Eur. Phys. J. D **25**, 203–238 (2003)
DOI: 10.1140/epjd/e2003-00270-x

THE EUROPEAN PHYSICAL JOURNAL D

Evaluation of the two-loop self-energy correction to the ground state energy of H-like ions to all orders in $Z\alpha$

V.A. Yerokhin[1,2], P. Indelicato[2,a], and V.M. Shabaev[1]

[1] Department of Physics, St. Petersburg State University, Oulianovskaya 1, Petrodvorets, St. Petersburg 198504, Russia
[2] Laboratoire Kastler-Brossel, École Normale Supérieure et Université P. et M. Curie, Case 74, 4 place Jussieu, 75252 Paris Cedex 05, France

Received 14 July 2003
Published online 3 September 2003 –

Abstract. We present an evaluation of the complete gauge-invariant set of the two-loop self-energy diagrams carried out to all orders in the parameter $Z\alpha$. The calculation is performed for the ground state of H-like ions with $Z \geq 40$. As a result, we significantly improve the accuracy of theoretical values for the ground-state Lamb shift in high-Z H-like ions. We provide a compilation of various contributions to the ground-state energy of H-like ions and estimate uncertainties of the corresponding theoretical predictions.

PACS. 31.30.Jv Relativistic and quantum electrodynamic effects in atoms and molecules – 31.10.+z Theory of electronic structure, electronic transitions, and chemical binding – 31.30.-i Corrections to electronic structure

Introduction

Lamb-shift measurements in atomic systems presently provide one of the most stringent tests of quantum electrodynamics (QED). They are also used for the determination of fundamental physical constants with an outstanding accuracy [1]. The experimental precision for the 1S–2S transition in hydrogen has already reached 2 parts in 10^{14} [2] and is likely to be improved in the future. To theoretically describe bound systems on an adequate level of accuracy is a challenging problem. Currently, one of the most important limiting factors for the theoretical determination of the Lamb shift is the understanding of the two-loop self-energy corrections [1].

Historically, investigations of radiative corrections to a given order in the fine-structure constant α rely on an expansion in the parameters $Z\alpha$ and $\ln[(Z\alpha)^{-2}]$ (Z is the nuclear charge number). For the two-loop self-energy correction this expansion reads

$$F(Z\alpha) = B_{40} + (Z\alpha)B_{50} + (Z\alpha)^2\Big[L^3 B_{63} + L^2 B_{62} + L\,B_{61} + B_{60}\Big] + \cdots\,, \qquad (1)$$

where $L = \ln[(Z\alpha)^{-2}]$ and the function $F(Z\alpha)$ is related to the corresponding energy shift ΔE by

$$\Delta E = m\left(\frac{\alpha}{\pi}\right)^2 \frac{(Z\alpha)^4}{n^3} F(Z\alpha)\,, \qquad (2)$$

where n is the principal quantum number of the valence state. The lowest-order term B_{40} is determined by the electron form factors and their derivatives at zero transferred momentum. This correction was evaluated long ago [3–6], and its numerical value for the ground state is

$$B_{40} = 1.409\,244\ldots \qquad (3)$$

The calculation of higher-order two-loop corrections became possible only relatively recently. A considerable amount of efforts has been applied in this direction during the last decade. The evaluation of the next-to-leading correction was accomplished independently by Pachucki [7] and by Eides and Shelyuto [8]. The numerical value of this term turned out to be surprisingly large,

$$B_{50} = -24.266(3). \qquad (4)$$

This result significantly influenced agreement with experimental values for the Lamb shift in hydrogen and in He^+. The leading logarithmic term $B_{63} = -8/27$ was first derived by Karshenboim [9] and later confirmed in [10,11]. (It should be noted that Karshenboim's evaluation, while yielding the right answer, is not completely correct, as will be discussed below.) Two remaining logarithmic corrections B_{62} and B_{61} have also been elaborated by Pachucki [11]. Complete n-dependence of the B_{61} term for S states was derived lately by Jentschura [12]. For the ground state, a small modification was found in that work for the B_{61} correction as compared to the previous result of [11]. The numerical values of these terms for the ground

[a] e-mail: paul@spectro.jussieu.fr

state are

$$B_{62} = -0.639\,669\ldots, \tag{5}$$

$$B_{61} = 49.838\,315. \tag{6}$$

Again, as in order $(Z\alpha)^5$, the result obtained turned out to be surprisingly large. Even for hydrogen, it reverses the sign of the total logarithmic contribution and significantly changes the theoretical prediction. The calculation of the next non-logarithmic correction B_{60} represents a calculational challenge and is not completed at present. Up to now, only its fine-structure difference has been reported in reference [13].

The above results show that the convergence of the $Z\alpha$ expansion (1) is remarkably slow even for the lightest ions. Keeping in mind the large value of the B_{61} term, one can only speculate about numerical values of higher-order terms. In particular, rather large error margins have been ascribed to the B_{60} term in [11], $B_{60} = 0 \pm 100$, which gives rise to the leading theoretical error for the Lamb shift in hydrogen. The situation for heavier ions is even more uncertain. This shows the necessity for the numerical evaluation of the two-loop self-energy correction to all orders in $Z\alpha$. Such an evaluation, especially in the low-Z region, is a very demanding problem. We remind the reader that an accurate numerical calculation of the *one-loop* self-energy correction for light H-like ions with $Z < 5$ was elaborated only very recently [14]. Evidently, carrying out a similar project for the two-loop case is much more difficult.

The calculation of the two-loop self-energy diagrams (Fig. 1) without an expansion in $Z\alpha$ started with the irreducible contribution of the diagram (a) (also known as the loop-after-loop (LAL) correction), which is the simplest part of the total set. Such an evaluation was first accomplished in [15] for high-Z ions, and later in [16] for all ions including hydrogen. The latter investigation demonstrated a rather peculiar behaviour of the LAL correction in the low-Z region. It was shown that already for hydrogen its actual value was of a different sign and magnitude than the value based on the first two terms of the $Z\alpha$ expansion. In addition, a different result was found in [16] for the leading logarithmic contribution B_{63} as compared to the analytical evaluation [9]. (We note that in the latter work the B_{63} term was evaluated for the complete set of the two-loop self-energy diagrams. However, it was argued that it originated from the LAL contribution only.) As a result, a question was raised in [16] about the possibility that the $Z\alpha$ expansion for the two-loop self-energy could be inadequate even for hydrogen. This speculation attracted attention and several investigations followed. The subsequent numerical calculation [17] claimed to be compatible with the analytical result. However, the third numerical evaluation by one of us [18] confirmed the first result [16]. At the same time, the total value of the B_{63} contribution was confirmed independently by several groups, *e.g.*, in [10]. To throw light on this intricate situation we performed [19] an analytical calculation of the B_{63} term separately for the LAL contribution and found agreement both with our previous numerical result and with that of [16]. Our conclusion was that the LAL correction provided an additional cubed logarithmic contribution that had been omitted in the original analytical calculation [9]. However, this additional term vanishes when the complete set of the two-loop self-energy diagrams is taken into account. Recently, analogous terms were reported for the leading logarithmic contribution for P states [20].

The evaluation of the remaining part of the two-loop self-energy diagrams is by far more difficult. It consists of the reducible part of the LAL diagram (a), the overlapping diagram (b), and the nested diagram (c). First attempts to evaluate them to all orders in $Z\alpha$ were made by Mallampalli and Sapirstein [21] and by Goidenko *et al.* [22]. In the former investigation, the contribution of interest was rearranged in 3 parts, referred to by the authors as the "M", "P", and "F" terms. (We discuss this separation in detail below.) Mallampalli and Sapirstein calculated only the M and F terms, while the P term was left out since a new numerical technique had to be developed for its computation. In addition, since the numerical procedure turned out to be very time consuming, the actual calculation of the M term was carried out only for two ions, uranium and bismuth. Subsequently, in the investigation by two of us [23] we accomplished the computation of the remaining P term for $Z = 83$, 90, and 92, which formally completed the calculation of the two-loop self-energy. However, as we will see, the rearrangement of the whole correction into the M, P, and F terms is artificial since all the three are divergent. A proper treatment should include these terms simultaneously. In addition, more than two points (in Z) are needed in order to analyze the Z dependence of the correction and to compare it with the known terms of the $Z\alpha$ expansion. All these issues are addressed to in the present investigation. First our results were published in [24]. In this work we present a detailed description of the formalism and the main features of our numerical procedure.

The paper is organized as follows. In the beginning of Section 1, we summarize the known results and basic formulas for the one-loop self-energy correction which serve as a basis for our study of two-loop contributions. Then we present general formulas for the two-loop corrections, isolate ultraviolet and infrared divergences, and separate the whole correction in 4 parts: the LAL contribution, the M, P, and F terms. The subsequent 3 sections describe the evaluation of the M, P, and F terms, respectively. In Section 5, we collect all contributions to the two-loop self-energy correction and discuss the present status of the Lamb shift in high-Z H-like ions.

Our calculation is carried out in the Feynman gauge and for the point model of the nuclear-charge distribution. The relativistic units ($\hbar = c = 1$) and the Heaviside charge units ($\alpha = e^2/4\pi$, $e < 0$) are used throughout the paper. We introduce here several notations that will be extensively used in what follows. The the photon propagator in the Feynman gauge is written as $D_{\mu\nu}(\omega, x_{12}) = g_{\mu\nu} D(\omega, x_{12})$, where

$$D(\omega, x_{12}) = \frac{\exp(\mathrm{i}\sqrt{\omega^2 + \mathrm{i}0}\, x_{12})}{4\pi x_{12}}, \tag{7}$$

the branch of the square root is fixed by the condition $\mathrm{Im}(\sqrt{\omega^2+\mathrm{i}0})>0$, and $x_{12}=|\mathbf{x}_1-\mathbf{x}_2|$. The operator of the electron-electron interaction is then

$$I(\omega)=e^2\alpha^\mu\alpha_\mu D(\omega), \tag{8}$$

where $\alpha^\mu=(1,\boldsymbol{\alpha})$ are the Dirac matrices. We also use the notations $\not{p}=p_\mu\gamma^\mu$, $\not{A}=\gamma_\mu A^\mu$, and $\hat{\mathbf{p}}=\mathbf{p}/|\mathbf{p}|$.

1 Basic analysis

1.1 One-loop self-energy

We start with some basic formulas for the first-order self-energy correction that will be needed in our investigation of two-loop contributions. The formal expression for the unrenormalized first-order self-energy matrix element in the Feynman gauge is given by

$$\Delta E^{\mathrm{unren}}_{\mathrm{SE}}=2\mathrm{i}\alpha\int_{-\infty}^{\infty}\mathrm{d}\omega\int\mathrm{d}\mathbf{x}_1\,\mathrm{d}\mathbf{x}_2\,\psi_a^\dagger(\mathbf{x}_1)\alpha_\mu \times G(\varepsilon_a-\omega,\mathbf{x}_1,\mathbf{x}_2)\alpha^\mu\psi_a(\mathbf{x}_2)D(\omega,x_{12}), \tag{9}$$

where G is the Dirac-Coulomb Green function, $G(\varepsilon)=(\varepsilon-H)^{-1}$, where H is the Dirac-Coulomb Hamiltonian. For the future use, we introduce the self-energy function

$$\Sigma(\varepsilon,\mathbf{x}_1,\mathbf{x}_2)=2\mathrm{i}\alpha\gamma^0\int_{-\infty}^{\infty}\mathrm{d}\omega \times D(\omega,x_{12})\,\alpha_\nu G(\varepsilon-\omega,\mathbf{x}_1,\mathbf{x}_2)\alpha^\nu. \tag{10}$$

In terms of the self-energy function, equation (9) is simply written as

$$\Delta E^{\mathrm{unren}}_{\mathrm{SE}}=\langle a|\gamma^0\Sigma(\varepsilon_a)|a\rangle. \tag{11}$$

We introduce the γ^0 matrix into the expression for the self-energy function Σ in order to be consistent with the standard definition of the *free* self-energy function $\Sigma^{(0)}$ [Eq. (234)], which should be obtained from Σ when the external binding field is switched off.

The renormalization of the one-loop self-energy is well known. In our work, we employ the method based on the expansion of the bound-electron propagator G in terms of the interaction with the nuclear Coulomb field [25]. For the detailed description of our renormalization procedure we refer the reader to [26]. The renormalized self-energy correction is then represented by the sum of the zero-, one-, and many-potential terms,

$$\Delta E_{\mathrm{SE}}=\Delta E^{\mathrm{zero}}_{\mathrm{SE}}+\Delta E^{\mathrm{one}}_{\mathrm{SE}}+\Delta E^{\mathrm{many}}_{\mathrm{SE}}, \tag{12}$$

where

$$\Delta E^{\mathrm{zero}}_{\mathrm{SE}}=\int\frac{\mathrm{d}\mathbf{p}}{(2\pi)^3}\,\overline{\psi}_a(\mathbf{p})\Sigma^{(0)}_R(\varepsilon_a,\mathbf{p})\psi_a(\mathbf{p}), \tag{13}$$

$$\Delta E^{\mathrm{one}}_{\mathrm{SE}}=\int\frac{\mathrm{d}\mathbf{p}_1}{(2\pi)^3}\frac{\mathrm{d}\mathbf{p}_2}{(2\pi)^3}\,\overline{\psi}_a(\mathbf{p}_1) \times\Gamma^0_R(\varepsilon_a,\mathbf{p}_1;\varepsilon_a,\mathbf{p}_2)V_C(\mathbf{q})\psi_a(\mathbf{p}_2)\ , \tag{14}$$

where $V_C(\mathbf{q})=-4\pi\alpha Z/|\mathbf{q}|^2$ is the Coulomb potential, $\mathbf{q}=\mathbf{p}_1-\mathbf{p}_2$, $\overline{\psi}_a(\mathbf{p})=\psi_a^\dagger(\mathbf{p})\gamma^0$, and $\Sigma^{(0)}_R(p)$ and $\Gamma^\mu_R(p_1,p_2)$ are the renormalized free self-energy and vertex functions in 4 dimensions introduced in Appendix A. The expression for $\Delta E^{\mathrm{many}}_{\mathrm{SE}}$ is given by equation (9) where the Green function G is replaced with $G^{(2+)}$,

$$G^{(2+)}=G-G^{(0)}-G^{(1)}, \tag{15}$$

where $G^{(0)}$ is the free Dirac Green function, and $G^{(1)}$ is the one-potential Green function,

$$G^{(1)}(\varepsilon,\mathbf{x}_1,\mathbf{x}_2)=\int\mathrm{d}\mathbf{z}\,G^{(0)}(\varepsilon,\mathbf{x}_1,\mathbf{z})V_C(\mathbf{z})G^{(0)}(\varepsilon,\mathbf{z},\mathbf{x}_2). \tag{16}$$

We now discuss the contour of the ω integration in the many-potential term because this will be an important point in the two-loop case. It is widely accepted that it is advantageous to deform the integration contour to be parallel to the imaginary axis. This provides additional exponential damping factors from the electron and photon propagators and makes the integration much more easy to perform numerically. We mention here two ways to deform the contour that are most widely used in self-energy calculations. The first choice is to perform the standard Wick rotation of the contour to the imaginary axis ($\omega\to\mathrm{i}\omega$). In this case, one or several pole terms arise induced by the intermediate states in the spectral decomposition of the electron propagator that are more (or equally) deeply bound than the valence state (see, *e.g.*, [25]). For the first-order self-energy, these pole terms are quite simple, but in the two-loop case their structure becomes much more complicated.

It is possible also to deform the integration contour in a way that is free from this disadvantage. We define the contour C_{LH} that consists of two parts, the low-energy (C_L) and the high-energy (C_H) ones, $C_{LH}=C_L+C_H$, $C_L=[\Delta-\mathrm{i}0,-\mathrm{i}0]+[\mathrm{i}0,\Delta+\mathrm{i}0]$, and $C_H=(\Delta-\mathrm{i}\infty,\Delta-\mathrm{i}0]+[\Delta+\mathrm{i}0,\Delta+\mathrm{i}\infty)$. Here Δ is an auxiliary parameter that can be chosen arbitrary within the interval $\Delta\in(0,m+\varepsilon_a)$. Such contour (with $\Delta=\varepsilon_a$) was first used by Mohr [27]. Various modifications of this contour were employed in our investigations [26,28], where the low-energy part of the contour was bent into the complex plane in order to escape poles from virtual states more deeply bound than the valence state. Employing the C_{LH} contour, we can write the expression for the many-potential term as (a is assumed to be the ground state)

$$\Delta E^{\mathrm{many}}_{\mathrm{SE}}=-\frac{\alpha}{\pi}\int_0^{\Delta}\mathrm{d}\omega\int\mathrm{d}\mathbf{x}_1\,\mathrm{d}\mathbf{x}_2\,\psi_a^\dagger(\mathbf{x}_1)\alpha_\mu \times G^{(2+)}(\varepsilon_a-\omega)\,\alpha^\mu\psi_a(\mathbf{x}_2)\frac{\sin(\omega x_{12})}{x_{12}} +\frac{\alpha}{\pi}\mathrm{Re}\int_{\Delta}^{\Delta+\mathrm{i}\infty}\mathrm{i}\,\mathrm{d}\omega\int\mathrm{d}\mathbf{x}_1\,\mathrm{d}\mathbf{x}_2\,\psi_a^\dagger(\mathbf{x}_1)\alpha_\mu \times G^{(2+)}(\varepsilon_a-\omega)\,\alpha^\mu\psi_a(\mathbf{x}_2)\frac{\exp(\mathrm{i}\omega x_{12})}{x_{12}}\cdot \tag{17}$$

Fig. 1. Two-loop self-energy diagrams. Individual graphs are referred to as the loop-after-loop (LAL) diagram (a), the overlapping diagram (b), and the nested diagram (c). Double line indicates an electron propagating in the Coulomb nuclear field. It is understood that the corresponding mass counterterms are subtracted from the diagrams.

In this case no pole terms arise from the point $\omega = 0$ since the behavior of the integrand is softened due to the presence of $\sin(\omega x_{12})$ that vanishes at $\omega = 0$.

1.2 Two-loop self-energy diagrams: basic formulas and renormalization

The two-loop self-energy diagrams are presented in Figures 1a–1c. They are denoted as the loop-after-loop (LAL) diagram (a), the overlapping diagram (b), and the nested diagram (c). The contribution of the LAL diagram is usually divided into 2 parts that are referred to as the irreducible and the reducible one. The reducible contribution is defined as a part of the diagram in which the intermediate states in the spectral decomposition of the middle electron propagator coincide with the initial valence state. The irreducible part is the remainder (also referred to as the LAL correction). This contribution can be shown to be invariant under the covariant gauge transformations (see, *e.g.*, Appendix of [29]). Formal expressions for the corresponding energy shift can easily be derived, *e.g.*, by the two-time Green function method [30]. For the first time they were obtained by Mills and Kroll [31]. The LAL correction is given by

$$\Delta E_{\rm LAL} = \langle a|\gamma^0 \widetilde{\Sigma}(\varepsilon_a)\, G^{\rm red}\, \gamma^0 \widetilde{\Sigma}(\varepsilon_a)|a\rangle, \qquad (18)$$

where $\widetilde{\Sigma}(\varepsilon_a) = \Sigma(\varepsilon_a) - \delta m^{(1)}$, $\Sigma(\varepsilon)$ is the self-energy function (10), $\delta m^{(1)}$ is the one-loop mass counterterm, $G^{\rm red}$ is the reduced Dirac-Coulomb Green function.

The reducible part of the LAL diagram should be evaluated together with the nested and overlapping contributions since only the sum of all these terms is ultraviolet (UV) and infrared (IR) finite. It is given by

$$\Delta E_{\rm red} = \Delta E_{\rm SE}\ \langle a|\ \gamma^0 \frac{\partial}{\partial\varepsilon}\widetilde{\Sigma}(\varepsilon)\Big|_{\varepsilon=\varepsilon_a} |a\rangle, \qquad (19)$$

where $\Delta E_{\rm SE}$ is the one-loop self-energy correction (12). The contribution of the nested (N) diagram reads

$$\Delta E_N = 2{\rm i}\alpha \int_{-\infty}^{\infty} {\rm d}\omega_1 \int {\rm d}\mathbf{x}_1 \ldots {\rm d}\mathbf{x}_4\, D(\omega_1, x_{14}) \times\psi_a^\dagger(\mathbf{x}_1)\, \alpha_\mu G(\varepsilon_a - \omega_1)\gamma^0 \widetilde{\Sigma}(\varepsilon_a - \omega_1) \times G(\varepsilon_a - \omega_1)\, \alpha^\mu \psi_a(\mathbf{x}_4) - {\rm m.c.t.}\,, \qquad (20)$$

where m.c.t. denotes the corresponding second-order mass-counterterm contribution. For brevity, we omit radial arguments in G and Σ that can be easily restored. The overlapping (O) contribution is given by

$$\Delta E_O = 2{\rm i}\alpha \int_{-\infty}^{\infty} {\rm d}\omega_1 \int {\rm d}\mathbf{x}_1 \ldots {\rm d}\mathbf{x}_4\, D(\omega_1, x_{13}) \times\psi_a^\dagger(\mathbf{x}_1)\alpha_\mu G(\varepsilon_a - \omega_1)\gamma^0 \Lambda^\mu(\varepsilon_a - \omega_1, \varepsilon_a)\psi_a(\mathbf{x}_4) - {\rm m.c.t.}, \qquad (21)$$

where the vertex function is defined as

$$\Lambda^\mu(\varepsilon_a - \omega_1, \varepsilon_a) = 2{\rm i}\alpha\gamma^0 \int_{-\infty}^{\infty} {\rm d}\omega_2\, D(\omega_2, x_{24})\, \alpha_\nu \times G(\varepsilon_a - \omega_1 - \omega_2)\alpha^\mu G(\varepsilon_a - \omega_2)\alpha^\nu. \qquad (22)$$

In our derivation we utilize an approach where the mass counterterm is included from the very beginning into the Lagrangian of the system (see, *e.g.*, [32]). In this approach, each (sub-) graph g giving a contribution to the self-energy is accompanied by the corresponding piece of δm called $\delta m^{(g)}$. We indicate this by adding a tilde to the self-energy function, $\widetilde{\Sigma}^{(g)} = \Sigma^{(g)} - \delta m^{(g)}$. In this way, the mass renormalization is performed implicitly, and we do not draw any diagrammatic representation for mass counterterms. With the discussion of formal mass renormalization completed, the next step is to consider the charge renormalization. For completeness, we present it in some detail here, largely repeating the original description by Fox and Yennie [33]. Other studies of the renormalization of two-loop self-energy diagrams can be found in [34,35].

The general approach is based on the external-field expansion of the bound-electron propagator

$$\frac{1}{\not p - e\not A - m} = \frac{1}{\not p - m} + \frac{1}{\not p - m} e\not A \frac{1}{\not p - m} + \cdots \qquad (23)$$

where A is the external electromagnetic potential $A^\mu(x) = (\varphi(x), \mathbf{A}(\mathbf{x}))$. This expansion, applied to the lowest-order self-energy function $\widetilde{\Sigma}$ yields

$$\widetilde{\Sigma} = \widetilde{\Sigma}^{(0)} + \widetilde{\Sigma}^{(1)} + \widetilde{\Sigma}^{(2+)}, \qquad (24)$$

where the superscript indicates the power in $\not A$, and

$$\widetilde{\Sigma}^{(2+)} = \Sigma^{(2+)} = \sum_{n=2}^{\infty} \Sigma^{(n)}. \qquad (25)$$

All terms $\Sigma^{(i)}$ with $i \geq 2$ are finite. For the first two terms we have (see Appendix A)

$$\widetilde{\Sigma}^{(0)} = B^{(1)}\,(\not p - m) + \Sigma_R^{(0)}, \qquad (26)$$

$$\widetilde{\Sigma}^{(1)} = L^{(1)}\, e\not A + \Sigma_R^{(1)}, \qquad (27)$$

where $B^{(1)}$ and $L^{(1)}$ are the one-loop renormalization constants, and the subscript R indicates that the corresponding contribution is UV finite.

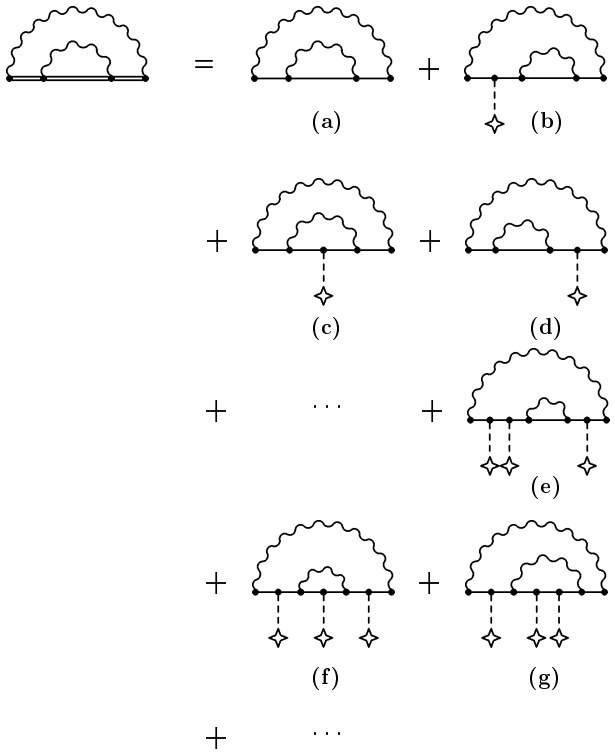

Fig. 2. Expansion of the nested part of the two-loop self-energy function in powers of $e\not{A}$.

Taking into account the Ward identity ($B^{(1)} = -L^{(1)}$), we obtain the following representation for the self-energy function,

$$\widetilde{\Sigma} = B^{(1)}\,(\not{p} - e\not{A} - m) + \Sigma_R^{(0)} + \Sigma_R^{(1)} + \Sigma^{(2+)}. \quad (28)$$

The last three terms here are finite, and the fist term vanishes when its expectation value is evaluated with the Dirac wave functions. Then,

$$\langle a|\gamma^0\widetilde{\Sigma}|a\rangle = \langle a|\gamma^0\Sigma_R^{(0)}|a\rangle + \langle a|\gamma^0\Sigma_R^{(1)}|a\rangle + \langle a|\gamma^0\Sigma_R^{(2+)}|a\rangle = \Delta E_{\rm SE}, \quad (29)$$

which yields the known decomposition (12).

Now we turn to the two-photon case. Starting with the nested diagram, we expand it as shown in Figure 2. The diagram (a) yields

$$\widetilde{\Sigma}_N^{(0)} = B^{(2N)}\,(\not{p} - m) + B^{(1)}\,\widetilde{\Sigma}^{(0)} + \Sigma_{N,R}^{(0)}, \quad (30)$$

where $B^{(2N)}$ is the overall two-loop divergent constant and $B^{(1)}$ comes from the renormalization of the inner self-energy loop. The combination of Figures 2b, 2c, and 2d contribute a net result

$$\widetilde{\Sigma}_N^{(1)} = L^{(2N)}\,e\not{A} + \left(2B^{(1)} + L^{(1)}\right)\widetilde{\Sigma}^{(1)} + \Sigma_{N,R}^{(1)}. \quad (31)$$

The contribution from the graphs containing n interactions with the potential are

$$\widetilde{\Sigma}_N^{(n)} = \left[(n+1)B^{(1)} + nL^{(1)}\right]\widetilde{\Sigma}^{(n)} + \Sigma_{N,R}^{(n)}\,. \quad (32)$$

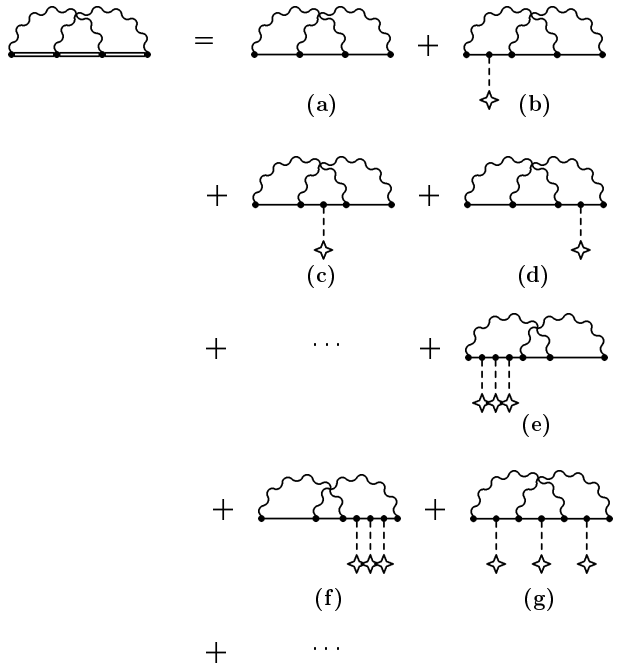

Fig. 3. Expansion of the overlapping part of the two-loop self-energy function in powers of $e\not{A}$.

Here the terms containing $B^{(1)}$ arise from graphs in which there are zero external potentials inside the inner self-energy loop [Fig. 2e], while those containing $L^{(1)}$ have just one external potential there [Fig. 2f]. Adding these results and using the Ward identity, one finds

$$\widetilde{\Sigma}_N = B^{(2N)}\,(\not{p} - e\not{A} - m) + B^{(1)}\,\widetilde{\Sigma} + \Sigma_{N,R}. \quad (33)$$

The same procedure can be used for the overlapping diagram, as indicated in Figure 3,

$$\widetilde{\Sigma}_O^{(0)} = B^{(2O)}\,(\not{p} - m) + 2L^{(1)}\,\widetilde{\Sigma}^{(0)} + \Sigma_{O,R}^{(0)}, \quad (34)$$

$$\widetilde{\Sigma}_O^{(1)} = L^{(2O)}\,e\not{A} + 2L^{(1)}\,\widetilde{\Sigma}^{(1)} + \Sigma_{O,R}^{(1)}. \quad (35)$$

For the higher-order contributions, there are two types: those which have all the potentials on the extreme right or left [Figs. 3e and 3f], and those with mixed insertions [Fig. 3g]. While the mixed insertions yield a finite result, the former diagrams have a divergent subgraph. The combined results for them yield

$$\widetilde{\Sigma}_O^{(n)} = 2L^{(1)}\,\widetilde{\Sigma}^{(n)} + \Sigma_{O,R}^{(n)}. \quad (36)$$

The net result is

$$\widetilde{\Sigma}_O = B^{(2O)}\,(\not{p} - e\not{A} - m) + 2L^{(1)}\,\widetilde{\Sigma} + \Sigma_{O,R}. \quad (37)$$

In our present notation equations (20) and (21) are just $\Delta E_N = \langle a|\gamma^0\widetilde{\Sigma}_N|a\rangle$ and $\Delta E_O = \langle a|\gamma^0\widetilde{\Sigma}_O|a\rangle$. Taking into account that $(\not{p} - e\not{A} - m)|a\rangle = 0$ and $\langle a|\gamma^0\widetilde{\Sigma}|a\rangle = \Delta E_{\rm SE}$, we have

$$\Delta E_N + \Delta E_O = L^{(1)}\,\Delta E_{\rm SE} + \Delta E_{N,R} + \Delta E_{O,R}\,. \quad (38)$$

The reducible part is then written as

$$\Delta E_{\rm red} = B^{(1)}\,\Delta E_{\rm SE} + \Delta E_{{\rm red},R}\,. \tag{39}$$

Now we explicitly see that the sum of these 3 terms for the energy shift is UV finite,

$$\Delta E_N + \Delta E_O + \Delta E_{\rm red} = \Delta E_{N,R} + \Delta E_{O,R} + \Delta E_{{\rm red},R}\,, \tag{40}$$

which concludes our analysis of the renormalization of the two-loop self-energy diagrams.

1.3 Infrared reference-state divergences

Infrared (IR) reference-state singularities can occur in bound-state QED calculations when the energy of intermediate states in the spectral decomposition of the electron propagators coincide with the valence-state energy. Considering first the reducible contribution (19), one can see that it is IR divergent when the valence state appears as intermediate in the spectral decomposition of the electron propagator in the self-energy function $\Sigma(\varepsilon)$. The corresponding (IR) contribution reads

$$\Delta E^{\rm IR}_{\rm red} = -\Delta E_{\rm SE}\,J, \tag{41}$$

where we introduced the IR-divergent integral J,

$$J = \frac{\rm i}{2\pi}\int_{-\infty}^{\infty}{\rm d}\omega \frac{1}{(\omega-{\rm i}0)^2}\sum_{\mu_{\overline{a}}}\langle a\overline{a}|I(\omega)|\overline{a}a\rangle\,. \tag{42}$$

Here, $\overline{a}$ indicates the valence state a with the angular momentum projection $\mu_{\overline{a}}$.

Turning to the nested contribution (20), we obtain its IR-divergent part by the substitution

$$G(\varepsilon_a-\omega_1) \to G^{(a)}(\varepsilon_a-\omega_1) = \sum_{\mu_{\overline{a}}}\frac{\psi_{\overline{a}}\,\psi^\dagger_{\overline{a}}}{-\omega_1+{\rm i}0} \tag{43}$$

applied to the *both* electron propagators to the left and to the right from the inner self-energy loop. Taking into consideration that the matrix element of the self-energy operator $\langle n|\Sigma|n\rangle$ is diagonal with respect to the angular momentum projection of $|n\rangle$ (and does not depend on it), we obtain the expression for the IR-divergent part:

$$\Delta E^{\rm IR}_N = \frac{\rm i}{2\pi}\int_{-\infty}^{\infty}{\rm d}\omega_1 \sum_{\mu_{\overline{a}}}\langle a\overline{a}|I(\omega_1)|\overline{a}a\rangle \times\frac{\langle a|\gamma^0\,\widetilde{\Sigma}(\varepsilon_a-\omega_1)|a\rangle}{(\omega_1-{\rm i}0)^2}. \tag{44}$$

In the limit $\omega_1\to 0$ we can replace $\widetilde{\Sigma}(\varepsilon_a-\omega_1)$ with $\widetilde{\Sigma}(\varepsilon_a)$, and the integrands of the reducible and the nested term can be seen to cancel. In other words, we separate $\Delta E^{\rm IR}_N$ into two parts, $\Delta E^{\rm IR}_N = \Delta E^{{\rm IR},1}_N + \Delta E^{{\rm IR},2}_N$. The first term $\Delta E^{{\rm IR},1}_N$ is obtained from $\Delta E^{\rm IR}_N$ by the substitution $\widetilde{\Sigma}(\varepsilon_a-\omega_1)\to\widetilde{\Sigma}(\varepsilon_a)$. Obviously,

$$\Delta E^{{\rm IR},1}_N = \Delta E_{\rm SE}\,J, \tag{45}$$

and it vanishes when added together with $\Delta E^{\rm IR}_{\rm red}$. The remainder is given by

$$\Delta E^{{\rm IR},2}_N = \frac{\rm i}{2\pi}\int_{-\infty}^{\infty}{\rm d}\omega_1 \sum_{\mu_{\overline{a}}}\langle a\overline{a}|I(\omega_1)|\overline{a}a\rangle \times\frac{\langle a|\gamma^0\left[\Sigma(\varepsilon_a-\omega_1)-\Sigma(\varepsilon_a)\right]|a\rangle}{(\omega_1-{\rm i}0)^2}. \tag{46}$$

Let us show that this expression is IR finite. To demonstrate this, it is sufficient to consider the reference-state contribution to the self-energy functions. Denoting it conventionally by ΔE_a, we write

$$\Delta E_a = \left(\frac{\rm i}{2\pi}\right)^2\int_{-\infty}^{\infty}{\rm d}\omega_1\,{\rm d}\omega_2 \times\sum_{\mu_{\overline{a}}\mu_{\hat{a}}}\frac{\langle a\overline{a}|I(\omega_1)|\overline{a}a\rangle\langle a\hat{a}|I(\omega_2)|\hat{a}a\rangle}{(\omega_1-{\rm i}0)^2} \times\left(\frac{1}{-\omega_1-\omega_2+{\rm i}0}-\frac{1}{-\omega_2+{\rm i}0}\right). \tag{47}$$

It is convenient to use here the momentum-space representation for the photon propagator that yields

$$D(\omega,x_{12}) = -\int\frac{{\rm d}\mathbf{k}}{(2\pi)^3}\frac{\exp({\rm i}\mathbf{k}\mathbf{x}_{12})}{\omega^2-\mathbf{k}^2+{\rm i}0}, \tag{48}$$

or, after integrating over the angular variables,

$$D(\omega,x_{12}) = -\int_0^\infty\frac{{\rm d}k}{2\pi^2}\frac{k}{\omega^2-k^2+{\rm i}0}\frac{\sin kx_{12}}{x_{12}}. \tag{49}$$

Using this representation, we perform the integrations over ω_1 and ω_2 in equation (47) by Cauchy's theorem, which yields

$$\Delta E_a = \frac{\alpha^2}{\pi^2}\int_0^\infty{\rm d}k_1\,{\rm d}k_2\,\frac{1}{k_1+k_2} \times\sum_{\mu_{\overline{a}}\mu_{\hat{a}}}\langle a\overline{a}|\alpha_\mu\alpha^\mu\frac{\sin k_1x_{14}}{k_1x_{14}}|\overline{a}a\rangle \times\langle a\hat{a}|\alpha_\nu\alpha^\nu\frac{\sin k_2x_{23}}{k_2x_{23}}|\hat{a}a\rangle. \tag{50}$$

This expression is obviously finite.

1.4 General scheme of the numerical evaluation

We are now going to rearrange the contributions under consideration to the form suitable for the numerical evaluation. Although we already demonstrated the cancellation of UV divergences, it is still to be discussed how to treat them in practical calculations. The standard method for extracting UV divergences in QED is developed for diagrams involving only free-electron propagators and treats them in momentum space. We note that this approach is the only consistent method of renormalization developed

up to now that can be applied to diagrams of arbitrary order. Hence, our strategy will be to subtract similar diagrams with electron propagators containing zero or one interaction with the binding Coulomb field in order to make the corresponding point-by-point difference UV finite. The subtracted diagrams can be then evaluated in momentum space or in the mixed momentum-coordinate representation.

For the first-order self-energy correction, this approach was first developed by Snyderman [25] and implemented by Blundell and Snyderman [36]. In case of the two-loop self-energy, the situation is essentially more difficult. Here, for the first time, we encounter *overlapping* UV divergences. For example, the diagram in Figure 1b can be considered as consisting of two overlapping vertex subgraphs, each of which is UV divergent. The presence of overlapping divergences makes the structure of subtraction terms much more elaborate than that in the first order. Moreover, some of these terms contain both bound-electron propagators *and* UV-divergent subgraphs. Such situation had never been encountered before, and a new numerical technique had to be developed for the evaluation of these subtraction terms.

We start with the simplest part of the set, the LAL correction given by equation (18). Its evaluation can be performed by a straightforward generalization of the first-order calculation. Introducing an effective wave function [15]

$$|\phi_{\rm SE}\rangle = \gamma^0 \widetilde{\Sigma}(\varepsilon_a)|a\rangle, \tag{51}$$

we write equation (18) as

$$\Delta E_{\rm LAL} = \langle\phi_{\rm SE}|G^{\rm red}|\phi_{\rm SE}\rangle. \tag{52}$$

The effective wave function $\phi_{\rm SE}$ can be treated exactly in the same way as the first-order self-energy matrix element. For details, we refer the reader to [15,18].

The remainder of the set of the diagrams in Figure 1 is rearranged into 3 parts. Following the original study by Mallampalli and Sapirstein [21], we refer to them as the M, P, and F terms. The M term is diagrammatically represented by Figure 4. It consists of 3 parts that originate from the nested diagram, the overlapping diagram, and the reducible part of the LAL diagram. The subtractions in the M term are chosen so that each of these 3 parts is separately UV finite. Next, we should account for the subtracted terms. Those that contain only free-electron propagators can be treated in momentum space using the standard Feynman-parametrization technique. For those that involve bound-electron propagators we introduce additional subtractions that remove *overlapping* UV divergences. This is graphically represented by Figure 5. The corresponding contribution is referred to as the P term. It consists of 3 parts, each containing only a single UV-divergent subgraph. Taking the first part of the P term as an example, we see that the difference shown in the picture is UV-divergent only due to the inner self-energy loop, while the divergence due to the outer self-energy loop is canceled. Finally, we collect all terms we have subtracted and denote them as the F term depicted in Figure 6. It consists of Feynman diagrams that contain free-electron propagators only.

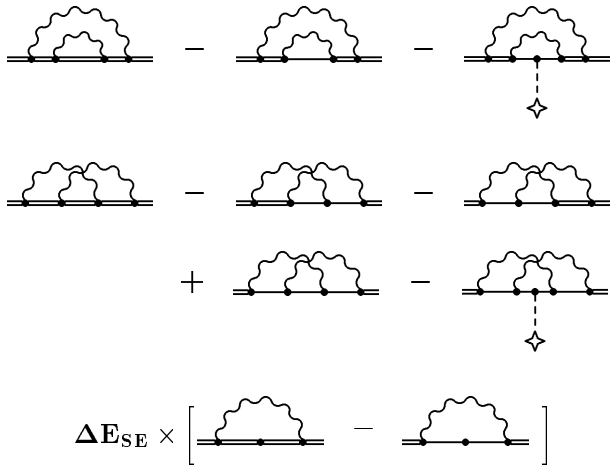

Fig. 4. Diagrammatic representation of the M term. It consists of 3 parts: the nested, overlapping, and reducible ones. Each of them is defined by the corresponding point-by-point difference, as indicated on the picture. The dashed line denotes the interaction with the binding Coulomb field. $\Delta E_{\rm SE}$ indicates the first-order self-energy correction. Drawing the diagrammatic representation for the reducible part, we used the identity for the derivative of the electron propagator, $\partial/(\partial\varepsilon)(\varepsilon - H)^{-1} = -(\varepsilon - H)^{-2}$.

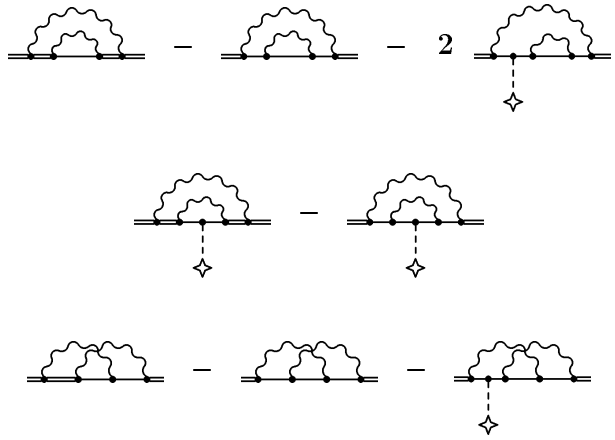

Fig. 5. Diagrammatic representation of the P term. It consists of 3 parts, the first two originate from the nested contribution and the last one from the overlapping contribution. The last part should be counted twice, accounting for two equivalent terms.

In this way we have divided the "non-trivial" part of the two-loop self-energy correction into 3 parts, the M, P, and F terms. All of these terms diverge: the M term is IR divergent, the F term is UV divergent, and the P term contains both types of divergences. The reason for this separation is that different numerical techniques are applied for the evaluation of each of these terms. The F terms consists of diagrams involving free-electron propagators only. It is thus evaluated in momentum space using the standard Feynman-parametrization technique within the dimensional regularization. The M term is UV finite,

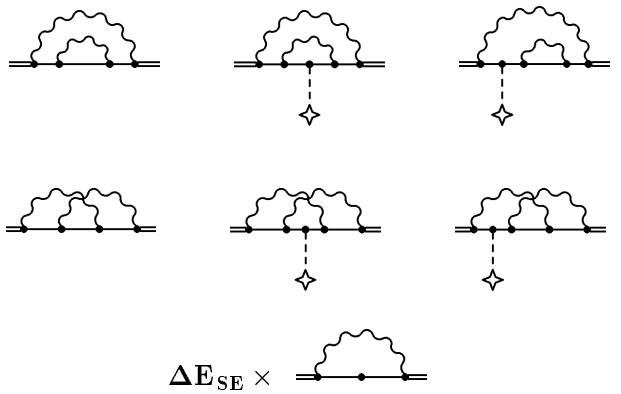

Fig. 6. Diagrammatic representation of the F term. The last diagrams from the right in the first two lines (the "side" graphs) should be counted twice, accounting for two equivalent diagrams.

which allows its treatment completely in coordinate space that is preferable for the evaluation of bound-electron propagators. In the present work as well as in the previous study [21], the Green-function approach is employed in numerical calculations of this contribution. The P term contains both UV-divergent subgraphs *and* the bound-electron propagators. Evaluating the corresponding diagrams, we treat the divergent subgraphs in momentum space (which allows the UV divergences to be easily isolated), while the remaining part of the diagram is kept in coordinate space. This approach involves a computation of the Dirac Green function in the mixed momentum-coordinate representation. This was implemented by using the finite-basis-set representation of the bound-electron propagator. All these issues are discussed in detail in the next sections.

2 M term

In this section, we discuss various contributions to the M term and write them in the form suitable for the numerical calculation. The basic scheme of the numerical evaluation of the M term is also explained in some detail.

The reducible part of the M term is relatively simple. It is given by equation (19) with the substitution $G \to G - G^{(0)}$ in the self-energy function $\Sigma(\varepsilon)$. As discussed in the previous section, the reducible M contribution is IR divergent when the valence state appears as intermediate in the spectral decomposition of the electron propagator. Thus we divide this contribution into two parts,

$$\Delta E_{\mathrm{red},M} = \Delta E^{\mathrm{IR}}_{\mathrm{red}} + \Delta E^{f}_{\mathrm{red},M}, \tag{53}$$

where the divergent contribution $\Delta E^{\mathrm{IR}}_{\mathrm{red}}$ is given by equation (41), and $\Delta E^{f}_{\mathrm{red},M}$ is finite and is obtained from equation (19) by the substitution $G \to G - G^{(0)} - G^{(a)}$ in the self-energy function $\Sigma(\varepsilon)$. The divergent contribution vanishes when all relevant terms are added together, whereas $\Delta E^{f}_{\mathrm{red},M}$ can be evaluated by a straightforward generalization of the numerical procedure for the first-order self-energy correction [26].

2.1 Nested diagram

As illustrated in Figure 4, the nested M term is given by

$$\begin{aligned}\Delta E_{N,M} = 2\mathrm{i}\alpha \int_{-\infty}^{\infty} \mathrm{d}\omega_1 \int \mathrm{d}\mathbf{x}_1 \ldots \mathrm{d}\mathbf{x}_4\, D(\omega_1, x_{14}) \\ \times \Big[\psi_a^\dagger(\mathbf{x}_1)\alpha_\mu G(\varepsilon_a - \omega_1)\,\gamma^0 \Sigma(\varepsilon_a - \omega_1) \\ \times G(\varepsilon_a - \omega_1)\,\alpha^\mu \psi_a(\mathbf{x}_4) - \text{subtractions}\Big],\end{aligned} \tag{54}$$

where the subtractions are symbolically defined by

$$G\gamma^0\Sigma G \to G\gamma^0\left(\Sigma - \Sigma^{(0)} - \Sigma^{(1)}\right) G = G\gamma^0\Sigma^{(2+)}G\,. \tag{55}$$

By employing elementary power-counting arguments, one can show that equation (54) is UV finite.

In order to facilitate the numerical evaluation of equation (54), it is convenient to deform the contour of the ω_1 integration in a way similar to that for the first-order self-energy correction. The necessary condition for a deformation of the contour is that the self-energy function $\Sigma(\varepsilon_a - \omega_1)$ can be analytically continued into the complex ω_1 plane. Analytical properties of the self-energy function are studied in Appendix B. Examining the analytical structure of the integrand in equation (54), we conclude that the deformation of the contour is possible just in the same way as it is for the first-order self-energy. To complete our analysis, we should present an explicit expression for the analytical continuation of the self-energy function. First, we give it utilizing the contour C_{LH} introduced in Section 1.1 (for simplicity, a is again assumed to be the ground state):

$$\Sigma(\varepsilon_a - \omega_1) = 2\mathrm{i}\alpha\gamma^0 \int_{C_{LH}} \mathrm{d}\omega_2\, D(\omega_2)\alpha_\nu G(\varepsilon_a - \omega_1 - \omega_2)\alpha^\nu. \tag{56}$$

This expression yields the analytical continuation of the self-energy function into the region where $\mathrm{Re}(\omega_1) \geq 0$ and $0 < \Delta + \mathrm{Re}(\omega_1) < m + \varepsilon_a$. In order to demonstrate this, it is sufficient to check that any point of this region can be connected with the point $\omega_1 = 0$ (where the validity of Eq. (56) is obvious) by a smooth contour that does not cross any singularities of the integrand.

The analytical continuation of the self-energy function can be also written in a different form that is valid for the imaginary values of ω_1 only ($\omega_1 = \mathrm{i}\omega$, $\omega \in \Re$),

$$\begin{aligned}\Sigma(\varepsilon_a - \mathrm{i}\omega) = 2\pi\alpha\gamma^0 \Bigg[D(\mathrm{i}\omega)\alpha_\nu \sum_{\mu\overline{a}} \psi_{\overline{a}}\, \psi_{\overline{a}}^\dagger\, \alpha^\nu \\ - \frac{1}{\pi} P \int_{-\infty}^{\infty} \mathrm{d}\omega_2\, D(\mathrm{i}\omega_2)\alpha_\nu G(\varepsilon_a - \mathrm{i}\omega - \mathrm{i}\omega_2)\alpha^\nu \Bigg],\end{aligned} \tag{57}$$

where P indicates the principal value of the integral that should be taken in a vicinity of the point $\omega_2 = -\omega$.

We conclude now that the contour of the ω_1 integration in equation (54) can be deformed into the complex plane, providing that it does not cross any branch cuts of the integrand and that the inner self-energy function is properly analytically continued. In particular, equation (54) still holds if we use the contour C_{LH} for the ω_1 *and* for the ω_2 integrations. The parameter of the contour Δ should then be chosen from the interval $0 < \Delta < (m + \varepsilon_a)/2$. The standard Wick rotation ($\omega_1 \to \mathrm{i}\omega_1$, $\omega_2 \to \mathrm{i}\omega_2$) is also possible. However, it leads to the appearance of a number of pole terms as will be discussed below.

The summation over the magnetic substates and the angular integrations in equation (54) can be conveniently carried out when the spectral decomposition of the electron propagators is employed,

$$\Delta E_{N,M} = \left(\frac{\mathrm{i}}{2\pi}\right)^2 \int_{C_{LH}} \mathrm{d}\omega_1\, \mathrm{d}\omega_2 \times \left[\sum_{n_1 n_2 n_3} \frac{\langle a n_3 | I(\omega_1) | n_1 a\rangle \langle n_1 n_2 | I(\omega_2) | n_2 n_3\rangle}{(\varepsilon_a - \omega_1 - \varepsilon_{n_1})(\varepsilon_a - \omega_1 - \omega_2 - \varepsilon_{n_2})} \times \frac{1}{(\varepsilon_a - \omega_1 - \varepsilon_{n_3})} - \text{subtractions} \right]. \quad (58)$$

Here and in what follows we assume that the intermediate-state energies have a small imaginary add-on, $\varepsilon_n = \varepsilon_n(1 - \mathrm{i}0)$.

We now introduce [40] a multipole expansion of the matrix element of the operator of the electron-electron interaction,

$$\langle ab | I(\omega) | cd\rangle = \alpha \sum_{J=0}^{\infty} I_J(abcd) R_J(\omega, abcd)\ , \quad (59)$$

where the function $I_J(abcd)$ contains the complete magnetic-substate dependence of the matrix element,

$$I_J(abcd) = \sum_{m_J} (-1)^{j_a - m_a + J - m_J + j_b - m_b} \times \begin{pmatrix} j_a & J & j_c \\ -m_a & m_J & m_c \end{pmatrix} \begin{pmatrix} j_b & J & j_d \\ -m_b & -m_J & m_d \end{pmatrix}, \quad (60)$$

and $(\ldots)$ denotes a $3j$-symbol. Expressions for the radial integrals $R_J(\omega, abcd)$ are given in Appendix C. Similar formulas were previously published in [37], with the corresponding derivation given in [40]. The summation over the magnetic substates can now easily be carried out, yielding

$$\Delta E_{N,M} = \left(\frac{\mathrm{i}\alpha}{2\pi}\right)^2 \int_{C_{LH}} \mathrm{d}\omega_1\, \mathrm{d}\omega_2 \left[\sum_{\substack{n_1 n_2 n_3 \\ J_1 J_2}} (-1)^{J_1 + J_2} X_N \times \frac{R_{J_1}(\omega_1, a n_3 n_1 a)\, R_{J_2}(\omega_2, n_1 n_2 n_2 n_3)}{(\varepsilon_a - \omega_1 - \varepsilon_{n_1})(\varepsilon_a - \omega_1 - \omega_2 - \varepsilon_{n_2})} \times \frac{1}{(\varepsilon_a - \omega_1 - \varepsilon_{n_3})} - \text{subtractions} \right], \quad (61)$$

where

$$X_N = \frac{(-1)^{j_2 - j_a} \delta_{\kappa_1 \kappa_3}}{(2j_a + 1)(2j_1 + 1)}, \quad (62)$$

j denotes the total angular momentum of the electron, and κ is the relativistic angular quantum number.

As discussed in Section 1.3, equation (61) is IR divergent when $n_1 = n_3 = a$. Thus we divide the nested M contribution into two parts,

$$\Delta E_{N,M} = \Delta E^{\mathrm{IR}}_{N,M} + \Delta E^{f}_{N,M}, \quad (63)$$

where the first term (the "infrared" part) corresponds to $n_1 = n_3 = a$, and the second one is the finite remainder.

2.1.1 Infrared part

By employing the arguments given in Section 1.3, we obtain

$$\Delta E^{\mathrm{IR}}_{N,M} = \Delta E^{\mathrm{IR},1}_{N,M} + \Delta E^{\mathrm{IR},2}_{N,M}, \quad (64)$$

$$\Delta E^{\mathrm{IR},1}_{N,M} = \Delta E^{\mathrm{many}}_{\mathrm{SE}}\, J, \quad (65)$$

where J is defined by equation (42), and

$$\Delta E^{\mathrm{IR},2}_{N,M} = \left(\frac{\mathrm{i}\alpha}{2\pi}\right)^2 \int_{C_{LH}} \mathrm{d}\omega_1\, \mathrm{d}\omega_2 \left[\sum_{n J_1 J_2} (-1)^{J_1 + J_2} \times X_N \frac{R_{J_1}(\omega_1, aaaa)\, R_{J_2}(\omega_2, anna)}{(-\omega_1 + \mathrm{i}0)^2} \times \left(\frac{1}{\varepsilon_a - \omega_1 - \omega_2 - \varepsilon_n} - \frac{1}{\varepsilon_a - \omega_2 - \varepsilon_n} \right) - \text{subtractions} \right]. \quad (66)$$

The integration over ω_1 for $n = a$, while formally converging, is somewhat difficult to evaluate numerically. In order to facilitate its computation, we separate the problematic part with $n = a$ and rewrite it using equation (50),

$$\Delta E^{\mathrm{IR},2\mathrm{a}}_{N,M} = \frac{\alpha^2}{\pi^2} \int_0^{\infty} \mathrm{d}k_1\, \mathrm{d}k_2\, \frac{X_N}{k_1 k_2 (k_1 + k_2)} \times \mathrm{Im}\Big[\sum_{J_1} (-1)^{J_1} R_{J_1}(k_1, aaaa) \Big] \times \mathrm{Im}\Big[\sum_{J_2} (-1)^{J_2} R_{J_2}(k_2, aaaa) \Big]. \quad (67)$$

For the point nuclear-charge distribution the radial integrations here are easily performed analytically. The remaining contribution to equation (66) is written as

$$\Delta E^{\mathrm{IR,2b}}_{N,M} = \frac{\alpha^2}{4\pi^2}\int_{C_{LH}} \mathrm{d}\omega_1\,\mathrm{d}\omega_2 \left[\sum_{\substack{n\neq a\\ J_1 J_2}} (-1)^{J_1+J_2} X_N \times \frac{R_{J_1}(\omega_1, aaaa)\, R_{J_2}(\omega_2, anna)}{\omega_1(\varepsilon_a-\omega_1-\omega_2-\varepsilon_n)(\varepsilon_a-\omega_2-\varepsilon_n)} - \mathrm{subtractions}\right]. \quad (68)$$

The integrand here is regular at $\omega_1 = 0$ due to the presence of $\sin(\omega_1 x_{12})$ in the low-energy part of the contour, as discussed in Section 1.1. Equivalently, we can write this expression as the integral over the imaginary axis plus the corresponding pole term.

Finally, the total IR contribution is given by the sum of equations (65), (67), and (68). We note that the contribution of equation (65) vanishes when all relevant terms are added together.

2.1.2 $\Delta E^{f}_{N,M}$ part

The contribution $\Delta E^{f}_{N,M}$ is given by

$$\Delta E^{f}_{N,M} = 2\mathrm{i}\alpha\int_{C_{LH}} \mathrm{d}\omega_1 \int \mathrm{d}\mathbf{x}_1\ldots\mathrm{d}\mathbf{x}_4\, D(\omega_1, x_{14}) \times\Big[\psi^\dagger_a(\mathbf{x}_1)\alpha_\mu G(\varepsilon_a-\omega_1)\gamma^0\Sigma(\varepsilon_a-\omega_1) \times G(\varepsilon_a-\omega_1)\alpha^\mu\psi_a(\mathbf{x}_4) - \mathrm{subtractions}'\Big], \quad (69)$$

where the self-energy function is assumed to be taken in the form (56), the parameter Δ of the contour C_{LH} should be within the interval $0 < \Delta < (m+\varepsilon_a)/2$, and the subtractions are given by the substitution

$$G\gamma^0\Sigma G \to G\gamma^0\Sigma^{(2+)}G - G^{(a)}\gamma^0\Sigma^{(2+)}G^{(a)}\,. \quad (70)$$

It is possible to evaluate $\Delta E^{f}_{N,M}$ directly according to equation (69). However, in order to check our analysis and the numerical procedure, we calculated this contribution also in a different way, utilizing the standard Wick rotation of the ω_1 and ω_2 integration contours. Below, we present the corresponding formulas for $\Delta E^{f}_{N,M}$. According to our experience, the numerical evaluation of these expressions is slightly faster, especially in the high-Z region, since one can employ less points for numerical integrations over the virtual photon energies.

First, we rotate the contour of the outer integration,

$$\Delta E^{f}_{N,M} = \Delta E^{\mathrm{pole},1}_{N,M} - 2\alpha\int_0^\infty \mathrm{d}\omega_1 \int \mathrm{d}\mathbf{x}_1\ldots\mathrm{d}\mathbf{x}_4 \times D(\mathrm{i}\omega_1, x_{14})\,\psi^\dagger_a(\mathbf{x}_1)\alpha_\mu \times\Big[G(\varepsilon_a-\mathrm{i}\omega_1)\gamma^0\Sigma(\varepsilon_a-\mathrm{i}\omega_1)G(\varepsilon_a-\mathrm{i}\omega_1) + G(\varepsilon_a+\mathrm{i}\omega_1)\gamma^0\Sigma(\varepsilon_a+\mathrm{i}\omega_1)G(\varepsilon_a+\mathrm{i}\omega_1) - \mathrm{subtractions}'\Big]\alpha^\mu\psi_a(\mathbf{x}_4), \quad (71)$$

where the pole term is given by

$$\Delta E^{\mathrm{pole},1}_{N,M} = \sum_{\mu_{\overline{a}}}\sum_{n}^{\varepsilon_n\neq\varepsilon_a} \frac{\langle a\overline{a}|I(0)|na\rangle}{\varepsilon_a-\varepsilon_n}\langle n|\gamma^0\Sigma^{(2+)}(\varepsilon_a)|\overline{a}\rangle. \quad (72)$$

Substituting the self-energy function in the form (57) into equation (71), we obtain

$$\Delta E^{f}_{N,M} = \Delta E^{\mathrm{pole},1}_{N,M} + \Delta E^{\mathrm{pole},2}_{N,M} + \Delta E^{\mathrm{Im}}_{N,M}, \quad (73)$$

$$\Delta E^{\mathrm{pole},2}_{N,M} = -\frac{1}{2\pi}\mathrm{Re}\int_0^\infty \mathrm{d}\omega_1 \times\sum_{\mu_{\overline{a}}}\sum_{n_1 n_3}^{(n_1 n_3)\neq(aa)} \frac{\langle an_3|I(\mathrm{i}\omega_1)|n_1 a\rangle\langle n_1\overline{a}|I(\mathrm{i}\omega_1)|\overline{a}n_3\rangle}{(\varepsilon_a-\mathrm{i}\omega_1-\varepsilon_{n_1})(\varepsilon_a-\mathrm{i}\omega_1-\varepsilon_{n_3})}, \quad (74)$$

and

$$\Delta E^{\mathrm{Im}}_{N,M} = 8\alpha^2\mathrm{Re}\int_0^\infty \mathrm{d}\omega_1\, P\int_{-\infty}^\infty \mathrm{d}\omega_2 \int \mathrm{d}\mathbf{x}_1\ldots\mathrm{d}\mathbf{x}_4 \times D(\mathrm{i}\omega_1, x_{14})\, D(\mathrm{i}\omega_2, x_{23})\psi^\dagger_a(\mathbf{x}_1)\alpha_\mu \times\Big[G(\varepsilon_a-\mathrm{i}\omega_1)\alpha_\nu G(\varepsilon_a-\mathrm{i}\omega_1-\mathrm{i}\omega_2)\alpha^\nu \times G(\varepsilon_a-\mathrm{i}\omega_1) - \mathrm{subtractions}'\Big]\alpha^\mu\psi_a(\mathbf{x}_4), \quad (75)$$

where the principal value of the ω_2 integral should be taken in a vicinity of the point $\omega_2 = -\omega_1$. We mention that the $\Delta E^{\mathrm{pole},1}_{N,M}$ and $\Delta E^{\mathrm{pole},2}_{N,M}$ pole terms are related to the screened self-energy correction and the two-photon exchange correction, respectively.

Finally, the $\Delta E^{f}_{N,M}$ contribution is given by equation (69) or, alternatively, by the sum of equations (72), (74), and (75).

2.2 Overlapping diagram

The overlapping M contribution is written as

$$\Delta E_{O,M} = 2\mathrm{i}\alpha\int_{-\infty}^\infty \mathrm{d}\omega_1 \int \mathrm{d}\mathbf{x}_1\ldots\mathrm{d}\mathbf{x}_4\, D(\omega_1, x_{13}) \times\Big[\psi^\dagger_a(\mathbf{x}_1)\alpha_\mu G(\varepsilon_a-\omega_1)\gamma^0\Lambda^\mu(\varepsilon_a-\omega_1,\varepsilon_a) \times\psi_a(\mathbf{x}_4) - \mathrm{subtractions}\Big], \quad (76)$$

where the vertex function is defined as

$$\Lambda^\mu(\varepsilon_a-\omega_1,\varepsilon_a) = 2\mathrm{i}\alpha\gamma^0\int_{-\infty}^{\infty}\mathrm{d}\omega_2\, D(\omega_2,x_{24})\,\alpha_\nu \times G(\varepsilon_a-\omega_1-\omega_2)\alpha^\mu G(\varepsilon_a-\omega_2)\alpha^\nu, \tag{77}$$

and the subtractions are symbolically represented by

$$G_1G_2G_3 \;\to\; G_1G_2G_3 - G_1G_2^{(0)}G_3^{(0)} - G_1^{(0)}G_2^{(0)}G_3 + G_1^{(0)}G_2^{(0)}G_3^{(0)} - G_1^{(0)}G_2^{(1)}G_3^{(0)}. \tag{78}$$

The expression (76) can be shown to be both UV and IR finite.

In order to deform the contour of the ω_1 integration in equation (76), we write the analytical continuation of the vertex function as follows (its existence is proven in Appendix B):

$$\Lambda^\mu(\varepsilon_a-\omega_1,\varepsilon_a) = 2\mathrm{i}\alpha\gamma^0\int_{C_{LH}}\mathrm{d}\omega_2\, D(\omega_2,x_{24})\,\alpha_\nu \times G(\varepsilon_a-\omega_1-\omega_2)\alpha^\mu G(\varepsilon_a-\omega_2)\alpha^\nu, \tag{79}$$

where $\mathrm{Re}(\omega_1)\geq 0$ and $0<\Delta+\mathrm{Re}(\omega_1)<m+\varepsilon_a$, and a is assumed to be the ground state. Now the contour of the ω_1 integration can be deformed, and we write the overlapping M contribution as

$$\Delta E_{O,M} = 2\mathrm{i}\alpha\int_{C_{LH}}\mathrm{d}\omega_1\int\mathrm{d}\mathbf{x}_1\ldots\mathrm{d}\mathbf{x}_4\, D(\omega_1,x_{13}) \times\psi_a^\dagger(\mathbf{x}_1)\alpha_\mu\Big[G(\varepsilon_a-\omega_1)\gamma^0\Lambda^\mu(\varepsilon_a-\omega_1,\varepsilon_a) -\text{subtractions}\Big]\psi_a(\mathbf{x}_4), \tag{80}$$

where the vertex function should be taken in the form (79), the subtractions are given by (78), and the parameter Δ of the contour C_{LH} should be within the interval $0<\Delta<(m+\varepsilon_a)/2$.

The summation over the magnetic substates and the angular integrations can be conveniently evaluated if we use the spectral decomposition of the electron propagators,

$$\Delta E_{O,M} = \left(\frac{\mathrm{i}}{2\pi}\right)^2\int_{C_{LH}}\mathrm{d}\omega_1\,\mathrm{d}\omega_2 \times\left[\sum_{n_1n_2n_3}\frac{\langle an_2|I(\omega_1)|n_1n_3\rangle\langle n_1n_3|I(\omega_2)|n_2a\rangle}{(\varepsilon_a-\omega_1-\varepsilon_{n_1})(\varepsilon_a-\omega_1-\omega_2-\varepsilon_{n_2})} \times\frac{1}{(\varepsilon_a-\omega_2-\varepsilon_{n_3})} - \text{subtractions}\right]. \tag{81}$$

Again, we assume that the intermediate-state energies have a small negative imaginary add-on, $\varepsilon_n=\varepsilon_n(1-\mathrm{i}0)$.

The angular integration yields

$$\Delta E_{O,M} = \left(\frac{\mathrm{i}\alpha}{2\pi}\right)^2\int_{C_{LH}}\mathrm{d}\omega_1\,\mathrm{d}\omega_2\left[\sum_{\substack{n_1n_2n_3\\J_1J_2}}X_O^{J_1J_2} \times\frac{R_{J_1}(\omega_1,an_2n_1n_3)\,R_{J_2}(\omega_2,n_1n_3n_2a)}{(\varepsilon_a-\omega_1-\varepsilon_{n_1})(\varepsilon_a-\omega_1-\omega_2-\varepsilon_{n_2})} \times\frac{1}{(\varepsilon_a-\omega_2-\varepsilon_{n_3})} - \text{subtractions}\right], \tag{82}$$

where

$$X_O^{J_1J_2} = \frac{(-1)^{j_1+j_2+j_3-j_a}}{2j_a+1}\begin{Bmatrix} j_2 & J_2 & j_1\\ j_a & J_1 & j_3\end{Bmatrix}. \tag{83}$$

2.2.1 Wick rotation

The overlapping M contribution can be calculated directly by utilizing equation (82). However, we present here also a different representation of this correction based on the Wick rotation of the integration contours. Agreement between numerical results based on these two representations for the overlapping M term served as an important check of our calculation. According to our experience, the numerical evaluation of expressions presented below is slightly faster, especially in the high-Z region. However, the corresponding analysis is essentially more awkward, and the final result consists of numerous parts.

Despite the fact that the overlapping diagram does not contain any IR divergences, we encounter terms with a nearly-singular IR behaviour when integrals run along the imaginary axis. These terms require some care and have to be evaluated separately. Conventionally, they are referred to as the "infrared" part $\Delta E_{O,M}^{\mathrm{IR}}$. Its expression can be obtained from equation (76) by the substitution

$$G_1G_2G_3 \;\to\; G_1^{(\mathrm{red})}G_2^{(a)}G_3^{(a)} + G_1^{(a)}G_2^{(a)}G_3^{(\mathrm{red})} + G_1^{(a)}G_2^{(a)}G_3^{(a)}, \tag{84}$$

where $G^{(a)}$ is defined by (43), and $G^{(\mathrm{red})}=G-G^{(a)}$. In this way, the overlapping M contribution is divided into two parts

$$\Delta E_{O,M} = \Delta E_{O,M}^{\mathrm{IR}} + \Delta E_{O,M}^{f}\,. \tag{85}$$

The contribution $\Delta E_{O,M}^{f}$ can be obtained from equation (76) by the substitution

$$G_1G_2G_3 \;\to\; G_1G_2G_3 - G_1G_2^{(0)}G_3^{(0)} - G_1^{(0)}G_2^{(0)}G_3 + G_1^{(0)}G_2^{(0)}G_3^{(0)} - G_1^{(0)}G_2^{(1)}G_3^{(0)} - G_1^{(\mathrm{red})}G_2^{(a)}G_3^{(a)} - G_1^{(a)}G_2^{(a)}G_3^{(\mathrm{red})} - G_1^{(a)}G_2^{(a)}G_3^{(a)}. \tag{86}$$

Analogously to the nested diagram, we evaluate the contribution of the last term in (84) to yield

$$\Delta E^{\mathrm{IR,a}}_{O,M} = -\frac{\alpha^2}{\pi^2}\int_0^\infty \mathrm{d}k_1\,\mathrm{d}k_2\,\frac{1}{k_1k_2(k_1+k_2)}\sum_{J_1J_2} X_O^{J_1J_2}\,\mathrm{Im}\left[R_{J_1}(k_1,aaaa)\right]\mathrm{Im}\left[R_{J_2}(k_2,aaaa)\right]. \tag{87}$$

The contribution of the two first terms in (84) is

$$\begin{aligned}\Delta E^{\mathrm{IR,b}}_{O,M} &= 2\left(\frac{\mathrm{i}\alpha}{2\pi}\right)^2\int_{-\infty}^\infty \mathrm{d}\omega_1\,\mathrm{d}\omega_2\sum_{\substack{n\neq a\\ J_1J_2}} X_O^{J_1J_2}\frac{R_{J_1}(\omega_1,aana)\,R_{J_2}(\omega_2,naaa)}{(\varepsilon_a-\omega_1-\varepsilon_n)(-\omega_1-\omega_2+\mathrm{i}0)(-\omega_2+\mathrm{i}0)}\\ &= 2\left(\frac{\mathrm{i}\alpha}{2\pi}\right)^2\int_{-\infty}^\infty \mathrm{d}\omega_1\,\mathrm{d}\omega_2\sum_{\substack{n\neq a\\ J_1J_2}} X_O^{J_1J_2}\frac{R_{J_1}(\omega_1,aana)\Big[R_{J_2}(\omega_2,naaa)-R_{J_2}(\omega_1,naaa)\Big]}{(\varepsilon_a-\omega_1-\varepsilon_n)(-\omega_1-\omega_2)(-\omega_2+\mathrm{i}0)}.\end{aligned} \tag{88}$$

In the last line, we have subtracted an additional contribution that vanishes after the integration over ω_2. At the same time, the subtracted term makes the integrand regular at $\omega_2=-\omega_1$ [we remind that $R_J(\omega_1)=R_J(-\omega_1)$]. Now we use the identity

$$\frac{1}{x+\mathrm{i}0} = P\frac{1}{x} - \mathrm{i}\pi\delta(x) \tag{89}$$

and separate the whole contribution (88) into a pole term and a principal-value integral,

$$\Delta E^{\mathrm{IR,b}}_{O,M}(\mathrm{pole}) = \frac{\mathrm{i}\alpha^2}{2\pi}\int_{-\infty}^\infty \mathrm{d}\omega_1\sum_{\substack{n\neq a\\ J_1J_2}} X_O^{J_1J_2}\frac{R_{J_1}(\omega_1,aana)\Big[R_{J_2}(\omega_1,naaa)-R_{J_2}(0,naaa)\Big]}{\omega_1(\varepsilon_a-\omega_1-\varepsilon_n)}, \tag{90}$$

$$\Delta E^{\mathrm{IR,b}}_{O,M}(\mathrm{Im}) = -\frac{\alpha^2}{2\pi^2}\int_{-\infty}^\infty \mathrm{d}\omega_1\,P\!\int_{-\infty}^\infty \mathrm{d}\omega_2\sum_{\substack{n\neq a\\ J_1J_2}} X_O^{J_1J_2}\frac{R_{J_1}(\omega_1,aana)\Big[R_{J_2}(\omega_2,naaa)-R_{J_2}(\omega_1,naaa)\Big]}{\omega_2(\varepsilon_a-\omega_1-\varepsilon_n)(\omega_1+\omega_2)}. \tag{91}$$

Rotating the integration contours ($\omega_1\to\mathrm{i}\omega_1$, $\omega_2\to\mathrm{i}\omega_2$) we obtain

$$\Delta E^{\mathrm{IR,b}}_{O,M}(\mathrm{pole}) = -\frac{\alpha^2}{\pi}\int_0^\infty \mathrm{d}\omega_1\sum_{\substack{n\neq a\\ J_1J_2}} X_O^{J_1J_2}\frac{R_{J_1}(\mathrm{i}\omega_1,aana)\Big[R_{J_2}(\mathrm{i}\omega_1,naaa)-R_{J_2}(0,naaa)\Big]}{\Delta_n^2+\omega_1^2}, \tag{92}$$

$$\Delta E^{\mathrm{IR,b}}_{O,M}(\mathrm{Im}) = \frac{2\alpha^2}{\pi^2}\mathrm{Re}\int_0^\infty \mathrm{d}\omega_1\,\mathrm{d}\omega_2\sum_{\substack{n\neq a\\ J_1J_2}} X_O^{J_1J_2}\frac{R_{J_1}(\mathrm{i}\omega_1,aana)\Big[R_{J_2}(\mathrm{i}\omega_2,naaa)-R_{J_2}(\mathrm{i}\omega_1,naaa)\Big]}{(\Delta_n-\mathrm{i}\omega_1)(\omega_1^2-\omega_2^2)}, \tag{93}$$

where $\Delta_n=\varepsilon_a-\varepsilon_n$. Finally, the total "infrared" contribution $\Delta E^{\mathrm{IR}}_{O,M}$ is given by the sum of equations (87), (92), and (93).

Similarly to that we rotate the integration contours in $\Delta E^f_{O,M}$, separating 3 pole contributions,

$$\Delta E^f_{O,M} = \Delta E^{\mathrm{pole},1}_{O,M} + \Delta E^{\mathrm{pole},2}_{O,M} + \Delta E^{\mathrm{pole},3}_{O,M} + \Delta E^{\mathrm{Im}}_{O,M}, \tag{94}$$

where

$$\Delta E^{\mathrm{pole},1}_{O,M} = \frac{\alpha^2}{4}\sum_{n_2\neq a}^{\kappa_1=\kappa_3=\kappa_a}\sum_{J_1J_2} X_O^{J_1J_2}\frac{R_{J_1}(0,an_2aa)R_{J_2}(0,aan_2a)}{\varepsilon_a-\varepsilon_{n_2}}, \tag{95}$$

$$\Delta E^{\mathrm{pole},2}_{O,M} = -\frac{\alpha^2}{\pi}\mathrm{Re}\int_0^\infty \mathrm{d}\omega_2\sum_{n_2\neq a,\,n_3}^{\kappa_1=\kappa_a}\sum_{J_1J_2} X_O^{J_1J_2}\frac{R_{J_1}(0,an_2an_3)\,R_{J_2}(\mathrm{i}\omega_2,an_3n_2a)}{(\varepsilon_a-\mathrm{i}\omega_2-\varepsilon_{n_2})(\varepsilon_a-\mathrm{i}\omega_2-\varepsilon_{n_3})} - \text{ free term}\Bigg], \tag{96}$$

$$\Delta E^{\mathrm{pole},3}_{O,M} = -\frac{\alpha^2}{2\pi}\mathrm{Re}\int_0^\infty \mathrm{d}\omega_1\sum_{n_1\neq a,\,n_3\neq a}^{\kappa_2=\kappa_a}\sum_{J_1J_2} X_O^{J_1J_2}\frac{R_{J_1}(\mathrm{i}\omega_1,aan_1n_3)\,R_{J_2}(\mathrm{i}\omega_1,n_1n_3aa)}{(\varepsilon_a-\mathrm{i}\omega_1-\varepsilon_{n_1})(\varepsilon_a+\mathrm{i}\omega_1-\varepsilon_{n_3})}, \tag{97}$$

$$\begin{aligned}\Delta E^{\mathrm{Im}}_{O,M} = \frac{\alpha^2}{2\pi^2}\mathrm{Re}\int_0^\infty \mathrm{d}\omega_1\,P\!\int_{-\infty}^\infty \mathrm{d}\omega_2\sum_{n_1n_2n_3}\sum_{J_1J_2} X_O^{J_1J_2}\\ \times\left[\frac{R_{J_1}(\mathrm{i}\omega_1,an_2n_1n_3)\,R_{J_2}(\mathrm{i}\omega_2,n_1n_3n_2a)}{(\varepsilon_a-\mathrm{i}\omega_1-\varepsilon_{n_1})(\varepsilon_a-\mathrm{i}\omega_1-\mathrm{i}\omega_2-\varepsilon_{n_2})(\varepsilon_a-\mathrm{i}\omega_2-\varepsilon_{n_3})} - \text{ subtractions}'\right].\end{aligned} \tag{98}$$

The subtractions in the last expression are defined by equation (86). Again, in order to avoid an evaluation of the principal value of the inner integral at $\omega_2 = -\omega_1$ and to make the integrand to behave smoothly, we add 3 additional terms that vanish identically after the ω_2 integration,

$$\Delta E^{\rm Im}_{O,M} = \frac{\alpha^2}{2\pi^2}{\rm Re}\int_0^\infty {\rm d}\omega_1\, P\!\int_{-\infty}^{\infty}{\rm d}\omega_2 \sum_{\substack{n_1 n_2 n_3\\ J_1 J_2}} X_O^{J_1 J_2}\left[\frac{R_{J_1}({\rm i}\omega_1, an_2n_1n_3)R_{J_2}({\rm i}\omega_2, n_1n_3n_2a)}{(\varepsilon_a - {\rm i}\omega_1 - \varepsilon_{n_1})(\varepsilon_a - {\rm i}\omega_1 - {\rm i}\omega_2 - \varepsilon_{n_2})(\varepsilon_a - {\rm i}\omega_2 - \varepsilon_{n_3})}\right.$$
$$- \frac{R_{J_1}({\rm i}\omega_1, aan_1n_3)R_{J_2}({\rm i}\omega_1, n_1n_3aa)}{(\varepsilon_a - {\rm i}\omega_1 - \varepsilon_{n_1})(-{\rm i}\omega_1 - {\rm i}\omega_2)(\varepsilon_a + {\rm i}\omega_1 - \varepsilon_{n_3})} + \frac{R_{J_1}({\rm i}\omega_1, aan_1a)R_{J_2}({\rm i}\omega_1, n_1aaa)}{{\rm i}\omega_1(-{\rm i}\omega_1 - {\rm i}\omega_2)(\varepsilon_a - {\rm i}\omega_1 - \varepsilon_{n_1})}$$
$$\left. + \frac{R_{J_1}({\rm i}\omega_1, aaan_3)R_{J_2}({\rm i}\omega_1, an_3aa)}{{\rm i}\omega_1({\rm i}\omega_1 + {\rm i}\omega_2)(\varepsilon_a + {\rm i}\omega_1 - \varepsilon_{n_3})} - \text{ subtractions}'\right] \quad (99)$$

where the subtractions are the same as in equation (98). The principal value of the ω_2 integral in the above expression should be evaluated only at the point $\omega_2 = 0$, which was accomplished by using quadratures that are symmetrical with respect to $\omega_2 \to -\omega_2$.

2.3 The total M term and its numerical evaluation

Finally, we bring together all contributions to the M term, separating explicitly its divergent part,

$$\Delta E_M = -\left(\Delta E^{\rm zero}_{\rm SE} + \Delta E^{\rm one}_{\rm SE}\right) J + \Delta E^f_M, \quad (100)$$
$$\Delta E^f_M = \Delta E^f_{{\rm red},M} + \Delta E^{{\rm IR},2}_{N,M} + \Delta E^f_{N,M} + \Delta E_{O,M}. \quad (101)$$

The IR-divergent part of ΔE_M vanishes when considered together with the corresponding part of the P term. We remind the reader the notations in the above expressions: $\Delta E^{\rm zero}_{\rm SE}$ and $\Delta E^{\rm one}_{\rm SE}$ are the zero-potential and the one-potential parts of the first-order self-energy correction (12), J is the IR divergent integral (42), $\Delta E^f_{{\rm red},M}$ is defined by equation (53), $\Delta E^{{\rm IR},2}_{N,M}$ is given by the sum of equations (67) and (68), $\Delta E^f_{N,M}$ is given by the equation (69) or, alternatively, by the sum of equations (72), (74), and (75); $\Delta E_{O,M}$ is given by the equation (82) or, alternatively, by the sum of equations (87), (92), (93), (95), (96), (97), and (99).

As can be readily seen, the general expressions for the nested and overlapping M terms [Eqs. (61, 82)] contain 5 summations over angular-momentum quantum numbers, namely, J_1, J_2, κ_1, κ_2, and κ_3. The first two parameters originate from the partial-wave decomposition of photon propagators, and the last three are the angular-momentum quantum numbers of intermediate electron states. Angular-momentum analysis leads to selection rules and makes only two of these parameters independent. In [21], the photon angular momenta L_1 and L_2 were chosen as independent expansion parameters. We found it technically more convenient to employ for this purpose the absolute values of the relativistic angular parameter κ of intermediate electron states, $|\kappa| = j + 1/2$. For the nested contribution, angular selection rules yield $\kappa_3 = \kappa_1$. Obviously, $|\kappa_1|$ and $|\kappa_2|$ can be taken as independent expansion parameters in this case. For the overlapping diagram the choice is less definitive. Empirically, we have found that choosing $|\kappa_1|$ and $|\kappa_3|$, we get a smooth expansion that yields a stable result for the extrapolated sum.

Most of the formulas above are written in terms of explicit summations over the Dirac spectrum, utilizing the spectral representation of the radial Green function,

$$G_\kappa(\varepsilon, x_1, x_2) = \sum_n \frac{\varphi_{\kappa,n}(x_1)\,\varphi^T_{\kappa,n}(x_2)}{\varepsilon - \varepsilon_{\kappa,n}}. \quad (102)$$

In our actual calculations we mainly use the analytical representation of the Dirac Green function in terms of the Whittaker functions (see, *e.g.*, [27]). In order to allow the immediate use of formulas presented so far, we write the radial Dirac Green function as

$$G_\kappa(\varepsilon, x_1, x_2) = -\psi_\kappa(\varepsilon, x_1; x_2)\,\tau^T_\kappa(\varepsilon, x_2; x_1)\,, \quad (103)$$

where

$$\psi_\kappa(\varepsilon, x_1; x_2) = \begin{cases} \phi^0_\kappa(\varepsilon, x_1), & x_1 < x_2\,, \\ \phi^\infty_\kappa(\varepsilon, x_1), & x_1 > x_2\,, \end{cases} \quad (104)$$

and

$$\tau_\kappa(\varepsilon, x_2; x_1) = \begin{cases} \phi^\infty_\kappa(\varepsilon, x_2), & x_1 < x_2\,, \\ \phi^0_\kappa(\varepsilon, x_2), & x_1 > x_2\,. \end{cases} \quad (105)$$

Here, ϕ^0_κ and ϕ^∞_κ are the two-component solutions of the radial Dirac equation bounded at the origin and infinity, respectively, and normalized in such a way that their Wronskian is unity. Taking into account equation (103), we can easily rewrite formulas involving summations over the Dirac spectrum in terms of the functions ψ_κ and τ_κ. The major complication is that the representation (103) is discontinuous at the point $x_1 = x_2$. Therefore, instead of the product of two-dimensional radial integrals $R_{J_1}(\omega_1)\,R_{J_2}(\omega_2)$, we now have a 4-fold radial integration.

The main problem of the numerical evaluation of the M term is its time consumption. Final expressions contain a 4-dimensional radial integration, a double integration over the virtual-photon energies, and two infinite summations over the angular-momentum quantum numbers. Taking equation (99) as a characteristic example,

we write symbolically a typical term of its partial-wave expansion as

$$t_{\kappa_1\kappa_3} \sim \int_0^\infty \mathrm{d}\omega_1\, P\!\int_{-\infty}^{\infty} \mathrm{d}\omega_2 \int_0^\infty \mathrm{d}x_1\, \mathrm{d}x_2\, \mathrm{d}x_3\, \mathrm{d}x_4 \times g_{L_1}(\mathrm{i}\omega_1, x_1, x_3)\, g_{L_2}(\mathrm{i}\omega_2, x_2, x_4)\, \varphi_a^i(x_1) \times G^{jk}_{\kappa_1}(\varepsilon_1, x_1, x_2)\, G^{lm}_{\kappa_2}(\varepsilon_2, x_2, x_3) \times G^{nr}_{\kappa_3}(\varepsilon_3, x_3, x_4)\, \varphi_a^s(x_4), \quad (106)$$

where the functions g_L originate from the partial-wave decomposition of photon propagators [see Eq. (271)], φ^i is a radial component of the wave function, and G^{ij}_κ is a radial component of the Green function. In the above expression, κ_1 and κ_3 are chosen to be the independent expansion parameters. For simplicity, all finite summations, subtractions, angular and overall factors are omitted there. The central part of the numerical procedure is the radial integration. In order to keep the computational time within reasonable limits, it is important to develop an efficient scheme for the evaluation of a 4-dimensional radial integral. We now address this topic in some detail.

In order to simplify the discussion, let us consider first a two-dimensional integral with similar properties:

$$L = \int_0^\infty \mathrm{d}x_1 \left(\int_0^{x_1} + \int_{x_1}^\infty\right) \mathrm{d}x_2\, F(x_<)\, G(x_>), \quad (107)$$

where $x_>$ ($x_<$) is the maximal (minimal) of the radial arguments. It is important that the integrand is a product of two functions, each depending on one radial argument only. For carrying out the numerical integration, we introduce the radial grid $\{r(i,j,k)\}$ on the interval $[0, r_{\max}]$. The parameter $r_{\max}$ (the cavity radius) was taken to be 1 a.u. for $Z = 80$; it was scaled by the factor of γ/Z for other values of Z, $\gamma = \sqrt{1-(Z\alpha)^2}$. First, we fill the elements $r(i,0,0)$ for $i = 0, ..., N_i$:

$$r(i,0,0) = r_0 \frac{1-t^2}{t^2}, \quad t = t_{\min} + (1-t_{\min})\frac{N_i - i}{N_i}, \quad (108)$$

where $t_{\min}$ is chosen so that $r(N_i,0,0) = r_{\max}$, and r_0 is the parameter of order of unity, adjusted empirically. Next, on each interval $[r(i,0,0), r(i+1,0,0)]$ we introduce the set of the Gauss-Legendre abscissae $\{r(i,j,0)\}_{j=1}^{N_j}$. In order to perform the outer radial integration, it is sufficient to know the integrand on the grid $\{r(i,j,0)\}$. This means that we have to evaluate the inner integral at each point of $\{r(i,j,0)\}$. We perform this by introducing a finer grid $\{r(i,j,k)\}$. For fixed values of i and j, the set $\{r(i,j,k)\}_{k=1}^{N_k}$ represents the Gauss-Legendre abscissae on the interval $[r(i,j,0), r(i,j+1,0)]$ if $j < N_j$ and on the interval $[r(i,j,0), r(i+1,0,0)]$ if $j = N_j$.

Finally we can see that when the functions F and G in equation (107) are stored on the radial grid $\{r(i,j,k)\}$, the numerical integration can be carried out by just summing up the stored numerical values. We mention that in actual situations the function F has often an exponentially-growing behaviour for large values of argument, whereas the function G is exponentially decreasing in this region. In order to avoid the numerical overflow in computing the product $F(x_1)\,G(x_2)$ for large values of the arguments, we store on the grid values $F(x)\mathrm{e}^{-ax}$ and $G(x)\mathrm{e}^{ax}$, where the factor $\mathrm{e}^{\pm ax}$ compensates the exponential behaviour of the functions F and G.

The procedure described for the evaluation of double integrals can be directly generalized for integrals of higher dimensions. For the computation of a 4-fold integral, we utilize the grid $\{r(i,j,k,l,m)\}$ introduced similarly to that for the two-dimensional integration. For fixed values of ω_1 and ω_2 in equation (106), the functions ϕ^0_κ and ϕ^∞_κ for each of the Green functions and Bessel functions for photon propagators are stored on this grid. After that the evaluation of radial integrals is reduced to simple manipulations with the stored numerical values. The following set of the grid parameters was employed in our numerical procedure: $\{N_j, N_k, N_l, N_m\} = \{4,3,2,1\}$. The parameter N_i was varied within the range $N_i = 8$–12.

The actual situation is somewhat more complicated due to the presence of finite summations over angular-momentum parameters (in Eq. (106) they would correspond to the summation over L_1, L_2, and κ_2) and of subtractions of free and one-potential contributions. In order to reduce the time of the computation, we stored all necessary functions on the radial grid for a fixed set $\{\kappa_1, \kappa_3, \omega_1, \omega_2\}$, and carried out all subtractions and finite angular-momentum summations before the radial integrations. In addition, we evaluated the integrand simultaneously for ω_2 and $-\omega_2$, reducing the corresponding integration over $(-\infty, \infty)$ to the interval $[0, \infty)$. In this way the principal value of the integral at the point $\omega_2 = 0$ is accounted for automatically.

The next step of the numerical procedure is to carry out integrations over the virtual-photon energies ω_1 and ω_2. For this purpose we used the Gauss-Legendre quadratures. The ω_2 integration was performed dividing the interval $[0, \infty)$ into two parts, $[0, \omega_1]$ and $[\omega_1, \infty)$. The typical number of integration points was 16–24 for the inner integration, and 12–16 for the outer one if the integrations were carried out along the imaginary axis. For the C_{LH} contour, we used the same number of integration points for the high-energy part and 4–8 points for the low-energy part. We found that in the high-Z region the numerical evaluation based on the integration along the imaginary axis is less time consuming. However, for lower values of Z, the C_{LH} contour becomes preferable due to the presence of the factor $\sin(\omega x_{12})$ in the low-energy part that softens the IR behaviour of the integrand and makes it smoother for small values of ω.

At this point of our numerical procedure the nested and overlapping M contributions are represented by tables consisting of elements of the partial-wave decomposition X_{κ_1,κ_3}. (We note that due to symmetry conditions for the overlapping diagram, it is sufficient to evaluate only a half of its non-diagonal elements.) We have now to estimate the sum of the double expansion for $\kappa_1 \to \infty$, $\kappa_3 \to \infty$. First,

Table 1. Finite parts of the reducible, nested, and overlapping contributions to the M term expressed in terms of the function $F(Z\alpha)$ defined by equation (2). In order to allow the term-by-term comparison with the previous calculation, finite parts of the $\Delta E^{\rm IR}_{{\rm red},M}$ and $\Delta E^{{\rm IR},1}_{N,M}$ contributions were subtracted from the results of [21] for the reducible and nested contributions (see the text for details).

Z	$\Delta E_{{\rm red},M}$	$\Delta E_{N,M}$	$\Delta E_{O,M}$	M term
40	−1.147	22.54(17)	−29.66(7)	−8.27(18)
50	−0.782	12.81(3)	−17.02(5)	−4.99(6)
60	−0.565	7.984(19)	−10.761(9)	−3.342(21)
70	−0.424	5.325(9)	−7.313(7)	−2.412(11)
83	−0.302	3.378(3)	−4.840(3)	−1.764(4)
	−0.302[a]	3.323(7)[a]	−5.456(8)[a]	−2.435(11)[a]
92	−0.239	2.563(2)	−3.837(2)	−1.513(3)
	−0.239[a]	2.553(5)[a]	−4.387(5)[a]	−2.074(7)[a]
100	−0.190	2.050(2)	−3.244(2)	−1.384(3)

[a] Reference [21].

we convert the table X_{κ_1,κ_3} to

$$X_{|\kappa_1|,|\kappa_3|} = \sum_{{\rm sign}(\kappa_1)} \sum_{{\rm sign}(\kappa_3)} X_{\kappa_1,\kappa_3}\,, \tag{109}$$

and then resum it once more,

$$X_{|\kappa_1|,|\kappa_3|} \to Y_{ij}\,, \tag{110}$$

where $i = ||\kappa_1| - |\kappa_3||$ and $j = (|\kappa_1| + |\kappa_3| - i)/2$. (This corresponds to the summation over diagonals of the matrix $X_{|\kappa_1|,|\kappa_3|}$.) Now we sum up the table Y_{ij}. First, we fix i and extrapolate the sum over j to infinity using 7–10 first expansion terms. Finally, we perform the summation over i and estimate the contribution of $i = i_{\rm max}, ..., \infty$, with $i_{\rm max}$ = 6–8. Several algorithms were used for the estimation of the tail of the expansion, including least-squares inverse-polynomial fitting and the ϵ resummation algorithm (see, *e.g.*, [38]).

We now discuss the computer time necessary for the evaluation of the M term. Certainly, the M term is the most time-consuming part of the total calculation. This is explained by the fact that we have to numerically evaluate the double infinite summation over the partial waves. In the previous evaluation by Mallampalli and Sapirstein, a total time of 7323 h was required for a given value of Z. In our numerical approach, the typical time of the evaluation of one element $X_{\kappa_1\kappa_3}$ is about 1 h for the IBM PWR3 processor with 350 MHz, both for the nested and the overlapping diagram. The typical number of the elements for a given Z was 440 for the nested diagram and 320 for the overlapping diagram. This shows that the time consumption in our numerical procedure is smaller than that of [21], although it is still very large.

In Table 1 we present the results of our numerical evaluation for finite parts of the M term that originate from the reducible, nested, and overlapping contributions, as given by equation (101). Our results are compared with the numerical values obtained by Mallapmalli and Sapirstein [21]. In order to make the term-by-term comparison possible, we have to account for a different treatment of the IR divergences in the present investigation as compared with that of [21]. Thus we perform a separate evaluation of the IR-divergent contributions $\Delta E^{\rm IR}_{{\rm red},M}$ and $\Delta E^{{\rm IR},1}_{N,M}$ exactly in the same way as it was done in [21]. (We remind that in our approach these contributions vanish identically in the sum with the P term and, therefore, there is no need in their actual evaluation.) We regulate IR divergences in J [Eq. (42)] by altering the valence energy ε_a to $\tilde{\varepsilon}_a = \varepsilon_a(1-\delta)$ and perform the calculation keeping a finite regulator δ. Finally, we fit our results for different values of δ to the form

$$J(\delta) = \frac{\alpha}{\pi}\Big[\ln\delta + J_c + O(\delta)\Big]\,. \tag{111}$$

Least-squares fit for J_c yields 1.2728 for $Z = 92$ and 1.4655 for $Z = 83$. In order to compare the results by Mallampalli and Sapirstein for the reducible and nested M terms with our values, we subtracted from their results the finite parts of $\Delta E^{\rm IR}_{{\rm red},M}$ and $\Delta E^{{\rm IR},1}_{N,M}$, which were obtained from equations (41) and (65) by replacing J to J_c.

Table 1 shows that our evaluation of the reducible and nested contributions agrees well with the previous calculation [21]. However, the results for the overlapping part differ by 13–14%, which corresponds to a deviation of about 40% for the total M term. Taking into account complexity of the computation, it is difficult to suppose what the reason for this disagreement could be. We only recall here the major tests for our numerical procedure that were carried out. As the first check, we treated the reference-state singularities similarly to that in [21], evaluating the limit $\delta \to 0$ numerically. Next, we performed our evaluation by employing two different contours for the ω integrations, as described above. In addition, we employed two different methods to evaluate pole terms (that appear when the integrations are carried out along the imaginary axis), using both the exact representation for the electron propagator and the basis-set technique.

3 P term

The P term is diagrammatically represented in Figure 5. The whole contribution consists of 3 parts,

$$\Delta E_P = \Delta E_{N1,P} + \Delta E_{N2,P} + 2\Delta E_{O,P}\,, \tag{112}$$

that correspond to the first, the second, and the third line of the figure, respectively. We refer to them as the first nested P term, the second nested P term, and the overlapping P term, respectively. The last contribution is counted twice accounting for two equivalent subtractions in the overlapping M term.

We now present basic formulas for the individual contributions to the P term. The first nested P contribution

is given by

$$\Delta E_{N1,P} = 2\mathrm{i}\alpha \int_{-\infty}^{\infty} \mathrm{d}\omega \int \frac{\mathrm{d}\mathbf{p}}{(2\pi)^3} \int \mathrm{d}\mathbf{x}_1 \mathrm{d}\mathbf{x}_2\, D(\omega, x_{12}) \times \psi_a^\dagger(\mathbf{x}_1)\alpha_\mu \Big[G(E, \mathbf{x}_1, \mathbf{p})\, \gamma^0 \widetilde{\Sigma}^{(0)}(E, \mathbf{p}) \times G(E, \mathbf{p}, \mathbf{x}_2) - \text{subtractions} \Big] \alpha^\mu \psi_a(\mathbf{x}_2), \tag{113}$$

where $E = \varepsilon_a - \omega$, the subtractions are symbolically given by

$$G\gamma^0 \Sigma G \to G\gamma^0 \Sigma G - G^{(0)}\gamma^0 \Sigma G^{(0)} - G^{(1)}\gamma^0 \Sigma G^{(0)} - G^{(0)}\gamma^0 \Sigma G^{(1)}, \tag{114}$$

the Green function in the mixed momentum-coordinate representation is defined by

$$G(\varepsilon, \mathbf{x}_1, \mathbf{p}) = \int \mathrm{d}\mathbf{x}_2\, \mathrm{e}^{\mathrm{i}\mathbf{p}\cdot\mathbf{x}_2} G(\varepsilon, \mathbf{x}_1, \mathbf{x}_2), \tag{115}$$

$$G(\varepsilon, \mathbf{p}, \mathbf{x}_2) = \int \mathrm{d}\mathbf{x}_1\, \mathrm{e}^{-\mathrm{i}\mathbf{p}\cdot\mathbf{x}_1} G(\varepsilon, \mathbf{x}_1, \mathbf{x}_2), \tag{116}$$

$\widetilde{\Sigma}^{(0)}(p) = \Sigma^{(0)}(p) - \delta m$, and $\Sigma^{(0)}(p)$ is the free self-energy function defined in Appendix A.

The second nested P contribution is given by

$$\Delta E_{N2,P} = 2\mathrm{i}\alpha \int_{-\infty}^{\infty} \mathrm{d}\omega \int \frac{\mathrm{d}\mathbf{p}_1}{(2\pi)^3} \frac{\mathrm{d}\mathbf{p}_2}{(2\pi)^3} \int \mathrm{d}\mathbf{x}_1 \mathrm{d}\mathbf{x}_2 \times \psi_a^\dagger(\mathbf{x}_1)\, \alpha_\mu \Big[G(E, \mathbf{x}_1, \mathbf{p}_1)\, \gamma^0 \Gamma^0(E, \mathbf{p}_1; E, \mathbf{p}_2) \times G(E, \mathbf{p}_2, \mathbf{x}_2) - \text{subtractions} \Big] \alpha^\mu \psi_a(\mathbf{x}_2) \times D(\omega, x_{12})\, V_C(\mathbf{q})\ , \tag{117}$$

where $E = \varepsilon_a - \omega$, $\mathbf{q} = \mathbf{p}_1 - \mathbf{p}_2$, V_C is the Coulomb potential, the subtractions are symbolically given by

$$G\gamma^0 \Gamma G \to G\gamma^0 \Gamma G - G^{(0)}\gamma^0 \Gamma G^{(0)}, \tag{118}$$

and $\Gamma^0(p_1, p_2)$ is the time component of the vertex function defined in Appendix A.

In order to obtain the expression for the overlapping P contribution, we first write the first-order self-energy matrix element in the mixed momentum-coordinate representation. It is obtained by applying the Fourier transformation over $\mathbf{x}_2$ to equation (9),

$$\Delta E_{\mathrm{SE}}^{\mathrm{unren}} = -2\mathrm{i}\alpha \int_{-\infty}^{\infty} \mathrm{d}\omega \int \frac{\mathrm{d}\mathbf{p}_1}{(2\pi)^3} \frac{\mathrm{d}\mathbf{p}_2}{(2\pi)^3} \times \int \mathrm{d}\mathbf{x}_1\, \frac{\exp(-\mathrm{i}\mathbf{q}\cdot\mathbf{x}_1)}{\omega^2 - \mathbf{q}^2 + \mathrm{i}0} \times \psi_a^\dagger(\mathbf{x}_1)\alpha_\mu G(E, \mathbf{x}_1, \mathbf{p}_1)\alpha^\mu \psi_a(\mathbf{p}_2). \tag{119}$$

The expression for $\Delta E_{O,P}$ is obtained from the formula above by making the substitution $\alpha^\mu \to \gamma^0 \Gamma^\mu$ and $G \to G^{(2+)}$,

$$\Delta E_{O,P} = -2\mathrm{i}\alpha \int_{-\infty}^{\infty} \mathrm{d}\omega \int \frac{\mathrm{d}\mathbf{p}_1}{(2\pi)^3} \frac{\mathrm{d}\mathbf{p}_2}{(2\pi)^3} \int \mathrm{d}\mathbf{x}_1 \times \frac{\exp(-\mathrm{i}\mathbf{q}\cdot\mathbf{x}_1)}{\omega^2 - \mathbf{q}^2 + i0}\, \psi_a^\dagger(\mathbf{x}_1)\alpha_\mu G^{(2+)}(E, \mathbf{x}_1, \mathbf{p}_1) \times \gamma^0 \Gamma^\mu(E, \mathbf{p}_1; \varepsilon_a, \mathbf{p}_2)\, \psi_a(\mathbf{p}_2). \tag{120}$$

3.1 Analysis of divergences

In this section we isolate divergent contributions from the general expressions for the P term presented so far. Taking into account the renormalization prescriptions for the one-loop functions

$$\widetilde{\Sigma}^{(0)}(p) = B^{(1)}(\not{p} - m) + \Sigma_R^{(0)}, \tag{121}$$

$$\Gamma^0(p_1, p_2) = L^{(1)}\gamma^0 + \Gamma_R^0(p_1, p_2), \tag{122}$$

the Ward identity $L^{(1)} = -B^{(1)}$ and the Dirac equation, we can separate UV divergences from the contributions to the P term:

$$\Delta E_{N1,P} + \Delta E_{N2,P} = B^{(1)} \Delta E_{\mathrm{SE},D}^{\mathrm{many}} + \Delta E_{N1,P}^R + \Delta E_{N2,P}^R, \tag{123}$$

$$2\Delta E_{O,P} = 2L^{(1)} \Delta E_{\mathrm{SE},D}^{\mathrm{many}} + 2\Delta E_{O,P}^R. \tag{124}$$

Here the index R labels the contributions that are free from UV divergences. Expressions for $\Delta E_{N1,P}^R$, $\Delta E_{N2,P}^R$, and $\Delta E_{O,P}^R$ are obtained from equations (113), (117), and (120) by the substitutions $\widetilde{\Sigma} \to \Sigma_R$ and $\Gamma^0 \to \Gamma_R^0$. In the above expressions, $\Delta E_{\mathrm{SE},D}^{\mathrm{many}}$ is the many-potential part of the one-loop self-energy correction, and the subscript D indicates that this term should be evaluated in D dimensions since it is multiplied by a divergent renormalization constant. (We mention that fortunately there is no need in its *actual* evaluation since the corresponding contribution vanishes identically in the sum with the F term.)

Both nested P contributions are also IR divergent. We obtain their IR-divergent part by the substitution $G \to G^{(a)}$ in equations (113) and (117). The same reasoning as for the nested M contribution yields

$$\Delta E_{N1,P}^R = \Delta E_{\mathrm{SE}}^{\mathrm{zero}}\, J + \Delta E_{N1,P}^{\mathrm{IR},2} + \Delta E_{N1,P}^f, \tag{125}$$

$$\Delta E_{N2,P}^R = \Delta E_{\mathrm{SE}}^{\mathrm{one}}\, J + \Delta E_{N2,P}^{\mathrm{IR},2} + \Delta E_{N2,P}^f, \tag{126}$$

where J is the divergent integral (42),

$$\Delta E_{N1,P}^{\mathrm{IR},2} = \frac{\mathrm{i}}{2\pi} \int_{-\infty}^{\infty} \mathrm{d}\omega \sum_{\mu_{\overline{a}}} \frac{\langle a\overline{a}|I(\omega)|\overline{a}a\rangle}{(-\omega + \mathrm{i}0)^2} \times \langle \overline{a}|\gamma^0 \Big[\Sigma_R^{(0)}(E) - \Sigma_R^{(0)}(\varepsilon_a) \Big] |\overline{a}\rangle, \tag{127}$$

$$\Delta E_{N2,P}^{\mathrm{IR},2} = \frac{\mathrm{i}}{2\pi} \int_{-\infty}^{\infty} \mathrm{d}\omega \sum_{\mu_{\overline{a}}} \frac{\langle a\overline{a}|I(\omega)|\overline{a}a\rangle}{(-\omega + \mathrm{i}0)^2} \times \langle \overline{a}|V_C\gamma^0 \Big[\Gamma_R^0(E) - \Gamma_R^0(\varepsilon_a) \Big] |\overline{a}\rangle. \tag{128}$$

We remind that $E=\varepsilon_a-\omega$, $\langle a|\gamma^0\Sigma_R^{(0)}(\varepsilon_a)|a\rangle=\Delta E_{\rm SE}^{\rm zero}$, and $\langle a|V_C\gamma^0\Gamma_R^0(\varepsilon_a)|a\rangle=\Delta E_{\rm SE}^{\rm one}$. The remaining part of the first nested P contribution is given by

$$\begin{aligned}\Delta E^f_{N1,P}=2{\rm i}\alpha\int_{-\infty}^{\infty}{\rm d}\omega\int\frac{{\rm d}\mathbf{p}}{(2\pi)^3}\int{\rm d}\mathbf{x}_1{\rm d}\mathbf{x}_2\,D(\omega,x_{12})\\ \times\psi_a^\dagger(\mathbf{x}_1)\alpha_\mu\Big[G(E,\mathbf{x}_1,\mathbf{p})\,\gamma^0\Sigma_R^{(0)}(E,\mathbf{p})\\ \times G(E,\mathbf{p},\mathbf{x}_2)-\text{subtractions}'\Big]\alpha^\mu\psi_a(\mathbf{x}_2),\end{aligned}\tag{129}$$

where the subtractions are given by the substitution

$$\begin{aligned}G\gamma^0\Sigma G\to G\gamma^0\Sigma G-G^{(0)}\gamma^0\Sigma G^{(0)}-G^{(1)}\gamma^0\Sigma G^{(0)}\\ -G^{(0)}\gamma^0\Sigma G^{(1)}-G^{(a)}\gamma^0\Sigma G^{(a)}.\end{aligned}\tag{130}$$

The remaining part of the second nested P contribution is written as

$$\begin{aligned}\Delta E^f_{N2,P}=2{\rm i}\alpha\int_{-\infty}^{\infty}{\rm d}\omega\int\frac{{\rm d}\mathbf{p}_1}{(2\pi)^3}\frac{{\rm d}\mathbf{p}_2}{(2\pi)^3}\int{\rm d}\mathbf{x}_1{\rm d}\mathbf{x}_2\\ \times\psi_a^\dagger(\mathbf{x}_1)\alpha_\mu\Big[G(E,\mathbf{x}_1,\mathbf{p}_1)\,\gamma^0\Gamma_R^0(E,\mathbf{p}_1;E,\mathbf{p}_2)\\ \times G(E,\mathbf{p}_2,\mathbf{x}_2)-\text{subtractions}'\Big]\alpha^\mu\psi_a(\mathbf{x}_2)\\ \times V_C(\mathbf{q})D(\omega,x_{12}),\end{aligned}\tag{131}$$

where the subtractions are symbolically given by the substitution

$$G\gamma^0\Gamma G\to G\gamma^0\Gamma G-G^{(0)}\gamma^0\Gamma G^{(0)}-G^{(a)}\gamma^0\Gamma G^{(a)}.\tag{132}$$

The finite part of the overlapping P term is given by

$$\begin{aligned}\Delta E^R_{O,P}=-2{\rm i}\alpha\int_{-\infty}^{\infty}{\rm d}\omega\int\frac{{\rm d}\mathbf{p}_1}{(2\pi)^3}\frac{{\rm d}\mathbf{p}_2}{(2\pi)^3}\int{\rm d}\mathbf{x}_1\\ \times\frac{\exp(-{\rm i}\mathbf{q}\cdot\mathbf{x}_1)}{\omega^2-\mathbf{q}^2+{\rm i}0}\,\psi_a^\dagger(\mathbf{x}_1)\alpha_\mu G^{(2+)}(E,\mathbf{x}_1,\mathbf{p}_1)\\ \times\gamma^0\Gamma^\mu_R(E,\mathbf{p}_1;\varepsilon_a,\mathbf{p}_2)\psi_a(\mathbf{p}_2).\end{aligned}\tag{133}$$

Summarizing, we write the total P term as

$$\Delta E_P=L^{(1)}\Delta E^{\rm many}_{{\rm SE},D}+\Big(\Delta E^{\rm zero}_{\rm SE}+\Delta E^{\rm one}_{\rm SE}\Big)\,J+\Delta E^f_P,\tag{134}$$

$$\begin{aligned}\Delta E^f_P=\Delta E^{\rm IR,2}_{N1,P}+\Delta E^f_{N1,P}+\Delta E^{\rm IR,2}_{N2,P}\\ +\Delta E^f_{N2,P}+2\Delta E^R_{O,P}.\end{aligned}\tag{135}$$

The IR-divergent part of equation (134) vanishes when considered together with the M term [Eq. (100)], whereas its UV-divergent part is canceled by the corresponding contribution from the F term [see Eq. (227)].

3.2 Angular integration

In this section, we illustrate how the integration over angular variables can be carried out in the P term. Since this integration is rather straightforward for the nested contributions, we concentrate here on the most problematic overlapping part. Utilizing the spectral representation for the Green function, we rewrite equation (133) as

$$\begin{aligned}\Delta E^R_{O,P}=-\frac{{\rm i}\alpha}{2\pi}\int_{-\infty}^{\infty}{\rm d}\omega\int\frac{{\rm d}\mathbf{p}_1}{(2\pi)^3}\frac{{\rm d}\mathbf{p}_2}{(2\pi)^3}\\ \times\left(\sum_n\psi_n^\dagger(\mathbf{p}_1)\gamma^0\Gamma^\mu_R(E,\mathbf{p}_1;\varepsilon_a,\mathbf{p}_2)\psi_a(\mathbf{p}_2)\right.\\ \left.\times\frac{A^{an}_\mu(\omega,\mathbf{q})}{E-\varepsilon_n(1-{\rm i}0)}-\text{subtractions}\right),\end{aligned}\tag{136}$$

where $E=\varepsilon_a-\omega$, $\mathbf{q}=\mathbf{p}_1-\mathbf{p}_2$, the subtractions are given by the replacement $G\to G-G^{(0)}-G^{(1)}=G^{(2+)}$, and

$$A^{an}_\mu(\omega,\mathbf{q})=\frac{4\pi}{\omega^2-\mathbf{q}^2+{\rm i}0}\int{\rm d}\mathbf{x}\,{\rm e}^{-{\rm i}\mathbf{q}\cdot\mathbf{x}}\,\psi_a^\dagger(\mathbf{x})\alpha_\mu\psi_n(\mathbf{x}).\tag{137}$$

The wave function in momentum space is defined as

$$\begin{aligned}\psi_a(\mathbf{p})&=\int{\rm d}^3\mathbf{x}\,{\rm e}^{-{\rm i}\mathbf{p}\cdot\mathbf{x}}\begin{pmatrix}g_a(x)\chi_{\kappa_a\mu_a}(\hat{\mathbf{x}})\\ {\rm i}\,f_a(x)\chi_{-\kappa_a\mu_a}(\hat{\mathbf{x}})\end{pmatrix}\\ &={\rm i}^{-l_a}\begin{pmatrix}g_a(p_r)\chi_{\kappa_a\mu_a}(\hat{\mathbf{p}})\\ f_a(p_r)\chi_{-\kappa_a\mu_a}(\hat{\mathbf{p}})\end{pmatrix},\end{aligned}\tag{138}$$

where $p_r=|\mathbf{p}|$, $l_a=|\kappa_a+1/2|-1/2$, and $\chi_{\kappa\mu}(\hat{\mathbf{x}})$ is the spin-angular spinor [39].

First, we integrate over the angular variables in equation (137). Since this part is written in coordinate space, the angular integration can be performed in a standard way. We make use of the following identities [40]:

$$\int{\rm d}\hat{\mathbf{x}}\,\chi^\dagger_{\kappa_b\mu_b}(\hat{\mathbf{x}})\,Y_{LM}(\hat{\mathbf{x}})\,\chi_{\kappa_a\mu_a}(\hat{\mathbf{x}})=s^{ba}_{LM}\,C_L(\kappa_b,\kappa_a),\tag{139}$$

$$\chi^\dagger_{\kappa_b\mu_b}(\hat{\mathbf{x}})\,\boldsymbol{\sigma}\chi_{\kappa_a\mu_a}(\hat{\mathbf{x}})=\sum_{JLM}s^{ab}_{JM}\,S_{JL}(\kappa_b,\kappa_a)\mathbf{Y}_{JLM}(\hat{\mathbf{x}})\,,\tag{140}$$

where $\boldsymbol{\sigma}$ denotes the vector incorporating Pauli matrices,

$$s^{ba}_{LM}=\frac{(-1)^{j_a-\mu_a}}{\sqrt{4\pi}}C^{LM}_{j_b\mu_b,j_a-\mu_a}\,,\tag{141}$$

Y_{LM} is the spherical harmonics, $\mathbf{Y}_{JLM}$ is the vector spherical harmonics [41],

$$\mathbf{Y}_{JLM}(\hat{\mathbf{x}})=\sum_{mq}C^{JM}_{Lm,1q}Y_{Lm}(\hat{\mathbf{x}})\,\mathbf{e}_q\,,\tag{142}$$

$C^{jm}_{j_1m_1,j_2m_2}$ is the Clebsh-Gordan coefficient, $\mathbf{e}_q$ are the spherical components of the unity vector, and the coefficients $C_L(\kappa_1,\kappa_2)$ and $S_{JL}(\kappa_1,\kappa_2)$ are given in Appendix C. The angular integration for $A_\mu=(A_0,\mathbf{A})$ in

$$\Delta E^R_{O,P} = -2\mathrm{i}\alpha^2 \int_{-\infty}^{\infty} \mathrm{d}\omega \int \frac{\mathrm{d}\mathbf{p}_1}{(2\pi)^3} \frac{\mathrm{d}\mathbf{p}_2}{(2\pi)^3} \frac{1}{\omega^2 - \mathbf{q}^2 + \mathrm{i}0} \left(\sum_{nJ} \frac{1}{E - \varepsilon_n(1-\mathrm{i}0)} \left\{ \mathrm{i}^{l_n - l_a - J} R^{1,an}_J(q_r) \left[\mathcal{F}^{na}_1 t_{l_n l_a} + \mathcal{F}^{na}_2 t_{\bar{l}_n \bar{l}_a} \right] \right.\right.$$
$$- \sum_L \mathrm{i}^{l_n - l_a - L + 1} R^{2,an}_{JL}(q_r) \left[\mathcal{R}^{na}_1 s_{l_n \bar{l}_a}(\boldsymbol{\sigma}) + \mathcal{R}^{na}_2 s_{\bar{l}_n l_a}(\boldsymbol{\sigma}) + p_{1r} \mathcal{R}^{na}_3 s_{l_n l_a}(\hat{\mathbf{p}}_1) + p_{2r} \mathcal{R}^{na}_4 s_{l_n l_a}(\hat{\mathbf{p}}_2) \right.$$
$$\left.\left. \left. + p_{1r} \mathcal{R}^{na}_5 s_{\bar{l}_n \bar{l}_a}(\hat{\mathbf{p}}_1) + p_{2r} \mathcal{R}^{na}_6 s_{\bar{l}_n \bar{l}_a}(\hat{\mathbf{p}}_2) \right] \right\} - \text{subtractions} \right) \quad (149)$$

$$\Delta E^R_{O,P} = -\frac{\mathrm{i}\alpha^2}{4\pi^4} \int_{-\infty}^{\infty} \mathrm{d}\omega \int_0^{\infty} \mathrm{d}p_{1r} \mathrm{d}p_{2r} \int_{-1}^{1} \mathrm{d}\xi \, \frac{p^2_{1r} p^2_{2r}}{\omega^2 - q^2_r + \mathrm{i}0} \left(\sum_{nJ} \frac{1}{E - \varepsilon_n(1-\mathrm{i}0)} \left\{ (-1)^{k_1} R^{1,an}_J(q_r) \left[\mathcal{F}^{na}_1 t_{l_n l_a} + \mathcal{F}^{na}_2 t_{\bar{l}_n \bar{l}_a} \right] \right.\right.$$
$$- \sum_L (-1)^{k_2} R^{2,an}_{JL}(q_r) \left[\mathcal{R}^{na}_1 s_{l_n \bar{l}_a}(\boldsymbol{\sigma}) + \mathcal{R}^{na}_2 s_{\bar{l}_n l_a}(\boldsymbol{\sigma}) + p_{1r} \mathcal{R}^{na}_3 s_{l_n l_a}(\hat{\mathbf{p}}_1) + p_{2r} \mathcal{R}^{na}_4 s_{l_n l_a}(\hat{\mathbf{p}}_2) \right.$$
$$\left.\left. \left. + p_{1r} \mathcal{R}^{na}_5 s_{\bar{l}_n \bar{l}_a}(\hat{\mathbf{p}}_1) + p_{2r} \mathcal{R}^{na}_6 s_{\bar{l}_n \bar{l}_a}(\hat{\mathbf{p}}_2) \right] \right\} - \text{subtractions} \right) \quad (152)$$

equation (137) yields:

$$A^{an}_0(\omega, \mathbf{q}) = \frac{16\pi^2}{\omega^2 - \mathbf{q}^2 + \mathrm{i}0} \sum_{JM} \mathrm{i}^{-J} s^{na}_{JM} Y_{JM}(\hat{\mathbf{q}}) R^{1,an}_J(q_r), \quad (143)$$

$$\mathbf{A}^{an}(\omega, \mathbf{q}) = \frac{16\pi^2}{\omega^2 - \mathbf{q}^2 + \mathrm{i}0} \sum_{JLM} \mathrm{i}^{1-L} \times s^{na}_{JM} \mathbf{Y}_{JLM}(\hat{\mathbf{q}}) R^{2,an}_{JL}(q_r), \quad (144)$$

with radial integrals defined as

$$R^{1,an}_J(q_r) = C_J(\kappa_n, \kappa_a) \int_0^{\infty} \mathrm{d}x \, x^2 j_J(q_r x) \times (g_a g_n + f_a f_n), \quad (145)$$

$$R^{2,an}_{JL}(q_r) = \int_0^{\infty} \mathrm{d}x \, x^2 j_L(q_r x) \Big[g_a f_n S_{JL}(\kappa_a, -\kappa_n) - f_a g_n S_{JL}(-\kappa_a, \kappa_n) \Big], \quad (146)$$

where $q_r = |\mathbf{q}|$, $g_a = g_a(x)$ and $f_a = f_a(x)$ are components of radial wave functions, and $j_l(z)$ is the spherical Bessel function.

Now we write the combination $\psi^\dagger_n(\mathbf{p}_1)\gamma^0 \times \Gamma^\mu_R(E, \mathbf{p}_1; \varepsilon_a, \mathbf{p}_2)\psi_a(\mathbf{p}_2)$ that enters equation (136) in a form convenient for carrying out the angular integration $\left[\Gamma^\mu_R = (\Gamma^0_R, \boldsymbol{\Gamma}_R)\right]$:

$$\psi^\dagger_n(\mathbf{p}_1)\gamma^0 \Gamma^0_R(E, \mathbf{p}_1; \varepsilon_a, \mathbf{p}_2)\psi_a(\mathbf{p}_2) = \frac{\alpha}{4\pi} \mathrm{i}^{l_n - l_a} \Big[\mathcal{F}^{na}_1 \chi^\dagger_{\kappa_n \mu_n}(\hat{\mathbf{p}}_1) \chi_{\kappa_a \mu_a}(\hat{\mathbf{p}}_2) + \mathcal{F}^{na}_2 \chi^\dagger_{-\kappa_n \mu_n}(\hat{\mathbf{p}}_1) \chi_{-\kappa_a \mu_a}(\hat{\mathbf{p}}_2) \Big], \quad (147)$$

$$\psi^\dagger_n(\mathbf{p}_1)\gamma^0 \boldsymbol{\Gamma}_R(E, \mathbf{p}_1; \varepsilon_a, \mathbf{p}_2)\psi_a(\mathbf{p}_2) = \frac{\alpha}{4\pi} \mathrm{i}^{l_n - l_a} \Big[\mathcal{R}^{na}_1 \chi^\dagger_{\kappa_n \mu_n}(\hat{\mathbf{p}}_1) \boldsymbol{\sigma} \chi_{-\kappa_a \mu_a}(\hat{\mathbf{p}}_2) + \mathcal{R}^{na}_2 \chi^\dagger_{-\kappa_n \mu_n}(\hat{\mathbf{p}}_1) \boldsymbol{\sigma} \chi_{\kappa_a \mu_a}(\hat{\mathbf{p}}_2) + (\mathcal{R}^{na}_3 \mathbf{p}_1 + \mathcal{R}^{na}_4 \mathbf{p}_2) \chi^\dagger_{\kappa_n \mu_n}(\hat{\mathbf{p}}_1) \chi_{\kappa_a \mu_a}(\hat{\mathbf{p}}_2) + (\mathcal{R}^{na}_5 \mathbf{p}_1 + \mathcal{R}^{na}_6 \mathbf{p}_2) \chi^\dagger_{-\kappa_n \mu_n}(\hat{\mathbf{p}}_1) \chi_{-\kappa_a \mu_a}(\hat{\mathbf{p}}_2) \Big]. \quad (148)$$

Explicit expressions for the functions $\mathcal{F}^{na}_i = \mathcal{F}^{na}_i(p_{1r}, p_{2r}, \xi)$ and $\mathcal{R}^{na}_i = \mathcal{R}^{na}_i(p_{1r}, p_{2r}, \xi)$ are given in Appendix A of [42] ($p_{1r} = |\mathbf{p}_1|$, $p_{2r} = |\mathbf{p}_2|$, and $\xi = \hat{\mathbf{p}}_1 \cdot \hat{\mathbf{p}}_2$).

Substituting equations (143), (144), (147), and (148) into equation (136), we obtain

see equation (149) above.

Here $l_i = |\kappa_i + 1/2| - 1/2$, $\bar{l}_i = |\kappa_i - 1/2| - 1/2$, and the angular factors $t_{l_1 l_2}$ and $s_{l_1 l_2}$ are defined by

$$t_{l_n l_a} = \frac{1}{2j_a + 1} \sum_{\mu_a \mu_n M} s^{na}_{JM} \chi^\dagger_{\kappa_n \mu_n}(\hat{\mathbf{p}}_1) Y_{JM}(\hat{\mathbf{q}}) \chi_{\kappa_a \mu_a}(\hat{\mathbf{p}}_2), \quad (150)$$

$$s_{l_n l_a}(\mathbf{r}) = \frac{1}{2j_a + 1} \sum_{\mu_a \mu_n M} s^{na}_{JM} \times \chi^\dagger_{\kappa_n \mu_n}(\hat{\mathbf{p}}_1) \mathbf{r} \cdot \mathbf{Y}_{JLM}(\hat{\mathbf{q}}) \chi_{\kappa_a \mu_a}(\hat{\mathbf{p}}_2), \quad (151)$$

where we have averaged over the magnetic substates of the initial state a. The angular factors with $\bar{l}_i$ instead of l_i are obtained by reversing the sign of κ_i. As can be shown by an explicit evaluation, the angular factors $t_{l_1 l_2}$ and $s_{l_1 l_2}$ depend on angles through $\xi = \hat{\mathbf{p}}_1 \cdot \hat{\mathbf{p}}_2$ only. Therefore, the integration over other angular variables in equation (149) can be carried out,

see equation (152) above,

where we have taken into account that due to angular selection rules the values of $J+l_a-l_n$ and $L+l_a-l_n-1$ should be even, $J+l_a-l_n=2k_1$ and $L+l_a-l_n-1=2k_2$.

The last remaining step is the explicit evaluation of the angular factors $t_{l_1 l_2}$ and $s_{l_1 l_2}$. Since expressions involved are rather lengthy, we do not present them here. An example of such derivation can be found in [42], where it is demonstrated for a particular case of $n=2p_{1/2}$ (compare Eq. (151) with Eqs. (79–82) of that work). We mention here that equation (B13) of Appendix B of [42] contains a misprint. The right-hand side of this equation should be multiplied by $(-1)^{l_2}$.

3.3 Numerical evaluation and results

In order to evaluate expressions given in the previous section numerically, we deform the contour of the ω integration in a way discussed for the first-order self-energy correction. From the analysis given for the M term it follows that the analytical continuation of the integrand is possible for both the nested and overlapping P contributions. An alternative proof of this fact is given in Appendices B and C of [23], where the analytical properties of the free self-energy and vertex functions are studied in momentum space. Expressions given in the previous section can be directly used for the numerical evaluation if we just substitute the ω integration over the real axis by the integration along the contour C_{LH}. An alternative way for their evaluation is the standard Wick rotation of the integration contour. As usual, this leads to the appearance of pole terms, which requires a more detailed analysis. For the corresponding expressions we refer the reader to our previous investigation [23]. Technical details of our numerical evaluation of the P term are also given in that paper. In this work, we discuss only the general features of this calculation. We note that our present treatment of IR divergences in the P term is different from that of our previous work [23]. The reason is that in the latter investigation we had to be compatible with the evaluation by Mallampalli and Sapirstein [21], since the results of two different calculations were to be added together.

An important feature of equations (129), (131), and (133) is that they contain the Dirac Coulomb Green function (DCGF) in the mixed momentum-coordinate representation [see Eqs. (115, 116)]. To develop an effective numerical scheme for the computation of DCGF in this representation is an important part of the evaluation of the P term. This problem has never been encountered before in calculations of radiative corrections. There are two main approaches to the computation of DCGF that have been employed up to now in calculations of QED effects, both using coordinate space. The first approach [27,43] employs the analytical representation of DCGF in terms of the Whittaker functions, whereas the other is based on various finite basis sets for the Dirac equation [44,45].

In momentum space, there is a representation of DCGF [46] that is based on the Sturmian expansion. However, it seems to be not very well suited for our purposes since the convergence of the Sturmian expansion becomes problematic for large values of the energy argument. This expansion proved to be a powerful tool for the evaluation of DCGF for real energies $\varepsilon < m$, especially for problems that can be solved analytically (see, *e.g.*, [47]). In the continuum part of the spectra $\varepsilon > m$, a resummation of the Sturmian expansion is needed [48]. To the best of our knowledge, the convergence of the Sturmian expansion for large complex values of ε has not been investigated so far.

Our numerical scheme for the evaluation of DCGF in the mixed momentum-coordinate representation is based on the finite basis set for the Dirac equation constructed with B splines [44]. This scheme was proposed and tested in our calculation of the LAL correction [18]. The B-spline method [44] for the Dirac equation provides a finite set of radial wave functions $\{\varphi^i_{\kappa,n}(x)\}_{n=1}^N$ and the corresponding set of energies $\{\varepsilon_{\kappa,n}\}_{n=1}^N$, where κ is the angular-momentum quantum number and the superscript $i=1,\,2$ indicates the upper and the lower component of the radial wave function, respectively. The radial wave functions are represented by linear combinations of the B splines [49],

$$\varphi^i_{\kappa,n}(x) = \frac{1}{x}\sum_m a^i(\kappa,n,m)\,B_m(x), \tag{153}$$

where $\{B_m(x)\}$ is the set of the B splines defined on the grid $\{x_l\}$ (see [44] for details). Since each of $B_m(x)$ is in fact a piecewise polynomial, we can write the corresponding piecewise-polynomial representation for the wave function,

$$\varphi^i_{\kappa,n}(x) = \frac{1}{x}\sum_k c^i_k(\kappa,n,l)\,(x-x_l)^k, \qquad x\in[x_l,x_{l+1}]\,. \tag{154}$$

Analogous representation can be written for radial components of DCGF, defined as

$$G^{ij}_\kappa(\varepsilon,x_1,x_2) = \sum_n \frac{\varphi^i_{\kappa,n}(x_1)\,\varphi^j_{\kappa,n}(x_2)}{\varepsilon-\varepsilon_{\kappa,n}}. \tag{155}$$

This representation reads

$$\begin{aligned} G^{ij}_\kappa(\varepsilon,x_1,x_2) = {}& \frac{1}{x_1x_2}\sum_{k_1k_2} A^{ij}_{k_1k_2}(\varepsilon,\kappa,l_1,l_2) \\ & \times (x_1-x_{l_1})^{k_1}(x_2-x_{l_2})^{k_2}, \\ & x_1\in[x_{l_1},x_{l_1+1}]\,,\ x_2\in[x_{l_2},x_{l_2+1}]\,, \end{aligned} \tag{156}$$

where the coefficients $A^{ij}_{k_1k_2}$ are given by

$$A^{ij}_{k_1k_2}(\varepsilon,\kappa,l_1,l_2) = \sum_n \frac{c^i_{k_1}(\kappa,n,l_1)\,c^j_{k_2}(\kappa,n,l_2)}{\varepsilon-\varepsilon_{\kappa,n}}. \tag{157}$$

The above expressions yield a piecewise-polynomial representation for the radial DCGF. It can be very convenient

for numerical evaluations. After the coefficients $A^{ij}_{k_1k_2}$ are stored for given values of κ and ε, the computation of the Green function is reduced to the evaluation of a simple polynomial over each of the radial variables. We note an additional advantage of this representation as compared to the closed analytical form for DCGF. The Green function in the form (156) and its derivatives are continuous functions of the radial arguments, while the exact analytical representation contains the discontinuous function $\theta(x_1 - x_2)$ (see Eqs. (103–105)). The main disadvantage of the piecewise-polynomial representation is the dependence of the final result on the number of the B splines in the set. For many problems this dependence can be kept well under control, but it often turns out to be the limiting factor for the accuracy of self-energy calculations. To our opinion, this rather poor convergence with respect to the size of the basis set is explained by the fact that a wide range of energies of intermediate states contributes significantly to the final result in this case.

The piecewise-polynomial representation turned out to be also convenient for a numerical Fourier transformation of DCGF over one or both radial variables. Taking the Fourier transform over the second radial argument as an example, we write the radial component of DCGF as

$$G^{ij}_\kappa(\varepsilon, x_1, p_2) = 4\pi s(L_j) \int_0^\infty \mathrm{d}x_2\, x_2^2 \times j_{L_j}(p_2 x_2)\, G^{ij}_\kappa(\varepsilon, x_1, x_2), \quad (158)$$

where $L_{1,2} = |\kappa \pm 1/2| - 1/2$, $s(L_1) = 1$, $s(L_2) = -\kappa/|\kappa|$, and $j_L(z)$ denotes the spherical Bessel function. Introducing the Fourier-transformed basic polynomials,

$$\Pi^{ik}_l(p) = 4\pi s(L_i) \int_{x_l}^{x_{l+1}} \mathrm{d}x\, x(x - x_l)^k\, j_{L_i}(px)\,, \quad (159)$$

we write the Green function in the mixed momentum-coordinate representation as

$$G^{ij}_\kappa(\varepsilon, x_1, p_2) = \frac{1}{x_1} \sum_{k_1} (x_1 - x_{l_1})^{k_1} \times \sum_{l_2 k_2} A^{ij}_{k_1 k_2}(\varepsilon, \kappa, l_1, l_2)\, \Pi^{jk_2}_{l_2}(p_2)\,,$$
$$x_1 \in [x_{l_1}, x_{l_1+1}]\,. \quad (160)$$

Certainly, the computation of DCGF in the mixed representation is essentially more time-consuming than that in coordinate space, due to necessity to evaluate the whole set of the integrals $\Pi^{jk_2}_{l_2}(p_2)$ for each new value of p_2. Still, in actual calculations we can perform the numerical integration over x_1 first, and the total time consumption of the numerical procedure can be kept reasonable.

For the calculation of the P term we need also to evaluate the free Green function $G^{(0)}$ and the one-potential Green function $G^{(1)}$ [Eq. (16)] in the momentum-coordinate representation. Whereas $G^{(0)}$ can be calculated along the same lines as DCGF by taking the limit $Z \to 0$, the one-potential Green function requires some care. Obviously, it can be evaluated according to its definition (16).

Table 2. Individual finite contributions to the P term expressed in terms of the function $F(Z\alpha)$ defined by equation (2).

Z	$\Delta E_{N1,P}$	$\Delta E_{N2,P}$	$2\,\Delta E_{O,P}$	P term
40	−8.97(8)	17.64(5)	−20.08(12)	−11.41(15)
50	−4.36(4)	8.44(3)	−9.49(6)	−5.41(8)
60	−2.46(2)	4.57(2)	−5.04(3)	−2.93(4)
70	−1.530(9)	2.688(9)	−2.915(22)	−1.757(25)
83	−0.869(4)	1.435(4)	−1.623(12)	−1.057(13)
92	−0.557(3)	0.921(3)	−1.176(9)	−0.812(10)
100	−0.306(2)	0.552(3)	−0.969(6)	−0.723(7)

However, this involves a double summation over the Dirac spectrum and is rather time consuming. We found that the one-potential Green function can be also evaluated by a direct numerical differentiation of the basis-set representation for DCGF,

$$G^{(1)}_\kappa(\varepsilon, x_1, x_2) = Z\, \frac{\mathrm{d}}{\mathrm{d}Z} G_\kappa(\varepsilon, x_1, x_2)\Big|_{Z=0} = Z\, \frac{G_\kappa(\varepsilon, x_1, x_2)[\epsilon] - G_\kappa(\varepsilon, x_1, x_2)[-\epsilon]}{2\epsilon} + O(Z\epsilon^2), \quad (161)$$

where G_κ denotes the radial DCGF and $G_\kappa[\epsilon]$ indicates that it should be evaluated for $Z = \epsilon$. So, in our calculations we store a set of coefficients $A^{ij}_{k_1k_2}$ for $G^{(1)}_\kappa$, each of which is obtained as a finite difference (161) of the corresponding coefficients of DCGF for $Z = \epsilon$ and $Z = -\epsilon$. After that the momentum-coordinate representation for $G^{(1)}$ is constructed along the same lines as for DCGF. For the further details of the numerical evaluation of the P term, we refer the reader to our previous investigation [23].

Our numerical results for finite contributions to the nested and overlapping P terms are presented in Table 2. The numerical uncertainties quoted in the table were estimated by investigating the sensitivity of the results with respect to the number of integration points, to the number of B splines in the basis set, and to the particular choice of the grid on which the B-spline set is generated. The number of B splines was varied between 45 and 75. Two types of radial-knots distributions were used in actual calculations, the exponential grid and a grid similar to the one proposed in [50]. The order of B splines was taken to be 5 or 6. The infinite summations over the angular-momentum quantum number κ of intermediate states was extended up to $|\kappa_{\max}| = 7$–9. The tail of the expansion was estimated by polynomial fitting in $1/|\kappa|$.

4 F term

The Feynman diagrams contributing to the F term are shown in Figure 6. We remind the reader that the corresponding mass counterterms are assumed to be subtracted from these graphs. The diagrams contain only

free-electron propagators and, therefore, they can be evaluated by using the standard Feynman-parametrization technique. In our investigation we regulate UV divergences by working in $D = 4 - 2\epsilon$ dimensions. A short summary of formulas needed for carrying out integrations over loop momenta in an arbitrary number of dimensions is given in Appendix D.

We note that in our evaluation of the F term we do not encounter any IR divergences. This is explained by the fact that the 4-momentum of the valence electron is off from the mass shell. In this case all would-be IR divergences are cut off by a nonzero virtuality of the valence electron, $\rho = (m^2 - p^2)/m^2 \sim (Z\alpha)^2$, where $p = (\varepsilon_a, \mathbf{p})$. (A different situation is encountered in calculations based on an expansion in the parameter $Z\alpha$, where the momentum of the incoming electron is often put to the mass shell.) However, some IR-divergent terms are known to appear in the Feynman gauge when the renormalization constants are extracted from the unrenormalized contributions in the standard way of free-electron QED (see, *e.g.*, [32]). Since this is the only source of IR divergences in our case, their appearance can be avoided by pulling out only the UV-divergent parts of the renormalization constants [21]. In this case no IR divergences appear at intermediate stages of the calculation.

All diagrams in Figure 6 except one contain the self-energy loop or the one-loop vertex as a subgraph. For the evaluation of these diagrams we should first obtain a convenient representation for the one-loop functions. Their detailed derivation is presented in Appendix A. It is clear that the proper choice of a representation for the one-loop functions is important and can significantly simplify the evaluation of two-loop diagrams. Specifically, since the self-energy function enters higher-order graphs in the combination

$$\frac{1}{\not p - m}\widetilde{\Sigma}^{(0)}(p)\frac{1}{\not p - m}\,,$$

it is useful to separate the factors $(\not p - m)^2$ and $(\not p - m)$ from $\widetilde{\Sigma}^{(0)}(p)$. Analogously, in the combination

$$\frac{1}{\not p_1 - m}\Gamma^{\mu}(p_1, p_2)\frac{1}{\not p_2 - m}$$

we pull out the factors $(\not p_1 - m)$ to the left and $(\not p_2 - m)$ to the right of the vertex function. It is worth mentioning that due to the presence of overlapping divergences in two-loop diagrams we have to keep the exact dependence on the dimensional parameter ϵ in the one-loop functions. The expansion in ϵ in two-loop functions can be carried out only after all integrations over the loop momenta are performed. This expansion yields divergent terms of order $1/\epsilon^2$ and $1/\epsilon$ that have to vanish in the final sum.

Finally, we make several remarks about our notations. The diagrams contributing to the F term are divided into the *zero-potential* and *one-potential* graphs, according to the number of interactions with the Coulomb field. They are labeled by the subscripts "zero" and "one", respectively. The contributions to the two-loop self-energy function are denoted by Σ, whereas ΔE stand for the contributions to the energy shift. The subscript R refers to the renormalized (*i.e.*, UV-finite) part of a contribution. For notational simplicity, we often omit the overall two-loop factor $\alpha^2 C_\epsilon^2/(16\pi^2)$ [the parameter C_ϵ is defined by Eq. (236)]. This fact will be indicated by a bar over the corresponding term.

4.1 Zero-potential term

We now discuss the evaluation of the free nested and overlapping diagrams. The corresponding contributions to the two-loop self-energy function are denoted by $\Sigma^{(2N)}_{\rm zero}$ and $\Sigma^{(2O)}_{\rm zero}$, respectively. The contributions to the energy shift ΔE_i are obtained from the corresponding parts of the self-energy function Σ_i by taking their expectation value with the wave function of the valence electron,

$$\Delta E_i = \int \frac{{\rm d}\mathbf{p}}{(2\pi)^3}\psi_a^\dagger(\mathbf{p})\gamma^0\widetilde{\Sigma}_i(p)\,\psi_a(\mathbf{p}), \tag{162}$$

where $\widetilde{\Sigma}_i = \Sigma_i - \delta m_i$, and $p = (\varepsilon_a, \mathbf{p})$. Taking into account that free contributions to the self-energy function can be expressed in the form $\widetilde{\Sigma}_i(p) = m\,a_i(\rho) + \not p\, b_i(\rho)$, the integration over the angular variables is easily carried out, which yields

$$\Delta E_i = \frac{1}{8\pi^3}\int_0^\infty {\rm d}p_r\, p_r^2\Big\{m\,a_i(\rho)(g_a^2 - f_a^2) + b_i(\rho)\big[\varepsilon_a(g_a^2 + f_a^2) + 2p_r g_a f_a\big]\Big\}, \tag{163}$$

where $p_r = |\mathbf{p}|$, $\rho = (m^2 - p^2)/m^2$, $p = (\varepsilon_a, \mathbf{p})$, and $g_a = g_a(p_r)$ and $f_a = f_a(p_r)$ denote the upper and lower radial components of $\psi_a(\mathbf{p})$, respectively.

4.1.1 Nested diagram

The free nested diagram yields one of the simplest contributions to the F term. However, we discuss its evaluation in detail here since it illustrates many essential features of the calculation of more difficult diagrams. The corresponding contribution to the two-loop self-energy function reads

$$\Sigma^{(2N)}_{\rm zero} = -4\pi{\rm i}\alpha\mu^{2\epsilon}\int\frac{{\rm d}^D k}{(2\pi)^D}\frac{1}{k^2}\gamma_\sigma\frac{1}{\not p - \not k - m} \times\Big[\Sigma_D^{(0)}(p-k) - \delta m^{(1)}\Big]\frac{1}{\not p - \not k - m}\gamma^\sigma, \tag{164}$$

where $\Sigma_D^{(0)}(p)$ is the one-loop self-energy function investigated in Appendix A, $\delta m^{(1)}$ is the corresponding mass counterterm, and μ is the mass parameter introduced in Appendix A.

First, we substitute the expression for the one-loop self-energy function (245) in the above equation and denote the contributions generated by the three parts of

equation (245) by Σ_1, Σ_2, and Σ_3, respectively. The first part is the simplest one. Obviously,

$$\Sigma_1(p) = -\frac{\alpha C_\epsilon}{4\pi}\frac{1}{\epsilon(1-2\epsilon)}\Sigma_D^{(0)}(p). \tag{165}$$

Substituting the explicit expression for the one-loop self-energy function and expanding in ϵ, we isolate a contribution to the mass counterterm (*i.e.*, the part that does not vanish when p is put on the mass shell) and a divergent part of the remainder,

$$\Sigma_1(p) = \delta m_1^{(2N)} + (\not{p} - m)B_1^{(2N)} - \frac{\alpha C_\epsilon^2}{4\pi\epsilon}\Sigma_{R,4}^{(0)}(p) + \Sigma_{1,R}(p), \tag{166}$$

with

$$\overline{\delta m}_1^{(2N)} = -\left(\frac{3}{\epsilon^2} + \frac{10}{\epsilon} + 28\right)m, \tag{167}$$

$$\overline{B}_1^{(2N)} = \frac{1}{\epsilon^2} + \frac{2}{\epsilon}, \tag{168}$$

$$\overline{\Sigma}_{1,R} = 12(\not{p} - m) - \int \mathrm{d}x\,\frac{\rho}{\Upsilon}\Big\{2\not{p} - 6m + [\not{p}(2-x) - 4m][2 - \ln(x\Upsilon)]\Big\}, \tag{169}$$

where $\Upsilon = x(1-\rho) + \rho$, $\Sigma_{R,4}^{(0)}$ is the renormalized self-energy function in 4 dimensions, and the bar over a contribution means that the corresponding term should be multiplied by the overall factor $\alpha^2 C_\epsilon^2/(16\pi^2)$. [Taking into account that $C_\epsilon = 1 + O(\epsilon)$ makes clear that finite contributions should be multiplied simply by $\alpha^2/(16\pi^2)$.] Here and in what follows we assume that all integrations over Feynman parameters extend from 0 to 1, if not stated otherwise.

The contribution Σ_2 is finite, and we can put $\epsilon = 0$ right from the beginning,

$$\overline{\Sigma}_2(p) = -2m^2\int \mathrm{d}x\,\frac{2+x}{1-x}\int\frac{\mathrm{d}^4k}{\mathrm{i}\pi^2} \times \frac{\gamma_\sigma(\not{p} - \not{k} + m)\gamma^\sigma}{k^2[(p-k)^2 - m^2][(p-k)^2 - m^2/(1-x)]}. \tag{170}$$

Joining the terms in the denominator and performing the integration over k, we have

$$\overline{\Sigma}_2(p) = \int \mathrm{d}x\,\mathrm{d}y\,\mathrm{d}z\,\frac{4(2+x)(2m - z\not{p})}{1 - xy - z(1-x)\,p^2/m^2}. \tag{171}$$

Now we separate the mass-counterterm part by putting $\not{p} = m$. The corresponding integrals can be evaluated analytically. Finally, we have

$$\overline{\Sigma}_2(p) = \overline{\delta m}_2^{(2N)} + \overline{\Sigma}_{2,R}(p), \tag{172}$$

$$\overline{\delta m}_2^{(2N)} = \left(\frac{16\pi^2}{3} - 8\right)m, \tag{173}$$

$$\overline{\Sigma}_{2,R}(p) = \int \mathrm{d}x\,\mathrm{d}y\,\mathrm{d}z\,\left[\frac{4(2+x)(2m - z\not{p})}{1 - xy - z(1-x)\,p^2/m^2} - \text{c.t.}\right], \tag{174}$$

where c.t. denotes the same contribution with the constraint $\not{p} = m$, $p^2 = m^2$.

The contribution Σ_3 is given by

$$\overline{\Sigma}_3(p) = \frac{m^{4\epsilon}}{\Gamma(1+\epsilon)(4\pi)^\epsilon}\int \mathrm{d}x\,\frac{x^{-\epsilon}}{[-(1-x)]^{1+\epsilon}} \times \frac{16\pi^2}{\mathrm{i}}\int\frac{\mathrm{d}^Dk}{(2\pi)^D}\frac{N(p-k)}{k^2[(p-k)^2 - m^2/(1-x)]^{1+\epsilon}}, \tag{175}$$

where the numerator N is

$$N(p-k) = \gamma_\sigma\left[2m\left(\frac{\epsilon}{1-2\epsilon} + x\right) - (\not{p} - \not{k})\left(\frac{2-2\epsilon}{1-2\epsilon} - x\right)\right]\gamma^\sigma. \tag{176}$$

Carrying out the integration over k, we have

$$\overline{\Sigma}_3(p) = -\frac{\Gamma(2\epsilon)}{[\Gamma(1+\epsilon)]^2}\int \mathrm{d}x\,\mathrm{d}z\,x^{-\epsilon}(1-z)^{-\epsilon} \times (1-x)^{-1+\epsilon}\frac{N(zp)}{[1 - z(1-x)\,p^2/m^2]^{2\epsilon}}. \tag{177}$$

This expression has UV divergences both explicitly in the gamma function and implicitly in the x integration, due to the singular factor $(1-x)^{-1+\epsilon}$. In order to isolate the implicit divergence, we rewrite the denominator as follows, employing equation (284):

$$\frac{1}{[1 - z(1-x)\,p^2/m^2]^{2\epsilon}} = 1 + \left(\frac{1}{[1 - z(1-x)\,p^2/m^2]^{2\epsilon}} - 1\right) = 1 + 2\epsilon\int \mathrm{d}u\,\frac{z(1-x)\,p^2/m^2}{[1 - z(1-x)\,p^2/m^2]^{1+2\epsilon}}. \tag{178}$$

We denote the contributions to $\overline{\Sigma}_3$ induced by the first and the second term of equation (178) by $\overline{\Sigma}_{3a}$ and $\overline{\Sigma}_{3b}$, respectively. Due to the appearance of additional factors of ϵ and $(1-x)$ in the second term of equation (178), the contribution $\overline{\Sigma}_{3b}$ is finite when $\epsilon \to 0$. Therefore, we have

$$\overline{\Sigma}_{3b}(p) = -p^2\int \mathrm{d}x\,\mathrm{d}z\,\mathrm{d}u\,\frac{z[8mx + 2z(2-x)\not{p}]}{m^2 - zu(1-x)\,p^2}. \tag{179}$$

The mass-counterterm part of this expressions is

$$\overline{\delta m}_{3b}^{(2N)} = \frac{291 - 34\pi^2}{12}m\,. \tag{180}$$

In order to evaluate $\overline{\Sigma}_{3a}$, we represent the numerator $N(zp)$ in the form $N(zp) = N_0 + (1-x)N_1$, where N_0 and N_1 are independent of x. The integrals over x can then be evaluated analytically,

$$\int \mathrm{d}x\,x^{-\epsilon}(1-x)^{\epsilon-1} = \Gamma(1-\epsilon)\Gamma(\epsilon), \tag{181}$$

$$\int \mathrm{d}x\,x^{-\epsilon}(1-x)^{\epsilon} = \Gamma(1-\epsilon)\Gamma(1+\epsilon). \tag{182}$$

Finally, the expression for $\overline{\Sigma}_{3a}$ is expanded in ϵ, and the remaining integration over z is trivial. Separating the mass-counterterm contribution and the divergent part of the remainder, we have

$$\overline{\Sigma}_{3a}(p) = \overline{\delta m}_{3a}^{(2N)} + (\not{p} - m)\overline{B}_{3a}^{(2N)} + \overline{\Sigma}_{3a,R}(p), \quad (183)$$

where

$$\overline{\delta m}_{3a}^{(2N)} = -\left(\frac{9}{2\epsilon^2} + \frac{15}{4\epsilon} + \frac{103+12\pi^2}{8}\right) m, \quad (184)$$

$$\overline{B}_{3a}^{(2N)} = -\frac{1}{2\epsilon^2} - \frac{7}{4\epsilon}, \quad (185)$$

$$\overline{\Sigma}_{3a,R}(p) = -\frac{69+4\pi^2}{24}(\not{p} - m). \quad (186)$$

Collecting all contributions to $\Sigma_{\rm zero}^{(2N)}$, we have

$$\Sigma_{\rm zero}^{(2N)}(p) = \delta m^{(2N)} + (\not{p} - m)B^{(2N)} - \frac{\alpha C_\epsilon^2}{4\pi\epsilon}\Sigma_{R,4}^{(0)}(p) + \Sigma_{{\rm zero},R}^{(2N)}(p)\,, \quad (187)$$

where

$$\delta m^{(2N)} = -\frac{\alpha^2 C_\epsilon^2}{16\pi^2}\, m \left(\frac{15}{2\epsilon^2} + \frac{55}{4\epsilon} + \frac{197-8\pi^2}{8}\right), \quad (188)$$

$$B^{(2N)} = \frac{\alpha^2 C_\epsilon^2}{16\pi^2}\left(\frac{1}{2\epsilon^2} + \frac{1}{4\epsilon}\right), \quad (189)$$

and

$$\Sigma_{{\rm zero},R}^{(2N)}(p) = \Sigma_{1,R}(p) + \Sigma_{2,R}(p) + \Sigma_{3a,R}(p) + \Sigma_{3b,R}(p). \quad (190)$$

4.1.2 Overlapping diagram

The contribution of the free overlapping diagram to the two-loop self-energy function reads

$$\Sigma_{\rm zero}^{(2O)}(p) = -4\pi{\rm i}\alpha\mu^{2\epsilon}\int\frac{{\rm d}^D k}{(2\pi)^D}\frac{1}{k^2} \times\gamma_\sigma\frac{1}{\not{p}-\not{k}-m}\Gamma_D^\sigma(p-k,p), \quad (191)$$

where $\Gamma_D^\sigma(p_1,p_2)$ is the one-loop vertex function investigated in Appendix A. A calculation similar to that for the nested diagram yields

$$\Sigma_{\rm zero}^{(2O)}(p) = \delta m^{(2O)} + (\not{p} - m)B^{(2O)} + \frac{\alpha C_\epsilon^2}{2\pi\epsilon}\Sigma_{R,4}^{(0)}(p) + \Sigma_{{\rm zero},R}^{(2O)}(p), \quad (192)$$

where

$$\delta m^{(2O)} = \frac{\alpha^2 C_\epsilon^2}{16\pi^2}\, m\left(\frac{3}{\epsilon^2} + \frac{5}{2\epsilon} + \eta\right), \quad (193)$$

$$B^{(2O)} = \frac{\alpha^2 C_\epsilon^2}{16\pi^2}\left(-\frac{1}{\epsilon^2} + \frac{1}{2\epsilon}\right), \quad (194)$$

where the constant η was evaluated numerically to be $\eta = -1.07561$.

Putting together (188) and (193) we obtain the gauge-invariant two-loop mass counterterm,

$$\delta m^{(2)} = \frac{\alpha^2 C_\epsilon^2}{16\pi^2}\, m\left(-\frac{9}{2\epsilon^2} - \frac{45}{4\epsilon} + \pi^2 - \frac{197}{8} + \eta\right). \quad (195)$$

This is in agreement with the known analytical result [51] that yields $12\zeta(3) + 24(1-2\ln 2)\zeta(2) - 1/4 = -1.07561\ldots$ for the constant η. We mention also studies of the two-loop mass counterterm within the Pauli-Willars regularization performed in [52,53].

The final result for the free two-loop self-energy function is given by the sum of the nested and overlapping contributions,

$$\Sigma_{\rm zero}^{(2)}(p) = \delta m^{(2)} + (\not{p} - m)B^{(2)} + \frac{\alpha C_\epsilon^2}{4\pi\epsilon}\Sigma_{R,4}^{(0)}(p) + \Sigma_{{\rm zero},R}^{(2)}(p)\,, \quad (196)$$

where the renormalization constant $B^{(2)}$ reads

$$B^{(2)} = \frac{\alpha^2 C_\epsilon^2}{16\pi^2}\left(-\frac{1}{2\epsilon^2} + \frac{3}{4\epsilon}\right), \quad (197)$$

and $\Sigma_{{\rm zero},R}^{(2)} = \Sigma_{{\rm zero},R}^{(2N)} + \Sigma_{{\rm zero},R}^{(2O)}$.

4.2 One-potential term

There are 4 nonequivalent one-potential two-loop diagrams which can be obtained from the free graphs by inserting the Coulomb interaction into electron propagators in all possible ways. When the Coulomb interaction is added to the central propagator we refer to the corresponding contribution as the *ladder* ("lad") term. Otherwise, it is denoted as the *side* contribution.

As we will show, one-potential contributions to the two-loop self-energy function can be written in the same form,

$$\Sigma_i(p_1,p_2) = \gamma^0 L_i^{(2)} + \frac{\alpha C_\epsilon^2}{4\pi\epsilon}\, a_i\, \Gamma_{R,4}^0(p_1,p_2) + \Sigma_{i,R}(p_1,p_2)\,, \quad (198)$$

where $L_i^{(2)}$ is a part of the renormalization constant, $\Gamma_{R,4}^0$ is the time component of the renormalized one-loop vertex function in 4 dimensions, and a_i is an integer factor. The corresponding contributions to the energy shift are obtained by

$$\Delta E_i = \int\frac{{\rm d}\mathbf{p}_1\,{\rm d}\mathbf{p}_2}{(2\pi)^6}\psi_a^\dagger(\mathbf{p}_1)V_C(\mathbf{q})\gamma^0\Sigma_i(p_1,p_2)\psi_a(\mathbf{p}_2)\,, \quad (199)$$

where V_C is the Coulomb potential, $V_C(\mathbf{q}) = -4\pi Z\alpha/\mathbf{q}^2$, $p_1 = (\varepsilon_a, \mathbf{p}_1)$, $p_2 = (\varepsilon_a, \mathbf{p}_2)$, $q = p_1 - p_2 = (0, \mathbf{p}_1 - \mathbf{p}_2)$.

One-potential contributions to the self-energy function Σ_i depend on two independent momenta, p_1 and p_2. Considering the matrix structure of Σ_i, we conclude that there are 8 possible independent basic elements: I, γ^0, $\not{p}_1$, $\not{p}_2$, $(\not{p}_1\gamma^0\not{p}_2)$, $(\not{p}_1\gamma^0)$, $(\gamma^0\not{p}_2)$, $(\not{p}_1\not{p}_2)$, (I is the unity

matrix). Denoting them by $\phi_1 \dots \phi_8$, we write the matrix structure of the self-energy function symbolically as $\Sigma_i(p_1,p_2) \equiv \Sigma_i(\phi_1,...,\phi_8)$. Next, we introduce the basic functions

$$\Phi_i = \frac{4\pi}{2j_a+1}\sum_{\mu_a}\psi_a^\dagger(\mathbf{p}_1)\,\gamma^0\phi_i\,\psi_a(\mathbf{p}_2), \tag{200}$$

where j_a and μ_a are the total angular momentum of the valence state and its projection. The functions Φ_i can be shown to depend on $p_{1r}=|\mathbf{p}_1|$, $p_{2r}=|\mathbf{p}_2|$, and $\xi=\hat{\mathbf{p}}_1\cdot\hat{\mathbf{p}}_2$ only. Then the angular integrations in equation (199) can be easily carried out, yielding

$$\Delta E_i = -\frac{Z\alpha}{8\pi^4}\int_0^\infty \mathrm{d}p_{1r}\,\mathrm{d}p_{2r}\int_{-1}^1 \mathrm{d}\xi\,\frac{p_{1r}^2p_{2r}^2}{q_r^2}\Sigma_i(\Phi_1,...,\Phi_8). \tag{201}$$

4.2.1 Overlapping ladder diagram

The overlapping ladder diagram is the only one from the set in Figure 6 that does not contain the one-loop self-energy loop or vertex as a subgraph. We consider the corresponding evaluation in some detail here since it contains all characteristic features of the general calculation.

We start from the basic expression for the overlapping ladder diagram,

$$\overline{\Sigma}^{(2O)}_{\mathrm{lad}}(p_1,p_2) = \frac{m^{2\epsilon}}{\Gamma(1+\epsilon)(4\pi)^\epsilon}\frac{16\pi^2}{\mathrm{i}}\int\frac{\mathrm{d}^Dk}{(2\pi)^D} \times\frac{1}{k^2}\gamma_\sigma\frac{1}{\not p_1-\not k-m}\Omega^\sigma(p_1,k,p_2), \tag{202}$$

where we again omitted the overall two-loop factor, and

$$\Omega^\sigma(p_1,k,p_2) = \frac{m^{2\epsilon}}{\Gamma(1+\epsilon)(4\pi)^\epsilon}\frac{16\pi^2}{\mathrm{i}}\int\frac{\mathrm{d}^Dl}{(2\pi)^D}\frac{1}{l^2} \times\gamma_\alpha\frac{1}{\not p_1-\not k-\not l-m}\gamma^0\frac{1}{\not p_2-\not k-\not l-m} \times\gamma^\sigma\frac{1}{\not p_2-\not l-m}\gamma^\alpha. \tag{203}$$

First, we evaluate the one-loop function Ω^σ. Joining the terms in the denominator, we have

$$\frac{1}{l^2[(p_1-k-l)^2-m^2][(p_2-k-l)^2-m^2][(p_2-l)^2-m^2]} = 6\int \mathrm{d}s\,\mathrm{d}t\,\mathrm{d}r\,\frac{s^2t}{[(l-s\zeta)^2-s\Delta]^4}, \tag{204}$$

where $\zeta=\eta-uk$, $\eta=(1-t)p_1+tp_2$, $\Delta=-uw(k^2-2k\xi-M)$, $\xi=(1-t)/u\,p_1+t(w-r)/(uw)\,p_2$, $M=[s\eta^2+m^2-(1-t)p_1^2-tp_2^2]/(uw)$, $u=1-tr$, and $w=1-su$.

Denoting the numerator in (203) as $N^\sigma(k,l)$,

$$N^\sigma(k,l) = \gamma_\alpha(\not p_1-\not k-\not l+m)\gamma^0(\not p_2-\not k-\not l+m) \times\gamma^\sigma(\not p_2-\not l+m)\gamma^\alpha, \tag{205}$$

and shifting the momentum variable $l\to l+s\zeta$, we have

$$\Omega^\sigma(p_1,k,p_2) = \frac{6m^{2\epsilon}}{\Gamma(1+\epsilon)(4\pi)^\epsilon}\int \mathrm{d}s\,\mathrm{d}t\,\mathrm{d}r\,s^2t \times\frac{16\pi^2}{\mathrm{i}}\int\frac{\mathrm{d}^Dl}{(2\pi)^D}\frac{N^\sigma(k,l+s\zeta)}{(l^2-s\Delta)^4}. \tag{206}$$

Now we write the numerator N in the form

$$N^\sigma(k,l+s\zeta) = N_0^\sigma + N_1^{\sigma\mu}l_\mu + N_2^{\sigma\mu\nu}l_\mu l_\nu + N_3^{\sigma\mu\nu\rho}l_\mu l_\nu l_\rho, \tag{207}$$

and carry out the momentum integration:

$$\Omega^\sigma(p_1,k,p_2) = m^{2\epsilon}\int \mathrm{d}s\,\mathrm{d}t\,\mathrm{d}r\,s^{-\epsilon}t \times\left[\frac{(1+\epsilon)N_0^\sigma}{\Delta^{2+\epsilon}}-\frac{sN_2^\sigma}{2\Delta^{1+\epsilon}}\right], \tag{208}$$

where $N_2^\sigma = N_2^{\sigma\mu\nu}g_{\mu\nu}$. Both parts of (208) induce divergent contributions to the self-energy function. In actual calculations, it is convenient to isolate the divergent part and evaluate the remainder in 4 dimensions. We consider here the contribution of the second part of (208) to the self-energy function (202) and denote it Σ_2. It reads

$$\overline{\Sigma}_2(p_1,p_2) = -\frac{m^{4\epsilon}}{2\Gamma(1+\epsilon)(4\pi)^\epsilon}\int \mathrm{d}s\,\mathrm{d}t\,\mathrm{d}r \times\frac{s^{1-\epsilon}t}{(-uw)^{1+\epsilon}}\frac{16\pi^2}{\mathrm{i}}\int\frac{\mathrm{d}^Dk}{(2\pi)^D} \times\frac{\gamma_\sigma(\not p_1-\not k+m)N_2^\sigma}{k^2[(p_1-k)^2-m^2][k^2-2k\xi-M]^{1+\epsilon}}\,. \tag{209}$$

The parametrization of the denominator yields

$$\frac{1}{k^2[(p_1-k)^2-m^2][k^2-2k\xi-M]^{1+\epsilon}} = (1+\epsilon)(2+\epsilon)\int \mathrm{d}x\,\mathrm{d}y\,\frac{x(xy)^\epsilon}{[(k-x\varrho)^2-x\mathcal{D}]^{3+\epsilon}}, \tag{210}$$

where $\varrho=(1-y)p_1+y\xi$, $\mathcal{D}=x\varrho^2+(1-y)(m^2-p_1^2)+yM$. Denoting the numerator in (209) by $\mathcal{M}(k)$, shifting the momentum variable $k\to k+x\varrho$, representing $\mathcal{M}(k+x\varrho)$ as $\mathcal{M}(k+x\varrho)=\mathcal{M}_0+\mathcal{M}_1^\mu k_\mu+\mathcal{M}_2^{\mu\nu}k_\mu k_\nu$, and integrating over momentum, we have

$$\overline{\Sigma}_2(p_1,p_2) = \frac{m^{4\epsilon}\Gamma(1+2\epsilon)}{[\Gamma(1+\epsilon)]^2}\int \mathrm{d}s\,\mathrm{d}t\,\mathrm{d}r\,\mathrm{d}x\,\mathrm{d}y\,\frac{st}{uw} \times\left(\frac{y}{xsuw}\right)^\epsilon\left[-\frac{\mathcal{M}_0}{2\mathcal{D}^{1+2\epsilon}}+\frac{x\mathcal{M}_2}{8\epsilon\,\mathcal{D}^{2\epsilon}}\right], \tag{211}$$

where $\mathcal{M}_2=\mathcal{M}_2^{\mu\nu}g_{\mu\nu}$. Expanding the result in ϵ and omitting terms of order ϵ and higher, we obtain

$$\overline{\Sigma}_2(p_1,p_2) = -\frac{\gamma^0}{\epsilon}+\frac{7\gamma^0}{2}+\int \mathrm{d}s\,\mathrm{d}t\,\mathrm{d}r\,\mathrm{d}x\,\mathrm{d}y\,\frac{st}{uw} \times\left[8x(2-3w)\gamma^0\ln\mathcal{D}-\frac{\mathcal{M}_0}{2\mathcal{D}}\right]. \tag{212}$$

Table 3. Contributions to the renormalization constant $L^{(2)}$ and to the overall factor a originating from the one-potential two-loop diagrams, as defined by equation (198).

	$\overline{L}^{(2)}$	a
$\Sigma^{2N}_{\rm lad}$	$1/(2\epsilon^2)+5/(4\epsilon)$	1
$\Sigma^{2N}_{\rm side}$	$-1/\epsilon^2-3/(2\epsilon)$	-2
$\Sigma^{2O}_{\rm lad}$	$-2/\epsilon$	0
$\Sigma^{2O}_{\rm side}$	$1/\epsilon^2+3/(2\epsilon)$	2
Total	$1/(2\epsilon^2)-3/(4\epsilon)$	1

Since the numerator $\mathcal{M}_0$ is a polynomial in x, the x integration can be carried out analytically. After that equation (212) is expressed in terms of elementary integrals I_i, L_1:

$$I_i \equiv \int \mathrm{d}x\, \frac{x^i}{\varrho^2 x + Y}, \tag{213}$$

$$L_1 \equiv \int \mathrm{d}x\, x\, \ln[\varrho^2 x + Y], \tag{214}$$

where $Y = (1-y)(m^2-p_1^2)+yM$. Four remaining parametric integrations were evaluated numerically.

The contribution induced by the first term in (208) is calculated in a similar way. The most difficult part of the evaluation is to keep control over numerators. While the corresponding manipulations are simple, the expressions involved are very lengthy. In this part of the calculation, the technical computing system MATHEMATICA [54] was a great help. Also evaluating other one-potential diagrams, most part of manipulations with numerators and expansions in ϵ were carried out by employing the MATHEMATICA system.

Finally, the overlapping ladder contribution to the self-energy function is written in the standard form (198). The corresponding results for $L_i^{(2)}$ and a_i are listed in Table 3.

4.2.2 Other one-potential diagrams

General expressions for the remaining one-potential contributions to the self-energy function are given by

$$\Sigma^{(2O)}_{\rm side}(p_1,p_2) = -8\pi\mathrm{i}\alpha\mu^{2\epsilon}\int\frac{\mathrm{d}^D k}{(2\pi)^D}\frac{1}{k^2}\gamma_\sigma\frac{1}{\not p_1-\not k-m} \times\gamma^0\frac{1}{\not p_2-\not k-m}\Gamma^\sigma_D(p_2-k,p_2), \tag{215}$$

$$\Sigma^{(2N)}_{\rm lad}(p_1,p_2) = -4\pi\mathrm{i}\alpha\mu^{2\epsilon}\int\frac{\mathrm{d}^D k}{(2\pi)^D}\frac{1}{k^2}\gamma_\sigma\frac{1}{\not p_1-\not k-m} \times\Gamma^0_D(p_1-k,p_2-k)\frac{1}{\not p_2-\not k-m}\gamma^\sigma, \tag{216}$$

$$\Sigma^{(2N)}_{\rm side}(p_1,p_2) = -8\pi\mathrm{i}\alpha\mu^{2\epsilon}\int\frac{\mathrm{d}^D k}{(2\pi)^D}\frac{1}{k^2}\gamma_\sigma\frac{1}{\not p_1-\not k-m} \times\Big[\Sigma^{(0)}_D(p_1-k)-\delta m^{(1)}\Big] \times\frac{1}{\not p_1-\not k-m}\gamma^0\frac{1}{\not p_2-\not k-m}\gamma^\sigma, \tag{217}$$

where an overall factor of 2 is included in the side contributions, accounting for two equivalent diagrams. After the separation of divergent terms, these contributions are written in the form (198), with the results for $L_i^{(2)}$ and a_i summarized in Table 3.

According to Table 3, the total one-potential part of the two-loop self-energy function reads

$$\Sigma^{(2)}_{\rm one}(p_1,p_2) = \gamma^0 L^{(2)} + \frac{\alpha C_\epsilon^2}{4\pi\epsilon}\,\Gamma^0_{R,4}(p_1,p_2) + \Sigma^{(2)}_{{\rm one},R}(p_1,p_2)\,, \tag{218}$$

where

$$L^{(2)} = \frac{\alpha^2 C_\epsilon^2}{16\pi^2}\left(\frac{1}{2\epsilon^2}-\frac{3}{4\epsilon}\right). \tag{219}$$

We note that $L^{(2)} = -B^{(2)}$, as required by the Ward identity.

4.3 The total F term

As illustrated in Figure 6, the F term consists of the zero-potential, the one-potential and the free reducible contribution,

$$\Delta E_F = \Delta E^{(2)}_{\rm zero} + \Delta E^{(2)}_{\rm one} + \Delta E^{\rm zero}_{\rm red}\,. \tag{220}$$

The free reducible contribution is given by

$$\Delta E^{\rm zero}_{\rm red} = \Delta E_{{\rm SE},D}\,\langle a|\,\frac{\partial}{\partial p^0}\Sigma^{(0)}_D(p)\Big|_{p^0=\varepsilon_a}|a\rangle\,, \tag{221}$$

where $\Delta E_{{\rm SE},D}$ is the one-loop self-energy correction calculated in D dimensions. We remind the reader that $\Delta E_{{\rm SE},D}$ is represented by the sum [Eq. (12)] of the free, one-potential, and many-potential contributions,

$$\Delta E_{{\rm SE},D} = \Delta E^{\rm zero}_{{\rm SE},D} + \Delta E^{\rm one}_{{\rm SE},D} + \Delta E^{\rm many}_{{\rm SE},D}\,, \tag{222}$$

where we introduced the subscript D in order to indicate that in all these contributions the loop integrals are evaluated in D dimensions.

Expanding the one-loop functions in terms of ϵ according to (248) and (256), we have for the corresponding contributions to the energy shift

$$\Delta E^{\rm zero}_{{\rm SE},D} = C_\epsilon\left[\Delta E^{\rm zero}_{\rm SE} + \epsilon\,\Delta E^{\rm zero}_{{\rm SE},\epsilon} + O(\epsilon^2)\right]\,, \tag{223}$$

$$\Delta E^{\rm one}_{{\rm SE},D} = C_\epsilon\left[\Delta E^{\rm one}_{\rm SE} + \epsilon\,\Delta E^{\rm one}_{{\rm SE},\epsilon} + O(\epsilon^2)\right]\,. \tag{224}$$

Now expanding equation (221) in ϵ and disregarding terms of order ϵ and higher, we get the following expression for the free reducible contribution,

$$\Delta E^{\rm zero}_{\rm red} = -\frac{\alpha C_\epsilon^2}{4\pi\epsilon}\,(\Delta E^{\rm zero}_{\rm SE} + \Delta E^{\rm one}_{\rm SE}) + B^{(1)}\,\Delta E^{\rm many}_{{\rm SE},D} + \Delta E^{\rm zero}_{{\rm red},R}, \tag{225}$$

Table 4. Individual finite contributions to the F term expressed in terms of the function $F(Z\alpha)$ defined by equation (2). The results of our numerical evaluation are compared with those of [21]. Since the numerical errors were not explicitly indicated in [21], we assume them to be one last significant digit.

Z	$\Delta E^{(2)}_{\rm zero}$	$\Delta E^{(2)}_{\rm one}$	$\Delta E^{\rm zero}_{\rm red}$	F term	Ref. [21]
10	621.5(9)	−328.3(3)	528.31	821.5(9)	975(3)
20	79.21(2)	−42.08(2)	99.755	136.89(3)	
30	24.668(2)	−16.085(5)	36.1389	44.723(5)	
40	11.615(1)	−9.243(2)	17.1316	19.504(2)	
50	6.877(2)	−6.277(1)	9.4243	10.025(2)	10.018(6)
60	4.663(1)	−4.649(1)	5.7090	5.723(1)	
70	3.4457(4)	−3.6600(5)	3.7109	3.4966(6)	
83	2.5474(1)	−2.9230(2)	2.3134	1.9378(2)	1.9368(7)
92	2.1831(1)	−2.6767(2)	1.7691	1.2755(2)	1.2743(5)
100	1.9937(1)	−2.6353(5)	1.4667	0.8251(5)	0.8245(3)

Table 5. Various contributions to the F term for $Z = 92$. Units are a.u.

$\Delta E^{(2N)}_{{\rm zero},R}$	$\Delta E^{(2O)}_{{\rm zero},R}$	$\Delta E^{(2N)}_{{\rm lad},R}$	$\Delta E^{(2N)}_{{\rm side},R}$	$\Delta E^{(2O)}_{{\rm lad},R}$	$\Delta E^{(2O)}_{{\rm side},R}$	$\Delta E^{\rm zero}_{{\rm red},R}$	Total	Ref. [21]
0.002 48	0.042 45	−0.005 88	0.010 32	−0.035 99	−0.023 55	0.036 42	0.026 26	0.026 23

where the renormalized part of the contribution is given by

$$\Delta E^{\rm zero}_{{\rm red},R} = -\frac{\alpha}{4\pi}\left(\Delta E^{\rm zero}_{{\rm SE},\epsilon} + \Delta E^{\rm one}_{{\rm SE},\epsilon}\right) + \Delta E_{\rm SE}\,\langle a|\,\frac{\partial}{\partial p^0}\Sigma^{(0)}_{R,4}(p)\Big|_{p^0=\varepsilon_a}|a\rangle\,, \quad (226)$$

where $\Delta E_{\rm SE} = \Delta E_{{\rm SE},D=4}$.

Finally, adding together the contributions to the energy shift originating from the zero-potential part of the self-energy function (196), from the one-potential part (218), and from the reducible part (225), we get the total result for the F term,

$$\Delta E_F = B^{(1)}\,\Delta E^{\rm many}_{{\rm SE},D} + \Delta E^{(2)}_{{\rm zero},R} + \Delta E^{(2)}_{{\rm one},R} + \Delta E^{\rm zero}_{{\rm red},R}, \quad (227)$$

where we have taken into account the Dirac equation and the Ward identity. We see that the total F term is still UV divergent. The divergent contributions vanishes only when it is considered together with the P term [Eq. (134)].

We now discuss briefly the numerical calculation of the F term. Whereas the free part is relatively simple, the evaluation of one-potential contributions requires some care since it involves a 3-dimensional integration over the momentum variables and up to 4 Feynman-parameter integrations. The numerical evaluation of equation (201) was carried out after the change of variables [26]: $\{p_{1r}, p_{2r}, \xi\} \to \{x, y, q_r\}$, where $x = p_{1r} + p_{2r}$, $y = |p_{1r} - p_{2r}|$, $q_r^2 = p_{1r}^2 + p_{2r}^2 - 2p_{1r}p_{2r}\xi$. This yields

$$\int_0^\infty {\rm d}p_{1r}\,{\rm d}p_{2r}\int_{-1}^{1}{\rm d}\xi\,F(p_{1r},p_{2r},\xi) = \int_0^\infty {\rm d}x\int_0^x {\rm d}y\int_y^x {\rm d}q_r\,\frac{q_r}{2p_{1r}p_{2r}} \times\Big[F(p_{1r},p_{2r},\xi)+F(p_{2r},p_{1r},\xi)\Big]. \quad (228)$$

All integrations were carried out by using the Gauss-Legendre integration formulas. A typical integrand is a combination of basic integrals like (213), (214) that are easily expressed in terms of elementary functions. Taking I_2 as an example, we have

$$I_2 = \frac{1}{2\varrho^2} - \frac{Y}{\varrho^4} + \frac{Y^2}{\varrho^6}\ln\left(1+\frac{\varrho^2}{Y}\right). \quad (229)$$

It should be mentioned that ϱ vanishes for certain combinations of integration variables. The whole integral I_2 stays finite for $\varrho = 0$, as can be seen from its definition (213). However, individual parts of equation (229) are divergent when $\varrho \to 0$. This may lead to instabilities in the numerical calculation. In order to avoid them, we evaluate the basic integrals I_i by a series expansion when ϱ is small.

The results of our numerical evaluation of the F term are listed in Table 4. We see that our values agree well with the results of Mallampalli and Sapirstein [21] for all cases except $Z = 10$. Individual contributions to the F term for the H-like uranium are given in Table 5. Comparing our results with those of [21], one should keep in mind that the parameter C_ϵ^2 in our definition of the renormalization constants differs from the analogous parameter $D = (4\pi)^{2\epsilon}\Gamma(1+2\epsilon)$ in [21] by terms of order ϵ^2.

Table 6. Individual contributions to the two-loop self-energy correction expressed in terms of $F(Z\alpha)$. Our results for the LAL correction, the F and M terms are compared with the previous evaluations [15,16,21]. In order to allow the term-by-term comparison for the M term, the finite part of IR-divergent contributions is subtracted from the results of [21] (see the text and Tab. 1 for details).

Z	LAL	F term	P term	M term	Total
40	−0.871	19.50	−11.41(15)	−8.27(18)	−1.05(23)
50	−0.973	10.03	−5.41(8)	−4.99(6)	−1.34(10)
		10.02[a]			
60	−1.082	5.72	−2.93(4)	−3.342(21)	−1.63(4)
70	−1.216	3.497	−1.757(25)	−2.412(11)	−1.888(27)
	−1.216[b]				
	−1.216[c]				
83	−1.466	1.938	−1.057(13)	−1.764(4)	−2.349(14)
		1.937[a]		−2.435(11)[a]	
92	−1.734	1.276	−0.812(10)	−1.513(3)	−2.783(10)
	−1.733[b]	1.274[a]		−2.074(7)[a]	
	−1.734[c]				
100	−2.099	0.825	−0.723(7)	−1.384(3)	−3.381(8)
		0.825[a]			

[a] Reference [21]; [b] reference [16]; [c] reference [15].

5 Numerical results and Lamb shift in H-like ions

In Table 6 we collect all contributions to the two-loop self-energy correction for the ground state of H-like ions with $Z \geq 40$. As already mentioned, the LAL correction was previously evaluated by several groups, and our values agree well with the known results for this contribution. The F and M terms were previously calculated by Mallampalli and Sapirstein [21]. Our results for the F term are very close to those from [21]. However, a significant deviation is observed for the M term.

As in the case of the one-loop self-energy correction, the evaluation becomes problematic very fast as Z decreases. It is due in part to the fact that some individual contributions exhibit a nearly Z-independent behaviour, while the total correction scales as $(Z\alpha)^4$. Already for $Z = 40$, significant numerical cancellations occur that tend to increase very rapidly as Z decreases. In addition, numerical integrations become more difficult to control in the lower-Z region. All this restricted our calculation to the region $Z \geq 40$.

In Figure 7 we present our non-perturbative results together with predictions based on the $Z\alpha$ expansion. The solid line represents the contribution of the first two terms in equation (1), whereas the dashed line corresponds to the contribution of all known terms ($B_{40} \dots B_{61}$). We can see that the convergence of the $Z\alpha$ expansion is remarkably slow in this case. Although this comparison does not provide any information about the higher-order terms, it suggests that the results obtained by two different methods could be compatible. After the first results of our evaluation [24] had become known, it was shown by Jentschura [55] that the [2/2] Padé extrapolation applied

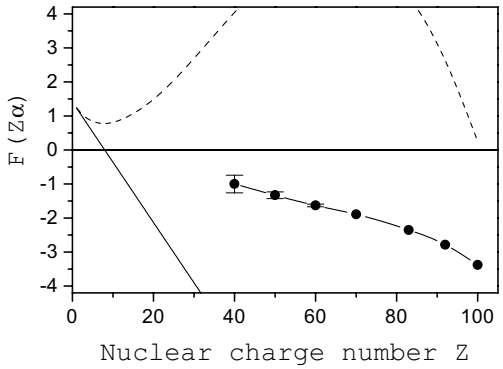

Fig. 7. The results of our numerical evaluation to all orders to $Z\alpha$ (dots) together with the first two terms of the $Z\alpha$ expansion (solid line) and all known terms of the $Z\alpha$ expansion (dashed line).

to the known terms of the $Z\alpha$ expansion agreed much better with our nonperturbative results than the plain sum of the these terms. Based on this extrapolation scheme, a tentative estimate for the higher-order term B_{60} was reported in that work, $B_{60} \approx -100(50)$.

In order to reach a definitive conclusion about the higher-order terms, it is important to extend the present calculation into the lower-Z region. Taking into account large numerical values of some of the known terms of the $Z\alpha$ expansion, one may speculate that the higher-order contribution could be of experimental interest even for hydrogen [11]. We believe that an extension of the present calculations to lower values of Z should be possible when the Fried-Yennie gauge is employed instead of the Feynman gauge. While increasing the complexity of the problem, one may hope that it will also remove a

Table 7. Two-loop QED contributions to the ground-state Lamb shift of H-like ions, in eV. The subsets SESE, VPVP, S(VP)E, and SEVP are introduced in Figure 8. Other labelling is as follows: VPVP(lad) indicates the diagram (d); VPVP(K-S) and VPVP(h.o.) refer to the diagrams (e, f), where (K-S) labels the Källén-Sabry part and (h.o.) stands for the higher-order contribution; SEVP(l.o) and SEVP(h.o.) denote the lowest-order and the higher-order part of the SEVP contributions, respectively.

Z	SESE	VPVP				S(VP)E	SEVP		Total
		(lad)	(K-S)	(h.o.)			(l.o.)	(h.o.)	
40	−0.021(5)	−0.001	−0.017		± 0.001	0.003	0.011	0.00	−0.025(5)
50	−0.065(5)	−0.003	−0.043		± 0.006	0.006(1)	0.034	0.00	−0.071(8)
54	−0.097(7)	−0.005	−0.059		± 0.009	0.009(1)	0.050	0.00	−0.102(11)
60	−0.165(4)	−0.010	−0.093		± 0.02	0.015(3)	0.085	0.00	−0.168(21)
70	−0.354(5)	−0.027	−0.185		± 0.05	0.030(8)	0.184	0.022	−0.330(51)
79	−0.666(8)	−0.065	−0.327	−0.01	± 0.11	0.056(19)	0.337	0.09	−0.59(11)
80	−0.713(8)	−0.071	−0.348	−0.01	± 0.12	0.060(20)	0.359	0.10	−0.62(12)
82	−0.816(8)	−0.086	−0.393	−0.017	± 0.14	0.070(25)	0.406	0.128	−0.71(14)
83	−0.872(5)	−0.095	−0.418	−0.02	± 0.15	0.075(28)	0.432	0.15	−0.75(15)
90	−1.369(8)	−0.181	−0.636	−0.03	± 0.27	0.118(51)	0.647	0.33	−1.12(27)
92	−1.559(6)	−0.217	−0.716	−0.038	± 0.32	0.134(60)	0.722	0.417	−1.26(33)
100	−2.643(6)	−0.446	−1.153		± 0.61	0.24(13)	1.096	1.0(1)	−1.91(63)

significant part of numerical cancellations between individual contributions, as it is the case for the LAL correction [18].

Turning to the experimental consequences of our evaluation, we mention that the two-loop self-energy correction provided the main uncertainty to theoretical predictions of the ground-state Lamb shift in heavy H-like ions. With our evaluation of this correction, we significantly improve the accuracy of the corresponding theoretical values. In Table 7 we compile the results available for the two-loop QED corrections to the ground-state energy of H-like ions. The complete set of these corrections is presented in Figure 8. It is traditionally divided into 4 gauge-invariant subsets: SESE (a–c), VPVP (d–f), SEVP (g–i), and S(VP)E (k). The calculation of the first subset SESE is carried out in the present investigation. The corresponding numerical values in Table 7 are obtained by interpolation of the results listed in Table 6. The other subsets in Figure 8 are easier to evaluate since all of them involve a vacuum-polarization loop that can be treated in the leading Uehling approximation with a reasonable accuracy. The ladder VPVP diagram (d) was evaluated to all orders in $(Z\alpha)$ in [56,57]. The values in the table are taken from the tabulation [57]. Two remaining VPVP diagrams (e) and (f) were calculated within the Uehling approximation in [58] for the point nucleus and in [59] for the extended nucleus. The Uehling part of this correction is often named after Källén and Sabry who first derived [60] the expression for the corresponding potential. In the table, the values from [59] were taken, with the corresponding entry labeled as VPVP(K-S). The corresponding higher-order contribution is presently calculated only for the diagram (e) [61]. While its numerical value was found to be rather small, one should keep in mind that the major contribution to the Källén-Sabry part comes from the diagram (f). We observe that for the diagram (e) the higher-order part contributes about one third of the value obtained within the Uehling approximation (for $Z = 92$ and 82). Taking this into account, we estimate the unknown higher-order part of the diagram (f) by multiplying the Källén-Sabry value by a factor of $(Z\alpha)^2$. Numerical results available for the higher-order part of the diagram (e) together with our estimations for the corresponding part of the diagram (f)

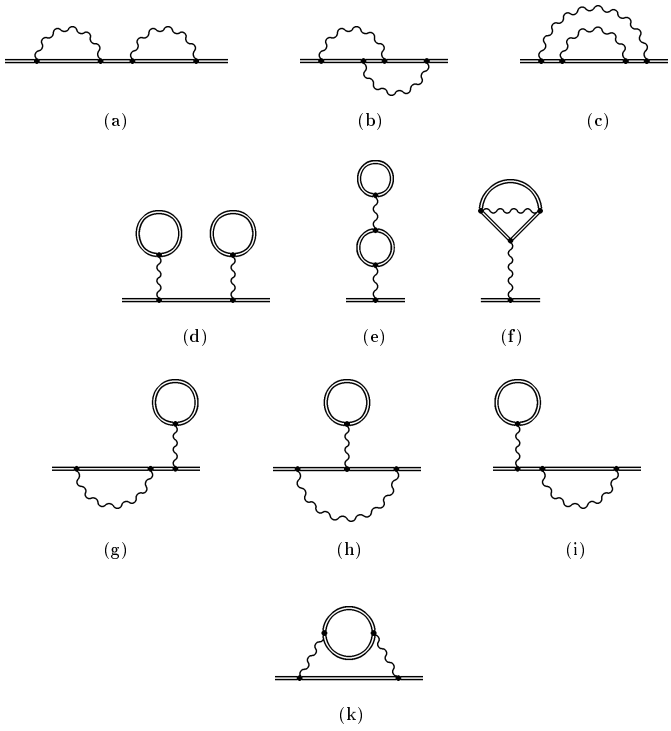

Fig. 8. One-electron QED corrections of second order in α. Gauge-invariant subsets are referred to as SESE (a–c), VPVP (d–f), SEVP (g–i), S(VP)E (k).

Table 8. The ground-state Lamb shift of H-like ions, in eV. In order to obtain the ground-state energy, one should add the Dirac-energy value $E_{\rm Dirac} = m\sqrt{1-(Z\alpha)^2}$. The labeling is as follows: "RMS" denotes the root-mean-square nuclear radii expressed in Fermi units, "Ext.Nuc." is the finite-nuclear-size effect, "SE" is the first-order self-energy correction, "Ueh" and "WK" are the Uehling and the Wichmann-Kroll parts of the first-order vacuum-polarization correction, respectively; "Two-loop" is the second-order QED correction, "Recoil" is the nuclear-recoil correction, "NP" is the nuclear-polarization correction, "Exp" indicates the experimental results.

Ion	RMS	Ext.Nuc.	SE	Ueh	WK	Two-loop	Recoil	NP	Total	Exp.
$^{90}_{40}$Zr	4.270	0.516(10)	18.394	−2.083	0.029	−0.025(5)	0.137		16.968(11)	
$^{120}_{50}$Sn	4.655	1.96(3)	39.198	−5.273	0.107	−0.071(8)	0.171		36.09(3)	
$^{132}_{54}$Xe	4.787	3.18(6)	50.997	−7.325	0.169	−0.102(11)	0.187		47.11(6)	54(10)[a]
$^{142}_{60}$Nd	4.914	6.25(11)	73.372	−11.606	0.319	−0.168(21)	0.215		68.38(11)	
$^{174}_{70}$Yb	5.317	19.57(33)	126.358	−23.399	0.825	−0.330(51)	0.269		123.29(33)	
$^{197}_{79}$Au	5.437	49.13(80)	196.684	−41.996	1.792(1)	−0.59(11)	0.33		205.36(81)	202(8)[b]
$^{202}_{80}$Hg	5.467(6)	54.67(13)	206.171	−44.729	1.942(1)	−0.62(12)	0.34		217.77(18)	
$^{208}_{82}$Pb	5.504(25)	67.23(51)	226.328	−50.701	2.284(1)	−0.71(14)	0.36	0.00	244.79(53)	
$^{209}_{83}$Bi	5.533(20)	74.79(44)	237.025	−53.956	2.476(1)	−0.75(15)	0.37		259.96(46)	
$^{232}_{90}$Th	5.802(4)	160.51(35)	325.016	−82.890	4.278(2)	−1.12(27)	0.44	−0.13(6)	406.10(45)	
$^{238}_{92}$U	5.860(2)	198.79(40)	355.046	−93.597	4.975(2)	−1.26(33)	0.46	−0.19(9)	464.22(53)	468(13)[c]
$^{257}_{100}$Fm	5.886	451(6)	503.487	−152.280	9.064(3)	−1.91(63)	0.61		810(6)	

[a] Reference [78]; [b] reference [79]; [c] reference [80].

are listed in the table under the entry VPVP(h.o.). Numerical values for Z other than 92 and 82 were obtained by a linear interpolation of available numerical results [61].

The SEVP correction is known to all orders in $Z\alpha$ for $Z = 70$, 82, and 92 [56]. For smaller values of Z, the lowest-order result for this correction [62] can be used,

$$\Delta E_{\rm SEVP} = m\left(\frac{\alpha}{\pi}\right)^2 (Z\alpha)^5\Big[1.920576 + O(Z\alpha)\Big]. \quad (230)$$

In the table, we separate the SEVP correction into the lowest-order ("l.o.") part given by the above formula, and the higher-order ("h.o.") contribution obtained from the results of [56]. The higher-order part scales as $(Z\alpha)^6$ and was estimated to contribute less than 0.01 eV for $Z \le 60$. For $Z > 60$, it was obtained by an interpolation of numerical results from [56].

Finally, the S(VP)E correction was evaluated within the Uehling approximation in [56,63]. The uncertainty due to the uncompleteness of the Uehling approximation was estimated in the same way as for the VPVP correction.

In Table 8 we collect all available contributions to the ground-state Lamb shift of high-Z H-like ions. First, we account for the finite-nuclear-size correction to the Dirac ground-state energy. This correction is easy to evaluate, but it is more difficult to provide a reliable estimate for its uncertainty. For most nuclei, experimental values are available for only their root-mean-square (rms) radii. Moreover, it is not completely clear what error bars should be ascribed to the existing experimental values. The nuclear rms radii used in the present compilation [64–67] are listed in the second column of Table 8. If not stated otherwise, we ascribe an uncertainty of 1% to them. For $Z = 80$, 82, 83, 90, and 92, the nuclear rms radii are considered to be known with higher precision. For uranium and thorium, we use the error estimate from the original studies [66,67]. For Hg, Pb, and Bi, the ascribed uncertainty corresponds to the deviation between different experimental values [64, 65]. The finite-nuclear-size correction was evaluated by using the two-parameter Fermi model for the nuclear-charge distribution

$$\rho(r) = \frac{N}{1+\exp\left[(r-c)/a\right]} \quad (231)$$

where the parameter a is fixed to be $a = 2.3/(4\ln 3)$ fm. The parameters c and N are obtained from the rms-radius by

$$c = \left[\frac{5}{3}\langle r^2\rangle - \frac{7}{3}a^2\pi^2\right]^{1/2}, \quad (232)$$

$$N = \frac{3}{4\pi c^3}\left(1+\frac{\pi^2 a^2}{c^2}\right)^{-1}. \quad (233)$$

The uncertainties ascribed to the nuclear-size corrections consist of two parts. The first one was obtained by varying the rms radii within the limits discussed above. The second one represents the dependence of the result on the model of the nuclear-charge distribution. It was estimated by taking the difference between the result obtained for the Fermi distribution and that for the homogeneously-charged sphere distribution with the same rms radius.

The first-order self-energy correction was taken from the recent tabulation in [68], which is based on the methods described in [27,69]. The results for the Uehling part of the first-order vacuum-polarization correction are taken from [70], where it was calculated using the Fermi model for the nuclear-charge distribution. A small deviation from the results of [72] is explained by a more realistic nuclear model employed in [70]. The Wichmann-Kroll part of the vacuum-polarization correction was taken from the tabulation in [68], which was obtained by the method developed in [71]. We mention a small (0.01 eV for $Z = 92$)

deviation between the results of [68,71] and the ones of the Swedish group [72]. A larger number of partial waves was accounted for in [72], but numerical values were presented only for a few ions.

The nuclear-recoil correction was calculated to first order in m/M and to all orders in $Z\alpha$ in [73] for the point nucleus and in [74] for the extended nucleus. The numerical values in the table are taken from [74]. Finally, the nuclear-polarization correction was evaluated in [75,76] for a few ions only, namely, uranium, thorium, and lead. For lead, these results were recently reproduced by an independent evaluation [77]. Since a number of experimental parameters and assumptions about nuclear models enters calculations of this type, the results obtained are considered to be an estimate only. We therefore ascribe to them an uncertainty of about 50%.

6 Conclusion and outlook

We have presented an evaluation of the complete gauge-invariant set of the two-loop self-energy diagrams for the ground-state of H-like ions with $Z \geq 40$. This calculation significantly improves the accuracy of the theoretical prediction for the ground-state energy in high-Z H-like ions. While the present experimental accuracy is not yet sufficient to probe the new contribution, it could be possible in the near future, when the experiment planned at GSI [80] is completed. The accuracy of 1 eV for H-like uranium aimed at in this experiment is comparable with the two-loop self-energy contribution of -1.6 eV obtained in this work. Finally, we have presented a compilation of all presently available contributions to the ground-state Lamb shift in high-Z H-like ions together with estimates of the uncertainty of the theoretical predictions. It should be noted that a possible "weak point" of these estimates is that the realistic uncertainty of the nuclear rms radii is difficult to determine. It can be illustrated, *e.g.*, by the fact that different experimental values of rms radii are often in serious disagreement with each other, well beyond the given error bars [64,65]. Since the present theoretical errors of the energy values specified in Table 8 are mainly determined by the uncertainty of the finite-nuclear-size effect, shifting of experimental values for the nuclear rms radii beyond the given error bars will also cause changes in the corresponding theoretical prediction.

We would like to indicate that the two-loop self-energy correction is, in some sense, the first "non-trivial" second-order QED correction that has been evaluated without an expansion in $Z\alpha$ up to now. All calculations of other second-order QED contributions presented in Figure 8 were accomplished by various generalizations of the numerical scheme developed for the first-order QED corrections. Contrary to that, a number of issues had to be addressed in the evaluation of the two-loop self-energy correction, which have not been encountered before. Among them are, *e.g.*, the evaluation of the bound-electron propagator in the mixed momentum-coordinate space and the double infinite summation over multipoles of photon propagators. We believe that the technique developed in this work can be applied to the evaluation of other non-trivial two-loop QED corrections as well.

Several systems can be mentioned at present, where evaluations of two-loop self-energy corrections would be of immediate experimental interest. First, of utmost importance is to extend our calculation to the lower-Z region, where the higher-order terms could enter at the level of the experimental interest even at $Z = 1$ [11]. Another problem is to perform a similar calculation for $2p-2s$ transitions in high-Z Li-like ions, where the present experimental accuracy is much higher than that in H-like ions. Particularly precise measurements were performed for the $2p_{1/2}-2s$ transition in Li-like uranium [81] and for the $2p_{3/2}-2s$ transition in Li-like bismuth [82]. In the latter investigation, the transition energy was obtained with an accuracy of 0.04 eV. This should be compared with an estimate of the corresponding two-loop self-energy correction of 0.11 eV obtained by a simple $1/n^3$ scaling of the ground-state result. We also mention that the present theoretical uncertainty of the corresponding theoretical values is mainly defined by the two-loop self-energy corrections [23,83].

Another system whose theoretical understanding is presently limited by two-loop QED corrections is the g factor of the bound electron in a H-like ion. Experimental and theoretical investigations of this system resulted in an independent determination of the electron mass [84, 85] with an accuracy that is 4 times better than that of the accepted value for the electron mass [1]. While the uncertainty of the new value of the electron mass is defined mainly by the present experimental error, significant progress is anticipated from the experimental side in the near future. We expect that the evaluation of the two-loop self-energy correction to the bound-electron g factor could be in principle carried out along the same lines as it is presented in this work.

We are grateful to Anton Artemyev for providing us with his numerical results for the first-order vacuum-polarization correction. We gratefully acknowledge valuable discussions with G. Soff, U. Jentschura, and Th. Beier. This study was supported in part by RFBR (Grant No. 01-02-17248), by Ministry of Education (Grant No. E02-3.1-49), and by the program "Russian Universities" (Grant No. UR.01.01.072). V.Y. acknowledges the support from the Ministère de l'Éducation Nationale et de la Recherche, the foundation "Dynasty", and International Center for Fundamental Physics. The computation was performed on the CINES and IDRIS French national computer centers. Laboratoire Kastler Brossel is Unité Mixte de Recherche du CNRS n° C8552.

Appendix A: Free one-loop functions

A.1 Self-energy function

The free one-loop self-energy function in the Feynman gauge and in D dimensions is given by

$$\Sigma_D^{(0)}(p) = -4\pi \mathrm{i}\alpha\mu^{2\epsilon} \int \frac{\mathrm{d}^D k}{(2\pi)^D} \frac{1}{k^2} \gamma_\sigma \frac{\not{p} - \not{k} + m}{(p-k)^2 - m^2} \gamma^\sigma, \tag{234}$$

where μ is the mass parameter which appearance is determined by the fact that in $D = 4 - 2\epsilon$ dimensions the electron charge is $e(D) = \mu^\epsilon e$. This parameter is introduced in order to keep the proper dimension of the interaction term in the Lagrangian. In the expression above the index D indicates the number of dimensions. We omit this subscript when the exact number of dimensions is irrelevant for the discussion.

The integration over the momentum k is easily evaluated after joining the denominators by the Feynman-parametrization formula (281), which yields

$$\Sigma_D^{(0)}(p) = -\frac{\alpha C_\epsilon}{2\pi\epsilon} \int_0^1 \mathrm{d}x \, \frac{(1-\epsilon)(1-x)\not{p} - (2-\epsilon)m}{(x\Upsilon)^\epsilon}, \tag{235}$$

where

$$C_\epsilon = \Gamma(1+\epsilon)(4\pi)^\epsilon \left(\frac{\mu^2}{m^2}\right)^\epsilon, \tag{236}$$

$\Upsilon = x(1-\rho) + \rho$, and ρ is the virtuality of the electron, $\rho = (m^2 - p^2)/m^2$. The mass counterterm is obtained from (235) by adding the on-mass-shell condition $\not{p} = m$,

$$\delta m^{(1)} = \frac{\alpha C_\epsilon}{4\pi\epsilon} \, \frac{3-2\epsilon}{1-2\epsilon} \, m \,. \tag{237}$$

The difference $\Sigma_D^{(0)}(p) - \delta m^{(1)}$ is still divergent when ϵ goes to zero. Separating explicitly the divergent part, we write

$$\Sigma_D^{(0)}(p) = \delta m^{(1)} + B^{(1)}(\not{p} - m) + \Sigma_{R,D}^{(0)}(p) \,, \tag{238}$$

where

$$B^{(1)} = -\frac{\alpha C_\epsilon}{4\pi\epsilon} \,, \tag{239}$$

and $\Sigma_{R,D}^{(0)}(p)$ is the renormalized self-energy function,

$$\Sigma_{R,D}^{(0)}(p) = -\frac{\alpha C_\epsilon}{2\pi} \left\{ \frac{\not{p} - m}{1-2\epsilon} + \frac{1}{\epsilon} \int_0^1 \mathrm{d}x \, \big[(1-\epsilon)(1-x)\not{p} - (2-\epsilon)m\big] \left(\frac{1}{x^\epsilon \Upsilon^\epsilon} - \frac{1}{x^{2\epsilon}}\right) \right\}. \tag{240}$$

In the limit $\epsilon \to 0$, this leads to the well-known expression

$$\Sigma_{R,4}^{(0)}(p) = \frac{\alpha}{4\pi} \left[2m \left(1 + \frac{2\rho}{1-\rho} \ln\rho\right) - \not{p} \, \frac{2-\rho}{1-\rho} \left(1 + \frac{\rho}{1-\rho} \ln\rho\right) \right]. \tag{241}$$

We note that our definition of the renormalization constant $B^{(1)}$ differs from that of the standard procedure of free-electron QED, where it is determined by the on-mass-shell condition

$$\overline{B}^{(1)} = \frac{\partial}{\partial \not{p}} \Sigma_D^{(0)}(p) \bigg|_{\not{p}=m} \,. \tag{242}$$

In fact, $B^{(1)}$ is just the UV-divergent part of $\overline{B}^{(1)}$. The reason for this modified definition is that $B^{(1)}$, unlike $\overline{B}^{(1)}$, does not contain any IR divergences.

Evaluating two-loop contributions, we have to keep the exact dependence of $\Sigma_R^{(0)}$ on ϵ since it can be multiplied by a divergent contribution of order $1/\epsilon$. However, equation (240) is not very convenient for practical applications since it involves auxiliary singularities when $\epsilon \to 0$. One could avoid them by joining the two terms in the last brackets by using equation (284). However, this will lead to an additional integration. Instead, we integrate (240) by parts and use the identity

$$x \left(\frac{1}{x^\epsilon \Upsilon^\epsilon} - \frac{1}{x^{2\epsilon}}\right)'_x = \frac{\epsilon\rho}{x^\epsilon \Upsilon^{\epsilon+1}} - 2\epsilon \left(\frac{1}{x^\epsilon \Upsilon^\epsilon} - \frac{1}{x^{2\epsilon}}\right). \tag{243}$$

We see that the integration by parts brings an additional power of ϵ in the numerator. Repeating this procedure, we get an expansion in the parameter ϵ that can be easily summed up in a closed form. This yields

$$\Sigma_{R,D}^{(0)}(p) = -\frac{\alpha C_\epsilon}{2\pi} \left\{ \frac{\not{p} - m}{1-2\epsilon} - \frac{\rho}{2} \int_0^1 \mathrm{d}x \, \frac{1}{x^\epsilon \Upsilon^{\epsilon+1}} \times \left[\not{p} \left(\frac{2-2\epsilon}{1-2\epsilon} - x \right) - m \frac{4-2\epsilon}{1-2\epsilon} \right] \right\}, \tag{244}$$

which agrees with the result of [21].

It is useful to obtain one more representation for the self-energy function, taking into account that it always enters higher-order diagrams accompanied by two electron propagators,

$$\frac{1}{\not{p} - m} \left[\Sigma_D^{(0)}(p) - \delta m^{(1)} \right] \frac{1}{\not{p} - m}.$$

Therefore, it is advantageous to separate explicitly powers of $(\not{p} - m)$ in (244). After simple manipulations, we get

$$\Sigma_D^{(0)}(p) - \delta m^{(1)} = \frac{\alpha C_\epsilon}{4\pi} (\not{p} - m) \left[-\frac{1}{\epsilon(1-2\epsilon)} + \Sigma_a(p^2) + (\not{p} - m)\Sigma_b(p) \right], \tag{245}$$

where

$$\Sigma_a(p^2) = 2m^{2+2\epsilon} \int_0^1 \mathrm{d}x \, \frac{x^{-\epsilon}}{[m^2 - p^2(1-x)]^{1+\epsilon}} \times \left(\frac{2}{1-2\epsilon} + x \right), \tag{246}$$

$$\Sigma_b(p) = m^{2\epsilon} \int_0^1 \mathrm{d}x \, \frac{x^{-\epsilon}}{[m^2 - p^2(1-x)]^{1+\epsilon}} \times \left[2m \left(\frac{\epsilon}{1-2\epsilon} + x \right) - \not{p} \left(\frac{2-2\epsilon}{1-2\epsilon} - x \right) \right]. \tag{247}$$

We introduce also an expansion of the self-energy function over the parameter ϵ,

$$\Sigma^{(0)}_{R,D}(p) = C_\epsilon \left(\Sigma^{(0)}_{R,4}(p) + \epsilon \Sigma^{(0)}_{R,\epsilon}(p) + O(\epsilon^2) \right) , \quad (248)$$

where $\Sigma^{(0)}_{R,4}(p)$ is given by (241). It is convenient to keep the overall constant C_ϵ in its closed form throughout the calculation.

For further useful representations of the self-energy function in a general covariant gauge (and, particularly, in the Fried-Yennie gauge) in framework of the dimensional regularization we refer the reader to the paper [86].

A.2 Vertex function

The free one-loop vertex function in the Feynman gauge and in D dimension is represented by

$$\Gamma^\alpha_D(p_1,p_2) = -4\pi \mathrm{i}\alpha\mu^{2\epsilon} \int \frac{\mathrm{d}^D k}{(2\pi)^D} \frac{1}{k^2} \gamma_\sigma \frac{\not p_1 - \not k + m}{(p_1-k)^2 - m^2} \times \gamma^\alpha \frac{\not p_2 - \not k + m}{(p_2-k)^2 - m^2} \gamma^\sigma . \quad (249)$$

While the evaluation of this expression is quite simple, we discuss it here in detail since it gives us an opportunity to illustrate some essential features of two-loop calculations. First we join the denominators by using the Feynman-parametrization formula (281):

$$\frac{1}{k^2[(p_1-k)^2-m^2][(p_2-k)^2-m^2]} = 2\int \mathrm{d}x\,\mathrm{d}y \frac{x}{[(k-xb)^2 - xD]^3}, \quad (250)$$

where $b = yp_1 + (1-y)p_2$, and $D = xb^2 + m^2 - yp_1^2 - (1-y)p_2^2$. Here and in what follows we assume that all integrations over Feynman parameters extend from 0 to 1, if not stated otherwise. Shifting the momentum variable $k \to k + xb$, we have

$$\Gamma^\alpha_D(p_1,p_2) = \frac{\alpha\mu^{2\epsilon}}{2\pi} \int \mathrm{d}x\,\mathrm{d}y\, x \times \frac{16\pi^2}{\mathrm{i}} \int \frac{\mathrm{d}^D k}{(2\pi)^D} \frac{N^\alpha(k+xb)}{(k^2 - xD)^3}, \quad (251)$$

where $N^\alpha(k)$ is the numerator in (249), $N^\alpha(k) = \gamma_\sigma(\not p_1 - \not k + m)\gamma^\alpha(\not p_2 - \not k + m)\gamma^\sigma$. Next, we represent the numerator $N^\alpha(k+xb)$ in the form $N^\alpha(k+xb) = N^\alpha_0 + N^{\alpha\mu}_1 k_\mu + N^{\alpha\mu\nu}_2 k_\mu k_\nu$, where the components N_i do not depend on k. [Obviously, $N^\alpha_0 = N^\alpha(xb)$.] The integration over k is carried out according formulas (282), (283). Finally, we obtain the following representation for the unrenormalized vertex function:

$$\Gamma^\alpha_D(p_1,p_2) = \frac{\alpha C_\epsilon m^{2\epsilon}}{4\pi} \int \mathrm{d}x\,\mathrm{d}y \times \left\{ \frac{(2-2\epsilon)^2\gamma^\alpha}{2\epsilon} \frac{x^{1-\epsilon}}{D^\epsilon} - \frac{x^{-\epsilon} N^\alpha(xb)}{D^{1+\epsilon}} \right\}, \quad (252)$$

where we have taken into account that contributions containing odd powers of k in the numerator vanish after the angular integration and that $N^{\alpha\mu\nu}_2 g_{\mu\nu} = (2-2\epsilon)^2\gamma^\alpha$. In the equation above, the constant C_ϵ is given by (236), and $N^\alpha(xb) = \gamma_\sigma(\not p_1 - x\not b + m)\gamma^\alpha(\not p_2 - x\not b + m)\gamma^\sigma$.

Another useful representation for the vertex function can be obtained by integrating by parts the first term in (252),

$$\Gamma^\alpha_D(p_1,p_2) = \frac{\alpha C_\epsilon m^{2\epsilon}}{4\pi} \left\{ \frac{(2-2\epsilon)^2}{2\epsilon(2-\epsilon)} \int \mathrm{d}y\, \frac{\gamma^\alpha}{D_0^\epsilon} + \int \mathrm{d}x\,\mathrm{d}y\, \frac{x^{-\epsilon}}{D^{1+\epsilon}} \left[\frac{(2-2\epsilon)^2}{2(2-\epsilon)} x^2 b^2 \gamma^\alpha - N^\alpha(xb) \right] \right\}, \quad (253)$$

where $D_0 = D(x=1) = m^2 - y(1-y)q^2$, and $q = p_1 - p_2$.

The divergent part of the vertex function can be easily separated,

$$\Gamma^\alpha_D(p_1,p_2) = L^{(1)}\gamma^\alpha + \Gamma^\alpha_{R,D}(p_1,p_2), \quad (254)$$

where

$$L^{(1)} = \frac{\alpha C_\epsilon}{4\pi\epsilon}, \quad (255)$$

and the renormalized vertex function $\Gamma^\alpha_{R,D}(p_1,p_2)$ is finite when ϵ goes to zero. Again, note that we pull out only the UV-divergent part of the renormalization constant in equation (255). The renormalized vertex function can be expanded in the parameter ϵ, which yields

$$\Gamma^\alpha_{R,D}(p_1,p_2) = C_\epsilon \Big[\Gamma^\alpha_{R,4}(p_1,p_2) + \epsilon \Gamma^\alpha_{R,\epsilon}(p_1,p_2) + O(\epsilon^2) \Big], \quad (256)$$

where

$$\Gamma^\alpha_{R,4}(p_1,p_2) = -\frac{\alpha}{4\pi} \left[\frac{3}{2}\gamma^\alpha + \int \mathrm{d}x\,\mathrm{d}y \times \left(\frac{N^\alpha(xb)}{D} + 2x\gamma^\alpha \ln D \right) \right]. \quad (257)$$

The integration over x in (257) can easily be carried out analytically. In this case we end up with the expression for the renormalized vertex function in 4 dimensions, analogous to those presented in [25,26,87]. (We note a large number of misprints in formulas of [25].)

In higher-order diagrams, the vertex function is accompanied by electron propagators from one or both sides. Hence, we may wish to separate the corresponding factors $(\not p_1 - m)$, $(\not p_2 - m)$ from the numerators in (253), (257). So, $N^\alpha(xb)$ can be represented in the form

$$N^\alpha(xb) = (\not p_1 - m)\gamma^\alpha(\not p_2 - m)\mathcal{L}_2 + (\not p_1 - m)\mathcal{L}^\alpha_{1r} + \mathcal{L}^\alpha_{1l}(\not p_2 - m) + \mathcal{L}^\alpha_0 , \quad (258)$$

where $\mathcal{L}_2 = 2(1-x)(1+\epsilon)$. Formulas for other functions $\mathcal{L}_i$ are obtained by simple algebraic manipulations. Here we present an explicit expression only for the function $\mathcal{L}^\alpha_0$ that is of particular importance since it yields the only

non-vanishing contribution to $N^\alpha(xb)$ when both p_1 and p_2 are put on the mass shell. The expression reads

$$\begin{aligned}\mathcal{L}_0^\alpha/2 = {}& mx(1-2y)[1+x(1-\epsilon)]q^\alpha \\ & - mx[1-x(1-\epsilon)]\mathrm{i}\sigma^{\alpha\beta}q_\beta \\ & + m^2[2-2x-x^2(1-\epsilon)]\gamma^\alpha \\ & - [1-x+x^2y(1-y)(1-\epsilon)]q^2\gamma^\alpha\,, \quad (259)\end{aligned}$$

where $\sigma^{\alpha\beta} = (\mathrm{i}/2)[\gamma^\alpha,\gamma^\beta]$. Equivalent formulas for $N^\alpha(xb)$ can be found in [88].

For completeness, we mention here some other representations for the one-loop vertex function available in the literature. In [89] the vertex function was studied in the Fried-Yennie gauge for the general case of D dimensions. The same gauge, but within the Pauli-Villars regularization, was used in [90]. The result for an arbitrary covariant gauge in 4 dimensions is presented in [91]. The vertex function in the Feynman gauge but within an old-fashioned regularization can be found in the book of Jauch and Rohrlich [92].

Appendix B: Analytical properties of the one-loop self-energy and vertex functions

In this section we investigate analytical properties of the self-energy function $\Sigma(\varepsilon_a-\omega_1)$ defined by equation (10) and the vertex function $\Lambda^\mu(\varepsilon_a-\omega_1,\varepsilon_a)$ defined by equation (22) as functions of ω_1. Our goal will be to demonstrate that these functions (defined originally for real values of ω_1) allow an analytical continuation into the complex plane.

We start with the self-energy function. Employing the spectral representation of the electron propagator, it is written as

$$\begin{aligned}\Sigma(\varepsilon_a-\omega_1) = {}& 2\mathrm{i}\alpha\gamma^0\int_{-\infty}^{\infty}\mathrm{d}\omega_2\, D(\omega_2,x_{12}) \\ & \times\sum_n \frac{\alpha_\nu\psi_n(\mathbf{x}_1)\psi_n^\dagger(\mathbf{x}_2)\alpha^\nu}{\varepsilon_a-\omega_1-\omega_2-\varepsilon_n(1-\mathrm{i}0)}. \quad (260)\end{aligned}$$

Using the momentum representation for the photon propagator (49), we write it as

$$\begin{aligned}\Sigma(\varepsilon_a-\omega_1) = {}& -\frac{\mathrm{i}\alpha}{\pi^2}\gamma^0\int_0^\infty \mathrm{d}k\,k\frac{\sin kx_{12}}{x_{12}} \\ & \times\sum_n \alpha_\nu\psi_n(\mathbf{x}_1)\psi_n^\dagger(\mathbf{x}_2)\alpha^\nu\, I_n(\omega_1,k), \quad (261)\end{aligned}$$

where

$$\begin{aligned}I_n(\omega_1,k) = {}& \int_{-\infty}^{\infty}\mathrm{d}\omega_2\,\frac{1}{(\omega_2^2-k^2+\mathrm{i}0)} \\ & \times\frac{1}{(\varepsilon_a-\omega_1-\omega_2-\varepsilon_n(1-\mathrm{i}0))}. \quad (262)\end{aligned}$$

This integral is evaluated by the Cauchy theorem to yield

$$I_n(\omega_1,k) = \begin{cases} \dfrac{-\mathrm{i}\pi}{k(\varepsilon_a-\varepsilon_n-k-\omega_1+\mathrm{i}0)}\,, & \varepsilon_n>0 \\ \dfrac{-\mathrm{i}\pi}{k(\varepsilon_a-\varepsilon_n+k-\omega_1-\mathrm{i}0)}\,, & \varepsilon_n<0. \end{cases} \quad (263)$$

Taking into account that $\varepsilon_a-\varepsilon_n-k\le 0$ for $\varepsilon_n>0$ (a is assumed to be the $1s$ state), and $\varepsilon_a-\varepsilon_n+k\ge\varepsilon_a+m$ for $\varepsilon_n<0$, we conclude that for $\omega_1\in(0,\varepsilon_a+m)$ the self-energy function $\Sigma(\varepsilon_a-\omega_1)$ can be analytically continued both into the upper and into the lower half-plane. However, for $\omega_1>\varepsilon_a+m$, it allows the analytical continuation into the upper half-plane only, and for $\omega_1<0$ in the lower half-plane only.

Analogously, considering the vertex function $\Lambda^\mu(\varepsilon_a-\omega_1,\varepsilon_a)$, we can conclude that its analytical properties are defined by the integrals $I_{n_1n_2}$,

$$\begin{aligned}I_{n_1n_2}(\omega_1,k) = {}& \int_{-\infty}^{\infty}\mathrm{d}\omega_2\,\frac{1}{(\omega_2^2-k^2+\mathrm{i}0)} \\ & \times\frac{1}{(\varepsilon_a-\omega_1-\omega_2-\varepsilon_{n_1}(1-\mathrm{i}0))}\frac{1}{(\varepsilon_a-\omega_2-\varepsilon_{n_2}(1-\mathrm{i}0))}. \quad (264)\end{aligned}$$

When ε_{n_1} and ε_{n_2} are of the same sign, we directly apply the Cauchy theorem that yields

$$I_{n_1n_2}(\omega_1,k) = \begin{cases} \dfrac{-\mathrm{i}\pi}{k(\varepsilon_a-\varepsilon_{n_1}-k-\omega_1+\mathrm{i}0)(\varepsilon_a-\varepsilon_{n_2}-k+\mathrm{i}0)}, \\ \varepsilon_{n_1}>0,\ \varepsilon_{n_2}>0 \\ \\ \dfrac{-\mathrm{i}\pi}{k(\varepsilon_a-\varepsilon_{n_1}+k-\omega_1-\mathrm{i}0)(\varepsilon_a-\varepsilon_{n_2}+k-\mathrm{i}0)}, \\ \varepsilon_{n_1}<0,\ \varepsilon_{n_2}<0. \end{cases} \quad (265)$$

For $\varepsilon_{n_1}>0$, $\varepsilon_{n_2}<0$, we use the identity

$$\begin{aligned}& \frac{1}{(\varepsilon_a-\omega_1-\omega_2-\varepsilon_{n_1}+\mathrm{i}0)(\varepsilon_a-\omega_2-\varepsilon_{n_2}-\mathrm{i}0)} = \\ & \qquad \frac{1}{\varepsilon_{n_1}-\varepsilon_{n_2}+\omega_1-\mathrm{i}0} \\ & \quad\times\left(\frac{1}{\varepsilon_a-\omega_1-\omega_2-\varepsilon_{n_1}+\mathrm{i}0}-\frac{1}{\varepsilon_a-\omega_2-\varepsilon_{n_2}-\mathrm{i}0}\right). \quad (266)\end{aligned}$$

Now the Cauchy theorem yields

$$\begin{aligned}I_{n_1n_2}(\omega_1,k) = {}& \frac{\mathrm{i}\pi}{k(\varepsilon_{n_2}-\varepsilon_{n_1}-\omega_1+\mathrm{i}0)} \\ & \times\left(\frac{1}{\varepsilon_a-\varepsilon_{n_1}-k-\omega_1+\mathrm{i}0}-\frac{1}{\varepsilon_a-\varepsilon_{n_2}+k-\mathrm{i}0}\right), \\ & \qquad \varepsilon_{n_1}>0,\ \varepsilon_{n_2}<0. \quad (267)\end{aligned}$$

The case $\varepsilon_{n_1} < 0, \varepsilon_{n_2} > 0$ is considered in the same way. Analyzing the integrals $I_{n_1 n_2}$ as functions of ω_1, we conclude that the vertex function $\Lambda^\mu(\varepsilon_a - \omega_1, \varepsilon_a)$ allows the analytical continuation to the upper half-plane for $\omega_1 > \varepsilon_a + m$, to the lower half-plane for $\omega_1 < 0$, and to both half-planes for $\omega_1 \in (0, \varepsilon_a + m)$.

Appendix C: Radial integrals

A derivation of the radial integral $R_J(\omega, abcd)$ defined by (59) (also called as the generalized Slater integral) can be found in [40]. For our purposes it is convenient to write it in the form:

$$R_J(\omega, abcd) = (2J+1)\int_0^\infty \mathrm{d}x_1\,\mathrm{d}x_2\, x_1^2 x_2^2 \times \Big[(-1)^J C_J(\kappa_a,\kappa_c)\, C_J(\kappa_b,\kappa_d) \times g_J(\omega,x_1,x_2)\, W_{ac}(x_1)\, W_{bd}(x_2) - \sum_L (-1)^L g_L(\omega,x_1,x_2)\, X_{ac}(x_1)\, X_{bd}(x_2)\Big], \tag{268}$$

$$W_{ab}(x) = g_a(x)g_b(x) + f_a(x)f_b(x), \tag{269}$$

$$X_{ab}(x) = g_a(x)f_b(x)S_{JL}(-\kappa_b,\kappa_a) - f_a(x)g_b(x)S_{JL}(\kappa_b,-\kappa_a), \tag{270}$$

where g_n, f_n are the upper and the lower radial components of the Dirac wave function, respectively. The function $g_L(\omega, x_1, x_2)$ is the radial part of the partial-wave expansion of the photon propagator,

$$\frac{\exp(\mathrm{i}\sqrt{\omega^2+\mathrm{i}0}\,x_{12})}{x_{12}} = \sum_L (2L+1) g_L(\omega,x_1,x_2) P_L(\xi), \tag{271}$$

where $P_L(\xi)$ is the Legendre polynomial, $\xi = \hat{\mathbf{x}}_1 \cdot \hat{\mathbf{x}}_2$. Explicitly,

$$g_L(0,x_1,x_2) = \frac{1}{2L+1}\frac{x_<^L}{x_>^{L+1}}, \tag{272}$$

$$g_L(\omega,x_1,x_2) = \mathrm{i}\overline{\omega} j_L(\overline{\omega}x_<) h_L^{(1)}(\overline{\omega}x_>), \tag{273}$$

where $\overline{\omega} = \sqrt{\omega^2+\mathrm{i}0}$, $j_l(z)$ and $h_l^{(1)}(z)$ are the spherical Bessel functions, $x_> = \max(x_1,x_2)$, $x_< = \min(x_1,x_2)$.

Nonvanishing angular coefficients $S_{JL}(\kappa_a,\kappa_b)$ for $J \neq 0$ are:

$$S_{J\,J+1}(\kappa_a,\kappa_b) = \sqrt{\frac{J+1}{2J+1}}\left(1+\frac{\kappa_a+\kappa_b}{J+1}\right) \times C_J(-\kappa_b,\kappa_a), \tag{274}$$

$$S_{J\,J}(\kappa_a,\kappa_b) = \frac{\kappa_a-\kappa_b}{\sqrt{J(J+1)}} C_J(\kappa_b,\kappa_a), \tag{275}$$

$$S_{J\,J-1}(\kappa_a,\kappa_b) = \sqrt{\frac{J}{2J+1}}\left(-1+\frac{\kappa_a+\kappa_b}{J}\right) \times C_J(-\kappa_b,\kappa_a). \tag{276}$$

For $J = 0$ there is only one nonzero coefficient $S_{01}(\kappa_a,\kappa_b) = C_0(-\kappa_b,\kappa_a)$. The coefficients $C_J(\kappa_b,\kappa_a)$ are given by

$$C_J(\kappa_b,\kappa_a) = (-1)^{j_b+1/2}\sqrt{(2j_a+1)(2j_b+1)} \times \begin{pmatrix} j_a & J & j_b \\ \frac{1}{2} & 0 & -\frac{1}{2}\end{pmatrix} \Pi(l_a,l_b,J), \tag{277}$$

where the symbol $\Pi(l_a,l_b,J)$ is unity if l_a+l_b+J is even, and zero otherwise.

We mention the following properties of the radial integrals:

$$R_J(\omega,abcd) = R_J(-\omega,abcd) = R_J(\omega,badc) = (-1)^{j_a-j_c}(-1)^{j_b-j_d} R_J(\omega,cdab), \tag{278}$$

$$R_J(\omega,abcd) \sim \Delta(j_a j_c J)\,\Delta(j_b j_d J)\,\left[1+(-1)^{l_a+l_b+l_c+l_d}\right], \tag{279}$$

where $\Delta(\cdots)$ denotes the triangle rule.

Appendix D: Integration over momenta in D dimensions

For completeness, we present here few basic formulas that are needed to carry out integrations over loop momenta in arbitrary number of dimensions.

In the evaluation of Feynman diagrams, integrals of the following form are encountered:

$$J = \frac{16\pi^2}{\mathrm{i}}\int \frac{\mathrm{d}^D k}{(2\pi)^D} \times \frac{N(k)}{(k^2+2p_1k+M_1^2)^{\alpha_1}\ldots(k^2+2p_nk+M_n^2)^{\alpha_n}}, \tag{280}$$

where $N(k)$ is a polynomial in k_μ; p_i and M_i do not depend on k.

First we use the following formula in order to combine the terms in the denominator:

$$\frac{1}{a_1^{\alpha_1}a_2^{\alpha_2}\cdots a_n^{\alpha_n}} = \frac{\Gamma(\alpha)}{\prod_{i=1}^n \Gamma(\alpha_i)} \times \int_0^1 \mathrm{d}x_1 \int_0^{x_1}\mathrm{d}x_2 \cdots \int_0^{x_{n-2}}\mathrm{d}x_{n-1} (1-x_1)^{\alpha_1-1} x_{n-1}^{\alpha_n-1}\prod_{i=2}^{n-1}(x_{i-1}-x_i)^{\alpha_i-1} \times \frac{1}{[(1-x_1)a_1+(x_1-x_2)a_2+\cdots+x_{n-1}a_n]^\alpha}, \tag{281}$$

where $\alpha = \sum_{i=1}^n \alpha_i$. The denominator in (281) can be rewritten in the form $(k^2-2pk-M)^\alpha = [(k-p)^2-\Delta]^\alpha$, with $\Delta = p^2+M$. Shifting the momentum variable $k \to k+p$, we end up with the integrals performed by the

following formulas ($D = 4 - 2\epsilon$):

$$\frac{16\pi^2}{\mathrm{i}} \int \frac{\mathrm{d}^D k}{(2\pi)^D} \frac{1}{(k^2 - \Delta)^a} = (-1)^a \frac{\Gamma(a - 2 + \epsilon)}{\Gamma(a)} \frac{(4\pi)^\epsilon}{\Delta^{a-2+\epsilon}}, \tag{282}$$

$$\frac{16\pi^2}{\mathrm{i}} \int \frac{\mathrm{d}^D k}{(2\pi)^D} \frac{k_\mu k_\nu}{(k^2 - \Delta)^a} = (-1)^{a+1} \frac{\Gamma(a - 3 + \epsilon)}{\Gamma(a)} \times \frac{(4\pi)^\epsilon}{\Delta^{a-3+\epsilon}} \frac{g_{\mu\nu}}{2}. \tag{283}$$

Similar integrals with odd powers of k_μ in the numerator vanish due to symmetry reasons.

Here is one more useful parametrization formula,

$$\frac{1}{\alpha^n} - \frac{1}{\beta^n} = -\int_0^1 \mathrm{d}z \frac{n(\alpha - \beta)}{[(\alpha - \beta)z + \beta]^{n+1}}. \tag{284}$$

References

1. P.J. Mohr, B.N. Taylor, Rev. Mod. Phys. **72**, 351 (2000)
2. M. Niering, R. Holzwarth, J. Reichert, P. Pokasov, T. Udem, M. Weitz, T.W. Hänsch, P. Lemonde, G. Santarelli, M. Abgrall, P. Laurent, C. Salomon, A. Clairon, Phys. Rev. Lett. **84**, 5496 (2000)
3. T. Appelquist, S.J. Brodsky, Phys. Rev. Lett. **24**, (1970) 562; Phys. Rev. A **2**, (1970) 2293.
4. R. Barbieri, J.A. Mignaco, E. Remiddi, Nuovo Cim. A **6**, (1971) 21.
5. C.M. Sommerfield, Phys. Rev. **107**, 328 (1957); Ann. Phys. (NY) **5**, 26 (1958)
6. A. Peterman, Helv. Phys. Acta **30**, (1957) 407; Nucl. Phys. **3**, 689 (1957)
7. K. Pachucki, Phys. Rev. Lett. **72**, 3154 (1994)
8. M. Eides, V. Shelyuto, Phys. Rev. A **52**, 954 (1995)
9. S.G. Karshenboim, Zh. Eksp. Teor. Fiz. **103**, 1105 (1993) [Sov. Phys. JETP **76**, 541 (1993)]
10. A.V. Manohar, I.V. Stewart, Phys. Rev. Lett. **85**, 2248 (2000)
11. K. Pachucki, Phys. Rev. A **63**, 042503 (2001)
12. U.D. Jentschura, J. Phys. A **36**, L229 (2003)
13. U.D. Jentschura, K. Pachucki, J. Phys. A **35**, 1927 (2002)
14. U.D. Jentschura, P.J. Mohr, G. Soff, Phys. Rev. Lett. **82**, 53 (1999)
15. A. Mitrushenkov, L. Labzowsky, I. Lindgren, H. Persson, S. Salomonson, Phys. Lett. A **200**, 51 (1995)
16. S. Mallampalli, J. Sapirstein, Phys. Rev. Lett. **80**, 5297 (1998)
17. I. Goidenko, L. Labzowsky, A. Nefiodov, G. Plunien, G. Soff, Phys. Rev. Lett. **83**, 2312 (1999)
18. V.A. Yerokhin, Phys. Rev. A **62**, 012508 (2000)
19. V.A. Yerokhin, Phys. Rev. Lett. **86**, 1990 (2001)
20. U.D. Jentschura, I. Nándori, Phys. Rev. A **66**, 022114 (2002)
21. S. Mallampalli, J. Sapirstein, Phys. Rev. A **57**, 1548 (1998)
22. I. Goidenko, L. Labzowsky, A. Nefiodov, G. Plunien, S. Zschocke, G. Soff, in: *Hydrogen atom: Precision Physics of Simple Atomic System*, edited by S.G. Karshenboim *et al.* (Springer, Berlin, 2001).
23. V.A. Yerokhin, V.M. Shabaev, Phys. Rev. A **64**, 062507 (2001)
24. V.A. Yerokhin, P. Indelicato, V.M. Shabaev, Phys. Rev. Lett. **91**, 073001 (2003); `hep-ph/0302268` (2003)
25. N.J. Snyderman, Ann. Phys. (N.Y.) **211**, 43 (1991)
26. V.A. Yerokhin, V.M. Shabaev, Phys. Rev. A **60**, 800 (1999)
27. P.J. Mohr, Ann. Phys. (N.Y.) **88**, 26 (1974); *ibid.* 52 (1974)
28. V.A. Yerokhin, V.M. Shabaev, Phys. Rev. A **64**, 012506 (2001)
29. S.A. Blundell, Phys. Rev. A **47**, 1790 (1993)
30. V.M. Shabaev, Phys. Rep. **356**, 119 (2002)
31. R. Mills, N. Kroll, Phys. Rev. **98**, 1489 (1955)
32. C. Itzykson, J.-B. Zuber, *Quantum Field Theory* (McGraw-Hill, NY, 1980)
33. J.A. Fox, D.R. Yennie, Ann. Phys. (N.Y.) **81**, 438 (1973)
34. L. Labzowsky, A. Mitrushenkov, Phys. Rev. A **53**, 3029 (1996)
35. I. Lindgren, H. Persson, S. Salomonson, P. Sunnergren, Phys. Rev. A **58**, 1001 (1998)
36. S.A. Blundell, N.J. Snyderman, Phys. Rev. A **44**, R1427 (1991)
37. S.A. Blundell, Phys. Rev. A **46**, 3762 (1992)
38. C. Brezinski, *Algorithmes d'accélération de la convergence* (Éditions Technip, Paris, 1978)
39. E.M. Rose, *Relativistic Electron Theory* (Whiley, New York, 1961)
40. W.R. Johnson, S.A. Blundell, J. Sapirstein, Phys. Rev. A **37**, 2764 (1988)
41. D.A. Varshalovich, A.N. Moskalev, V.K. Khersonskii, *Quantum Theory of Angular Momentum* (World Scientific, Singapore, 1988)
42. V.A. Yerokhin, A.N. Artemyev, T. Beier, G. Plunien, V.M. Shabaev, G. Soff, Phys. Rev. A **60**, 3522 (1999)
43. E.H. Wichmann, N.M. Kroll, Phys. Rev. **101**, 843 (1956)
44. W.R. Johnson, S.A. Blundell, J. Sapirstein, Phys. Rev. A **37**, 307 (1988)
45. S. Salomonson, P. Öster, Phys. Rev. A **40**, 5548 (1989); *ibid.* 5559 (1989)
46. N.L. Manakov, L.P. Rapoport, S.A. Zaprjagaev, Phys. Lett. A **43**, 139 (1973)
47. B.A. Zon, N.L. Manakov, L.P. Rapoport, Yad. Fiz. **15**, 508 (1972) [Sov. J. Nucl. Phys. **15**, 282 (1972)]
48. N.L. Manakov, S.I. Marmo, A.G. Fainstein, Zh. Eksp. Teor. Fiz. **59**, 49 (1984)
49. C. de Boor, *A Practical Guide to Splines* (Springer, NY, 1978)
50. C.F. Fischer, F.A. Parpia, Phys. Lett. A **179**, 198 (1993)
51. G.S. Adkins, Y. Zhang, Can. J. Phys. **76**, 333 (1998)
52. L. Labzowsky, A. Mitrushenkov, V. Shelyuto, G. Soff, Phys. Lett. A **240**, 225 (1998)
53. L. Labzowsky, A. Mitrushenkov, V. Shelyuto, G. Soff, Phys. Rev. A **57**, 4038 (1998)
54. S. Wolfram, *Mathematica – A System for Doing Mathematics by Computer* (Reading, MA: Addison-Wesley, 1988)
55. U. Jentschura, Phys. Lett. B **564**, 225 (2003)
56. H. Persson, I. Lindgren, L. Labzowsky, G. Plunien, T. Beier, G. Soff, Phys. Rev. A **54**, 2805 (1996)
57. T. Beier, G. Plunien, M. Greiner, G. Soff, J. Phys. B **30**, 2761 (1997)
58. T. Beier, G. Soff, Z. Phys. D **8**, 129 (1988)
59. S.M. Schneider, W. Greiner, G. Soff, J. Phys. B **26**, L529 (1993)

60. G. Källén, A. Sabry, Mater. Fys. Medd. Dan. Vid. Selsk. **29**, 17 (1955)
61. G. Plunien, T. Beier, G. Soff, H. Persson, Eur. Phys. J. D **1**, 177 (1998)
62. K. Pachucki, Phys. Rev. A **48**, 2609 (1993)
63. S. Mallampalli, J. Sapirstein, Phys. Rev. A **54**, 2714 (1996)
64. G. Fricke, C. Bernhardt, K. Heilig, L.A. Schaller, L. Schellenberg, E.B. Shera, C.W. de Jager, At. Data Nucl. Data Tables **60**, 177 (1995)
65. H. de Vries, C.W. de Jager, C. de Vries, At. Data Nucl. Data Tables **36**, 495 (1987)
66. J.D. Zumbro, E.B. Shera, Y. Tanaka, C.E. Bemis Jr, R.A. Naumann, M.V. Hoehn, W. Reuter, R.M. Steffen, Phys. Rev. Lett. **53**, 1888 (1984)
67. J.D. Zumbro, R.A. Naumann, M.V. Hoehn, W. Reuter, E.B. Shera, C.E. Bemis Jr, Y. Tanaka, Phys. Lett. B **167**, 383 (1986)
68. T. Beier, P.J. Mohr, H. Persson, G. Soff, Phys. Rev. A **58**, 954 (1998)
69. P.J. Mohr, G. Soff, Phys. Rev. Lett. **70**, 158 (1993)
70. A.N. Artemyev, private communication.
71. G. Soff, P. Mohr, Phys. Rev. A **38**, 5066 (1988)
72. H. Persson, I. Lindgren, S. Salomonson, P. Sunnergren, Phys. Rev. A **48**, 2772 (1993)
73. A.N. Artemyev, V.M. Shabaev, V.A. Yerokhin, Phys. Rev. A **52**, 1884 (1995)
74. V.M. Shabaev, A.N. Artemyev, T. Beier, G. Plunien, V.A. Yerokhin, G. Soff, Phys. Rev. A **57**, 4235 (1998)
75. G. Plunien, G. Soff, Phys. Rev. A **51**, 1119 (1995); **53**, 4614 (1996)
76. A.V. Nefiodov, L.N. Labzowsky, G. Plunien, G. Soff, Phys. Lett. A **222**, 227 (1996)
77. A. Haga, Y. Horikawa, Y. Tanaka, Phys. Rev. A **65**, 052509 (2002)
78. J.P. Briand, P. Indelicato, A. Simionovici, V. San Vicente, D. Liesen, D. Dietrich, Europhys. Lett. **9**, 225 (1989)
79. H. Beyer, G. Menzel, D. Liesen, A. Gallus, F. Bosch, R. Deslattes, P. Indelicato, T. Stöhlker, O. Klepper, R. Moshammer, F. Nolden, H. Eickhoff, B. Franzke, M. Steck, Z. Phys. D **35**, 169 (1995)
80. T. Stöhlker, P.H. Mokler, F. Bosch, R.W. Dunford, F. Franzke, O. Klepper, C. Kozhuharov, T. Ludziejewski, F. Nolden, H. Reich, P. Rymuza, Z. Stachura, M. Steck, P. Swiat, A. Warczak, Phys. Rev. Lett. **85**, 3109 (2000)
81. J. Schweppe, A. Belkacem, L. Blumenfeld, N. Claytor, B. Feinberg, H. Gould, V.E. Kostroun, L. Levy, S. Misawa, J.R. Mowat, M.H. Prior, Phys. Rev. Lett. **66**, 1434 (1991)
82. P. Beiersdorfer, A. Osterheld, J. Scofield, J. Crespo Lopez-Urrutia, K. Widmann Phys. Rev. Lett. **80**, 3022 (1998)
83. J. Sapirstein, K.T. Cheng, Phys. Rev. A **64**, 022502 (2001)
84. H. Häffner, T. Beier, N. Hermanspahn, H.-J. Kluge, W. Quint, S. Stahl, J. Verdú, G. Werth, Phys. Rev. Lett. **85**, 5308 (2000)
85. V.A. Yerokhin, P. Indelicato, V.M. Shabaev, Phys. Rev. Lett. **89**, 143001 (2002)
86. G.S. Adkins, Phys. Rev. D **47**, 3647 (1993)
87. T. Beier, I. Lindgren, H. Persson, S. Salomonson, P. Sunnergren, H. Häffner, N. Hermanspahn, Phys. Rev. A **62**, 032510 (2000)
88. G.S. Adkins, R.N. Fell, J. Sapirstein, Phys. Rev. D **63**, 125009 (2001)
89. G.S. Adkins, M. Lymberopoulos, D.D. Velkov, Phys. Rev. D **50**, 4194 (1994)
90. M.I. Eides, V.A. Shelyuto, Eur. Phys. J. C **21**, 489 (2001)
91. A. Kizilersü, M. Reenders, M.R. Pennington, Phys. Rev. D **52**, 1242 (1995)
92. J.M. Jauch, F. Rohrlich, *The Theory of Photons and Electrons* (Springer Verlag, NY, 1976)